

**OSL dating of coastal sediments revealing coastal evolutions: case studies
in Songkhla (Thailand), Trassenheide (Germany), and Ephesus (Turkey)**

Dissertation

To obtain the academic degree of a Doctor of Natural Science
(Dr. rer. nat.)

Submitted to
Bayreuth Graduate School of
Mathematics and Natural Science (BayNat)
University of Bayreuth

Presented by
Prakrit Noppradit
born on 23rd February 1989
in Songkhla, Thailand

Bayreuth, 2018

This doctoral thesis was prepared at the Chair of Geomorphology at the University of Bayreuth from April 2014 until June 2018 and was supervised by Prof. Dr. Ludwig Zöller.

This is a full reprint of the dissertation submitted to obtain the academic degree of Doctor of Natural Science (Dr. rer. nat.) and approved by the Bayreuth Graduated School of Mathematical and Natural Science (BayNat) of the University of Bayreuth.

Date of the submission: 26.06.2018

Date of the defense: 09.11.2018

Acting director: Prof. Dr. Dirk Schüler

Doctoral Committee:

Prof. Dr. Ludwig Zöller (reviewer)

Prof. Dr. Gerhard Schellmann (reviewer)

Prof. Dr. Bernd Huwe (chairman)

PD Dr. Klaus-Martin Moldenhauer

Abstract

Understanding coastal processes is important to adapt possible coastal changes. The projection of coastal changes in the future is carried out by investigating the present and past coastal environment. For understanding the past coastal environment, which was reconstructed from the evidences preserved in the coastal sediments, time is required. Coastal sediments consist of organic material and/or minerals depends on their geological setting.

Optically-stimulated luminescence (OSL) is a powerful tool to date many geological materials. This study attempted to apply OSL dating to coastal sediments which are rich in mineral grains by using a single aliquot regenerative (SAR) dose protocol in three study areas. First at Songkhla in Southern Thailand, OSL was applied to fine sand-size quartz in wave, wind, lagoon, and fluvial environments to reveal the geological evolution. Second at Trassenheide at the Baltic Sea coast of Germany, coastal dunes which were classified based on colour of subsoil were dated by sand-size quartz. Third at Ephesus in Turkey, pre- and post-ancient harbour environments were dated using silt-sized quartz and feldspar (polymineral), which then were compared to nearby studies and radiocarbon ages.

After the measurement of luminescence signal and statistical methods were applied the equivalent dose showed values between 0.56 and 153 Gy. Dose rates of sand-rich sediments (average 0.91 Gy/ka) were lower than silt-rich sediments (average 2.74 Gy/ka). OSL ages ranging between ca. 160-0.6 ka showed less than 10% errors. There are two problems found: incomplete bleaching and weathering. At the study location at Songkhla, there was the observation of weathering due to very low potassium content (effect to dose rate) resulting in an overestimated age (proven by sea level history). This problem was solved by using a time dependent dose rate model. At the study location of Ephesus, harbour sediments were probably formed in turbid water and there was not enough sunlight for resetting the OSL signal. The incomplete bleaching lead to overestimated ages (inconsistent in age-depth plot). However, well bleached samples can be observed when there was an agreement of quartz and feldspar ages (in polymineral fractions).

In Songkhla, from sandy sediments OSL proved the hypothesis of sea level highstand both in the last interglacial (ca. 127 ka) and mid-Holocene (ca. 6 ka). After the sea level highstand at ca. 127 ka, the sea level regressed and Songkhla was several hundred km from the coastline. There were wind, fluvial, and lake environments during 50-17 ka, which were dated by OSL. In this study OSL was also used to date mixed fine and coarse sediments which were classified to be lagoonal (ca. 7 ka). OSL ages of Holocene samples agreed with the sea level curves predicted in previous studies.

In Trassenheide, OSL ages were the better timing tool to classify dune generations. Generations of dunes were defined by OSL ages of ca. 2.5-1.6 ka (Roman Warm Period) and of ca. 0.6 ka (after Medieval Warm Period). During 1.6-0.6 ka, there was no observation of any dune. This might relate to a strong coastal erosion in the Baltic Sea at that time.

In Ephesus, consistent OSL and ^{14}C ages described the geological evolution since ca. 3 ka when Ephesus was a marine environment. Around 2.5 ka, the delta advanced fast; OSL proved a very high deposition rate of up to 65 mm/year. An intensive harbour use was at around 2 ka. OSL ages agreed with previous ^{14}C ages from lake sediments using nearby core samples in the same study area.

Overall, OSL is a useful tool to provide the geochronological frame for coastal sediments and can well describe the geological evolution, the sea level change, and archaeological events since the Late Pleistocene. In combination with other evidences such as palaeontology, paleoclimatology, OSL is a part to contribute understanding the paleoenvironment studies in coastal areas.

Zusammenfassung

Küstenprozesse zu verstehen ist wichtig, um sich an mögliche Küstenveränderungen anpassen zu können. Eine Projektion von zukünftigen Küstenveränderungen kann nur auf der Grundlage eines gegenwärtigen und vergangen Küstenverständnisses durchgeführt werden. Das Verstehen der vergangenen Küstenbedingungen, welches auf den in den Küstensedimenten erhaltenen Hinweisen beruht, erfordert den Faktor Zeit. Küstensedimente bestehen aus organischem Material und/oder Mineralien, abhängig von ihren geologischen Ablagerungsbedingungen.

Optisch stimulierte Lumineszenz (OSL) ist ein leistungsfähiges Werkzeug zur Datierung verschiedener geologischer Materialien. In dieser Studie wurden in drei Untersuchungsgebieten OSL Datierungen mittels des Einzelproben-Protokolls mit regenerierter Dosis (SAR) an mineralreichen Küstensedimenten durchgeführt. Erstens wurde OSL in Songkhla in Südthailand auf Quarz-Feinkorn Sand aus Wellen-, Wind-, Lagunen- und Fluvialumgebungen angewendet, um die geologische Entwicklung aufzuzeigen. Zweitens wurden in Trassenheide an der Ostseeküste Deutschlands anhand von Quarzen in der Sand-Fraktion Küstendünen datiert, die bisher anhand der Bodenfarbe klassifiziert worden sind. Drittens wurden in Ephesos in der Türkei vor- und nach-antike Hafensedimente mit Quarzen und Feldspäten der Silt-Fraktion (Polyminal) datiert. Die Alter wurden dann mit Studien und Radiokohlenstoff-Alter aus der Umgebung verglichen.

Nach der Messung des Lumineszenzsignals und der Anwendung statistischer Methoden zeigte die Äquivalentdosis Werte zwischen 0,56 und 153 Gy. Die Dosisrate sand-reicher Sedimente (durchschnittlich 0,91 Gy / ka) war niedriger als die der schluffreichen Sedimente (durchschnittlich 2,74 Gy/ka). OSL Alter zwischen ca. 160-0,6 ka zeigten Fehler von weniger als 10%. Es wurden zwei Probleme gefunden: zum einen die unvollständige Bleichung und zum anderen der Einfluss der Verwitterung. In Songkhla wurde der Verwitterungseffekt aufgrund eines sehr niedrigen Kaliumgehalts (Effekt auf die Dosisrate) beobachtet, was zu einem überschätzten Alter führte (nachgewiesen durch den Meeresspiegeltrend). Dieses Problem wurde durch Verwendung eines zeitabhängigen Dosisratenmodells gelöst. In Ephesos wurden Hafensedimente wahrscheinlich in trübem Wasser gebildet und dort gab es dann auch nicht genügend Sonnenlicht zum Zurücksetzen des OSL-Signals. Das unvollständige Bleichen führte zu überschätzten Altern (nicht konsistent in der Alters-Tiefen-Kurve). Gut gebleichte Proben konnten jedoch beobachtet werden, wenn Quarz- und Feldspatalter (in den polymineralischen Fraktionen) übereinstimmten.

In Songkhla hat OSL anhand sandiger Sedimentproben die Hypothese eines Meeresspiegelhochstandes sowohl im letzten Interglazial (ca. 127 ka) als auch im mittleren Holozän (ca. 6 ka) bewiesen. Nach dem Meeresspiegelstand bei ca. 127 ka sank der Meeresspiegel und Songkhla war mehrere hundert Kilometer von der Küste entfernt. Vor 50 bis 17 ka gab es Wind-, Fluss-, und Seeablagerungen, die mittels OSL datiert werden konnten. In dieser Studie wurde OSL auch verwendet, um gemischte, feine und grobe Sedimente zu datieren, die als Lagune (ca. 7 ka) klassifiziert wurden. OSL-Alter von Holozänproben stimmten mit den in früheren Studien vorhergesagten Meeresspiegelkurven überein.

In Trassenheide waren OSL-Alter das bessere Datierungswerkzeug, um die Dünenentwicklung zu klassifizieren. Dünenbildungen wurden durch OSL-Alter auf ca. 2,5-1,6 ka (Römische Warmzeit) und auf ca. 0,6 ka (nach der Mittelalterlichen Warmzeit) datiert. Während 1,6-0,6 ka gab es keine Dünenbildung, was mit einer starken Küstenerosion in der Ostsee zu dieser Zeit zusammenhängen könnte.

In Ephesus beschrieben konsistente OSL- und ^{14}C -Alter die geologische Entwicklung seit ca. 3 ka, als Ephesus einen marinen Ablagerungsraum darstellte. Um etwas 2,5 ka entwickelte sich das Delta schnell; OSL-Alter zeigen eine sehr hohe Ablagerungsrate von bis zu 65 mm/Jahr. Eine intensive Hafennutzung fand um ca. 2 ka statt. OSL-Alter aus dieser Studie stimmen mit früheren ^{14}C -Altern an Seesedimenten überein, die aus nahe gelegene Kernproben im selben Untersuchungsgebiet stammten.

Zusammenfassend kann gesagt werden, dass OSL ein sehr nützliches Werkzeug ist, um den geochronologischen Rahmen für Küstensedimente zu liefern und mit ihr können die geologische Entwicklung, der Meeresspiegelwechsel und archäologische Ereignisse seit dem späten Pleistozän gut beschrieben werden. Durch Kombination mit anderen Methoden und Daten, wie z.B. Paläontologie, Paläoklimatologie, tragen OSL Datierungen dazu bei das Verständnis der Paläogeographie von Küstengebieten zu fördern.

Table of Contents

Abstract	I
Zusammenfassung	IV
Table of Contents	VI
List of Tables	IX
List of Figures.....	X
List of symbols and abbreviations	XIII
1 Synopsis.....	1
1.1 Introduction	2
1.1.1 Coastal zone and causes of the coastal change.....	2
1.1.2 Late Quaternary sea level	3
1.1.3 Luminescence dating	3
1.2 Aim and hypothesis	6
1.3 Methodology	7
1.3.1 Fieldwork and sample collections	7
1.3.2 Sample preparation	8
1.3.3 Luminescence measurement and statistical analysis.....	8
1.3.4 Dose rate and age calculation	12
1.4 Study areas, results and discussions	14
1.4.1 Study I: Songkhla, Thailand.....	14
1.4.2 Study II: Trassenheide, Germany.....	15
1.4.3 Study III: Ephesus, Turkey.....	16
1.5 Conclusion	18
1.6 References	18
2 Study I: Late Quaternary evolution of Songkhla coast, Southern Thailand, revealed by OSL dating.....	22
Abstract	24
1. Introduction	24
2. Geomorphology of Songkhla	26
3. Methodology	26
4. Results and discussion.....	30

Overestimated OSL age due to weathering and the interglacial highstand	30
Late Pleistocene events	31
Holocene events	32
5. Conclusion	34
Acknowledgement.....	34
References	34
3 Study II: Geological evolution and optically stimulated luminescence (OSL) dating of the coastal dunes at Trassenheide, Usedom Island, NE Germany	37
3.1 Abstract	39
3.2 Introduction	39
3.3 Study area	40
3.4 Methodology	42
3.5 Results	47
3.6 Discussion	48
3.7 Conclusion	51
3.8 Acknowledgement.....	52
3.9 References	52
4 Study III: Methodological approach for dating harbor sediments by using luminescence dating – a case study in Ephesus, Western Turkey	56
4.1 Abstract	58
4.2 Introduction	58
4.3 Drill cores from the Roman harbor basin	60
4.4 Methodology	61
4.5 Results and Interpretation.....	64
4.5.1 Sedimentology of Eph 395	64
4.5.2 Chronology	64
4.6 Discussion	67
4.6.1 Validity of luminescence ages	67
4.6.2 Comparison with other results in the Roman harbor and canal	70
4.7 Conclusion	72
4.8 Acknowledgement.....	74

4.9 References	74
Appendix	78
A1 Own and authors contribution statements.....	79
A2 D_e distribution in Study I, II, and III.....	81
A3 Example of fading rate determination of polymineral fine grain	85
A4 Acknowledgement	86
A5 Curriculum Vitae	87
A6 (Eidesstattliche) Versicherungen und Erklärungen	89

List of Tables

Synopsis

Table 1.1	Measurement steps of the single aliquot regenerative dose (SAR) protocol (Wintle and Murray, 2006)	10
-----------	--	----

Table 1.2	Integral and background subtraction ranges for Study I to III	12
-----------	---	----

Study I

Table 1	Details of sample collection and OSL dating	27
---------	---	----

Study II

Table 3.1	Sampling locations and OSL dating results	45
-----------	---	----

Study III

Table 4.1	¹⁴ C dating results of sediment core Eph 395 from the Roman harbor basin. Dating was carried out at the Radiocarbon Dating Facility, Queens University Belfast, UK. The conventional ages were calibrated with Calib 7.1 (Reimer et al. 2009). They are presented with 2 sigma standard deviation (probability of 95.5 %). b.s.l. below sea level; b.s. below surface	63
-----------	--	----

Table 4.2	Luminescence dating results, both polymineral and quartz	68
-----------	--	----

List of Figures

Synopsis

- Figure 1.1 Late Quaternary global sea level curve (modified from Benjamin et al., 2017). 3
- Figure 1.2 Description of the luminescence process based on the band theory: (a) mineral received ionizing radiation and electrons are trapped at the energy level below conduction band and accumulated, (b) after the crystal is exposed to heat or light, electrons dissipate their energy by recombining with the hole. The light emitted by this process is called luminescence. (c) Basic principle of how luminescence dating is applied to coastal sediment: During transportation (by water, wave, wind), grains are exposed to light, the luminescence signal is reset. After grains were buried without light, grains are irradiated by ionizing radiation and luminescence intensity increases..... 5
- Figure 1.3 Steps of sample preparation of equivalent dose determination for both coarse and fine grains. 9
- Figure 1.4 Example of natural OSL decay curve of BT1555 10
- Figure 1.5 Measuring cycles of SAR protocol, which in brackets show ordering of measurements (dashed line shows an equivalent dose in Gy) 11
- Figure 1.6 OSL measurements, data processing of equivalent dose, dose rate, and age calculation 13
- Figure 1.7 OSL dating results on the cross-section to the sea (right hand side). Unit B and F were sandy clay, while others were sandy rich 15
- Figure 1.8 (a) Location of cores in previous and this studies (395), (b) deposition environments and successfully dated results of the core 395 combined with the possible bathymetry during 500 BC and 1 AD/BC, (c) Bayesian age-depth model (Zeeden et al., 2018) from the successfully dated samples 17

Study I

- Figure 1 (a) Geographical location of Songkhla at the eastern coast of Southern Thailand, (b) Geomorphological map (redraw and modified from [11]), (c) Barometric altitude in m of the profile P-P' in (b) and sampling location; blue line indicates mean high water spring (MHWS), vertical scale shows orthometric height in meter 27

- Figure 2 Dose recovery test for samples BT1558 and BT1563 for determining an appropriate temperature for preheating in the SAR protocol. Top: Equivalent dose (D_e) over applied dose versus preheat temperature. Band shows $\pm 5\%$ deviation from unity. Bottom: Equivalent dose (D_e) versus preheat temperature (preheat plateau test), the horizontal lines indicate the D_e plateau in the temperature range 220-260 °C 28
- Figure 3 Time dependence dose rate model for estimating the age of the weathered sample BT1557, when the integral (area under the graph) of dose rate (\dot{D}) and time (t) is present day equivalent dose (D_e). 29
- Figure 4 Examples of OSL growth curves of BT1559, which has the highest D_e (top), and of BT1564, which has the lowest D_e 30
- Figure 5 Late Quaternary coastal evolution along Profile P-P' in Songkhla (see Figure 1). OSL ages are given in italics. (a) Last interglacial sea level highstand when the sea level was +5 m from today, (b, c, d) after sea level regress since the interglacial, wind and water affected the development in the area, (e) before the Holocene sea level highstand, a lagoonal system occupied the area behind the barrier, (f) during the Holocene sea level highstand the barrier moved landward, inducing coastal sand dunes, (g) with sea level regression after the highstand, the barrier developed seaward and a dune ridge formed 33
- Figure 6 Relative sea level changes over time. Comparison of this study (black square) to local sea level curve of [7] (model in grey line, data in grey circles) 34

Study II

- Figure 3.1 Study location: (a) overview map of the German-Polish coast in the southern Baltic Sea, where the blue colour shows the location of Usedom Island, (b) geomorphological map of northern Usedom (redrawn from Hoffmann and Lampe 2007), (c) 30 m digital elevation model (DEM) of Trassenheide and the nearby area, (d) topographic cross-section A-A' derived from the 5-m resolution DEM (www.geoportal-mv.de) as provided in the geomorphological map (b). Location of sediment coring sites (distance from coastline: 850 m for TRA I, 550 m for TRA II, and 350 m for TRA III). Moreover, the lithology of each core (brown italic text shows colours of illuvial horizon) and OSL laboratory numbers are presented..... 43

Figure 3.2 Results of dose recovery tests of samples BT1499 (top) and BT1506 (below). Three aliquots were measured at each preheat temperature setting, the results were then averaged. Error bars represent 1σ standard error	46
Figure 3.3 The OSL decay curve of sample BT1501 shows that the initial signal is dominated by the fast component (a), and D_e distribution of sample BT1501 presented in the form of an abanico plot (Dietze et al. 2016).....	48
Figure 3.4 OSL ages and evolution model of the (classified) Yellow Dunes in Trassenheide (vertical axis = elevation in m above recent sea level, horizontal axis = distance in m from recent coastline, according to Figure 3.1). TRA I developed around 2.3 ka, then around 1.8 ka the dunes from which cores TRA II and TRA III were taken were generated contemporaneously. The red and grey dash indicates the possible dune surface at 1.9 and 1.7 ka, respectively. For lithological information please see Figure 3.1	49
Figure 3.5 OSL dating results from this study (Trassenheide) and Swina with a relationship to Lampe (2005)'s hypothetic sea level curve (bar colour: brown = Brown Dune, yellow = Yellow Dune, white = White Dune; black line = OSL age).....	50
 <u>Study III</u>	
Figure 4.1 Location of the drill cores in the Roman harbor basin and the canal. Eph 395 is located in the southern part of the basin (Stock et al. 2016, modified).	62
Figure 4.2 Photo of drill core Eph 395 from the Roman harbor basin. In order to minimize the problems with collapsed material and compaction, the section between 3 and 11 m were drilled with 80 cm segments only (Photo: F. Stock 2015).	65
Figure 4.3 Left: Stratigraphy and the results of grain size analyses, loss on ignition and the chronology (^{14}C and luminescence ages). Right: Luminescence and ^{14}C ages (OSL: quartz age, IRSL: polymineral age) as well as age-depth model (gray band) following Zeeden et al. (2018).	66
Figure 4.4 Dose response curve of BT1409 polymineral (right) and Abanico plot showing the D_e distribution of BT1409 polymineral.	67
Figure 4.5 The results of the core Eph 395 from this study have been integrated into the harbor/canal sequence. Source: Stock et al. 2016, modified.	72
Figure 4.6 Possible harbor depth around decades before 500 BC (blue line), decades after 500 BC (blue dashed line) showing the very fast advance of the delta and around 1 AD/BC (green line) when the harbor was dredged.	73

List of symbols and abbreviations

\dot{D}	Dose rate in Gy/ka
D_e	Equivalent dose in Gy; Gy =J/kg
t	time
ka	time's unit expressing for thousand years
R	Name of the numerical programming language R (here written in bold letters)
CRAN	Comprehensive R Archive Network; http://cran.r-project.org
OSL	Optically-stimulated luminescence
IR	Infrared light
IRSL	Infrared stimulated luminescence
SAR	Single aliquot regenerative (dose protocol)
n/N	Number of accepted aliquots per measured aliquots
ADELE	Name of software to calculated dose rate and age for trapped charge dating developed by Kulig (2005)
MHWS	Mean high water springs
AD	Anno Domini
BC	before Christ
b.s.	below surface
b.s.l.	below sea level

1 Synopsis

1.1 Introduction

Coastal areas are important to various topics, as they have been changed both by nature and human activities. Recently, many coastal areas are facing various problems, for example sea level change due to climate change and/or coastal erosion (Williams, 2013). Understanding coastal changes via geological evidence is useful to forecast future situations, which can help mankind to plan for, prepare for, prevent, and protect livelihoods from possible future events (Rohling et al., 2008). Knowledge, which is applied to predict the future, is not only required at present but information from the past is also needed. However, often human history records are short and only a few records provide information in geological contexts. For this reason, evidence preserved in geological materials, such as rocks or sediments, is helpful to study past events which did not appear in human history.

1.1.1 Coastal zone and causes of the coastal changes

The coastal zone is the transition zone between terrestrial and marine systems (Finkl, 2004). Masselink et al. (2011) classified coastal areas based on the dominance of depositional systems into three types: wave, tide, and fluvial processes. When coastal areas face sea waves, which have higher energy levels compared to others, waves might erode the area and/or bring coarse sediments (e.g. sand, gravel, pebble) to deposition. This area is dominated by wave action. When wind flows passing the dry coastal sands, sand grains are transported by wind and deposited further inland, so called coastal dunes, which can commonly be found at wave-dominated coasts. If the coastal area has a protector (e.g. by barrier) and wave energy is not strong enough comparing to the tide, lagoonal environment can be formed. In the lagoonal system, silty to clayey sized sediments are generally observed. For coastal areas located near a river mouth where fresh and salt water meet a fluvial dominated coast can be explored, so-called delta. There are various sedimentary types that can be observed in the delta system which mainly depend on the strength of the river, tide, or wave.

Changes of the coastal area can be related to several processes. On the long-term scale sea level fluctuates due to the inclination of the earth's rotational axis which affects directly sea water volume (Shennan et al., 2015). This effect has a period of up to one hundred thousand years. Moreover, there are several smaller scale factors such as tectonic, sea level change, meteorology, tide, or human activities (Finkl, 2004; Shennan et al., 2015).

1.1.2 Late Quaternary sea level

During the Quaternary period, the climate has changed between dry and wet periods for several times. The sea level and the coastal area have been affected directly. During the last interglacial, ca. 128 ka ago (Murray-Wallace and Woodroffe, 2014), was the last time when the sea level was similar to the present state (Rohling et al., 2008). After that, the climate went into a colder period and reached the Last Glacial Maximum (LGM) around 20 ka when the sea level was at least 120 m below the present sea level (Figure 1.1). Afterwards, the climate became warmer and the sea level rose.

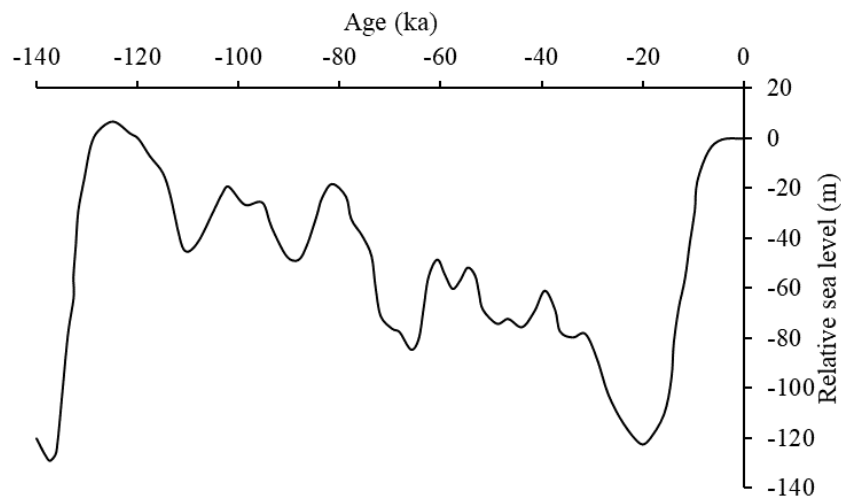


Figure 1.1 Late Quaternary global sea level curve (modified from Benjamin et al., 2017).

At the end of the Pleistocene through the beginning of the Holocene, ice volume had decreased and lead to higher volume of sea water. The sea level then rapidly rose and reached a maximum in the mid and low latitudes in the mid Holocene. After that the sea level has slightly decreased until today.

1.1.3 Luminescence dating

One of the keys to understand the past (paleo-) environments is the factor time. Many approaches have been applied to date geological materials depending on types of material and time ranges of each approach. Luminescence dating is a kind of trapped charge dating techniques providing the age of the last time a mineral in a sediment has been exposed to light or heat.

Luminescence is applied for many purposes, such as radiation measurement, or in the context of geosciences or archaeology (Bøtter-Jensen et al., 2003; Yukihiro and McKeever, 2011). In geoscience, luminescence dates minerals, which are generally found in sediments. Luminescence dating is useful for establishing the stratigraphy and chronology of stacked records. Therefore, it leads to a better understanding of geological processes. The basic principle of the origin and release of the luminescence signal in nature is described in the following paragraphs.

Radioactive elements, emitting ionizing radiation, are generally found in nature. This kind of radiation causes the environmental dose rate. Aitken (1985) separated the environmental dose rate into three types, cosmic (\dot{D}_c), external (\dot{D}_{ext}), and internal radiation (\dot{D}_{int}). First, the internal dose rate is the radiation related to radioactive element(s) inside minerals. Second, the environmental (external) dose rate is the radiation of the surrounding grains towards the mineral of interest. The cosmic radiation is the third factor affecting the dose rate. This radiation relates to cosmogenic particles that result from the interaction between solar radiation, earth magnetic field, and gases in the atmosphere.

In band theory, when a mineral is exposed to ionizing radiation, electrons in the valence band are stimulated. If the energy of the ionizing radiation is sufficient for electrons to reach the conduction band, electrons become attached to traps in the crystal lattice, which is at the electron energy level below the conduction band (Figure 1.2a). In case the accumulated electrons in the minerals are stimulated by sufficient energy from light or heat, trapped electrons are released, electrons energy decreases and the light is emitted, which is called luminescence (Figure 1.2b). The luminescence emitted from the heat stimulation is called thermoluminescence (TL). In addition, the luminescence emitted from photon stimulation is named optically stimulated luminescence (OSL). The intensity of luminescence emitted after stimulation depends on the duration and the intensity of the ionizing radiation.

Based on the luminescence principle, the burial time of geological material can be determined using its minerals. Mineral grains transported by water or wind were exposed to light and their luminescence signal was reset. When these grains were deposited and buried, no more light affected the grains. When the grains were irradiated by natural ionizing radiation, the luminescence signal accumulated (see summary in Figure 1.2c). The intensity of luminescence signal depends on the strength of ionizing radiation and duration. The strength of ionizing radiation can be estimated in the field or laboratory. The time since grains were buried can then be estimated.

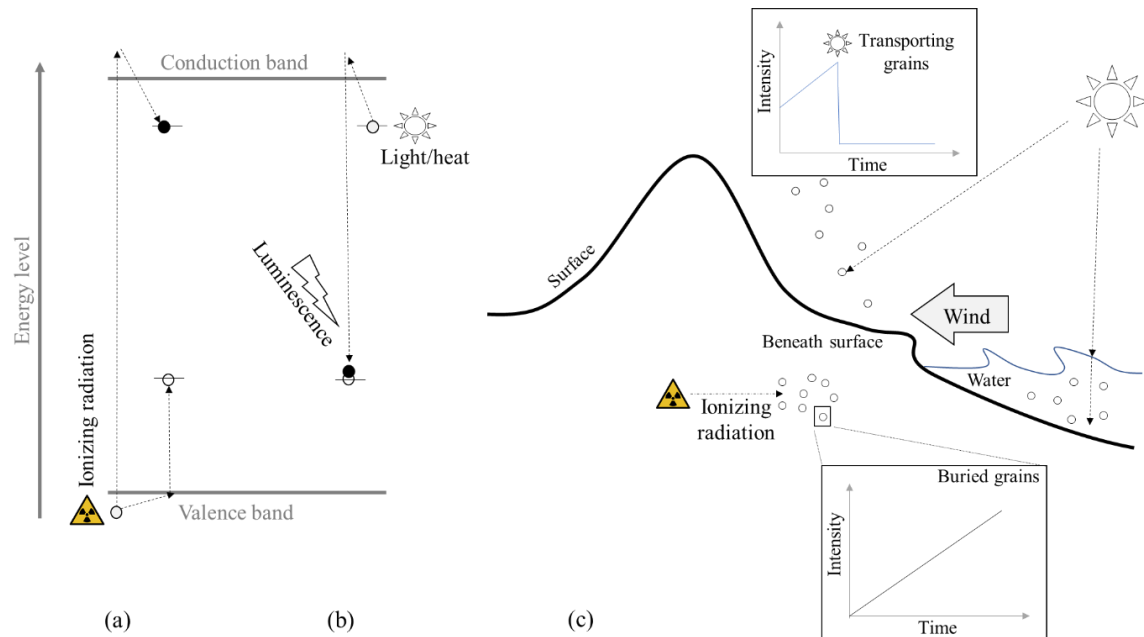


Figure 1.2 Description of the luminescence process based on the band theory: (a) mineral received ionizing radiation and electrons are trapped at the energy level below conduction band and accumulated, (b) after the crystal is exposed to heat or light, electrons dissipate their energy by recombining with the hole. The light emitted by this process is called luminescence. (c) Basic principle of how luminescence dating is applied to coastal sediment: During transportation (by water, wave, wind), grains are exposed to light, the luminescence signal is reset. After grains were buried without light, grains are irradiated by ionizing radiation and luminescence intensity increases.

Since 1953, many techniques in luminescence dating have been developed (Preusser, et al. 2008). At the beginning, TL was applied to ceramics and further applied to sediments. However, one major weakness of the TL technique is the luminescence signal is hard to be bleached, and some of the signals cannot be bleached by daylight (Godfrey-Smith et al., 1988). In consequence, OSL has been used instead of TL, since its signal is easier to be bleached by daylight.

To estimate how long the mineral has been buried, the equivalent dose (dose accumulated in the mineral since the last exposure; D_e) can be determined in a unit of Gray (Gy). There are two main methods, namely multiple aliquot additive dose (MAAD) and single aliquot regeneration (SAR) (Preusser et al., 2008). First, MAAD is a method based on adding laboratory doses on the natural

dose and extrapolating the dose response curve to the residual level. For SAR, after the measurement of the natural signal, the same aliquot's signal is regenerated by artificial irradiation. Then the growth curve, the graph in a relation between dose and signal intensity, is interpolated to find the D_e from its natural signal (Wintle and Murray, 2006). Later the age of the sample is calculated from the D_e divided by the dose rate.

Minerals are commonly found in almost all geological materials, leading to advantages of the luminescence dating over other methods. Several minerals were attempted to be dated by luminescence techniques, however, two common minerals are quartz and feldspar (Preusser et al., 2008; Wintle, 1997). The age range of the luminescence method depends on the strength of the dose rate and saturation of each mineral. For example, quartz has a lower saturation dose than feldspar.

For quartz OSL, the most efficient stimulations are between deep red and blue (Wintle, 1997). The emission spectrum of quartz is mainly in the UV range; centred at ca. 365 nm (Huntley et al., 1991). This quartz emission has a relationship to the 325 °C-thermoluminescence peak (Yukihara and McKeever, 2011), which can be rapidly bleached (Wintle, 1997). The feldspar OSL emission spectrum is mainly in the blue-violet range; centred at ca. 400 nm (Huntley et al., 1991). The general stimulation is carried out by the infrared range (Hütt et al., 1988; Wintle, 1997) to avoid unexpected signals which are closed to the emission spectrum.

Many sedimentary environments can be dated by the luminescence technique (Preusser et al., 2008). The same technique is also applied to sediments from a great variety of coastal areas, such as areas associated with dunes and lagoons, which are important for ecosystems and human settlements; thus, understanding the coastal processes is necessary. Normally, coastal sediments mainly are composed of minerals such as quartz or feldspar. Hence, the luminescence dating is a tool fitting to estimate the time scale of coastal transformation processes (Choi et al., 2013; Fuchs et al., 2012; Reimann et al., 2011). Furthermore, in many coastal research studies, luminescence dating has been applied to such various purposes as coastal development, tsunami-, or storm-deposits. This information is useful for land use, urban planning, hazard preparedness, and even historical studies.

1.2 Aim and hypothesis

The factor time is important in the understanding of paleocoastal processes, thus various dating techniques have been applied. So far OSL dating has been successful in dating several kinds of

sediments such as alluvial, aeolian, or others. In this study, OSL dating was applied to various coastal environments using quartz and/or polymineral grains from three locations.

Study I. Songkhla in Southern Thailand: wave, wind, and lagoon depositions were dated by using the coarse grain quartz technique to review the geological evolution, which was not chronologically confirmed yet.

Study II. Trassenheide in Germany: wind depositions were dated by using coarse grain quartz technique to determine the formation of parallel-to-coast sand dunes, which were classified without numerical ages.

Study III. Ephesus in Turkey: lake, harbour and delta depositions were dated by the fine grain technique (both quartz and polyminerals) to evaluate and determine periods before, during, and after the area was intensively used.

Problems of OSL dating in some environments, here mainly overestimated ages, were discussed related to their geological and archaeological contexts. A possibility of correcting overestimated ages due to weathering was invented. Age results and stratigraphy were utilized to understand the geological process in the coastal areas during the Late Quaternary. Coastal processes and evolution of the study areas were better understood via OSL dating.

1.3 Methodology

1.3.1 Fieldwork and sample collections

In preparation of the fieldwork, some information of the selected areas was required such as revision of previous studies, geoinformation, and others, with details described in the following chapters. As Study I was considering surface sedimentary units, samples were taken at ca. 1 m depth from surface by an auger (and shovel) and for deeper samples by a backhoe loader. In Study II and III, which considered deeper sediments, samples were drilled from the surface by vibracores with cylinders of 6 cm in diameter. Because the luminescence is sensitive to light, precautions were required to avoid light exposure. Sediments samples were collected by light-blocked cylinder tubes (PVC or metal) and immediately sealed by black plastic. Lithology information of the sampled cores was determined in the laboratory.

1.3.2 *Sample preparation*

Collected samples were opened in a dark room under red-light conditions (ca. 640 nm wavelength) and separated into two parts: luminescence measurement (from the middle part of a cylinder) and radioactivity analysis (from the outer part of a cylinder). The overall sample preparation is presented in Figure 1.3. For the dose measurement, samples were sieved at 90-200 μm for coarse grain fraction (fine sand size), and at $<63 \mu\text{m}$ for fine grain fraction. Samples were further treated with H_2O_2 for removal of organic materials and HCl for removal of carbonate materials. During the treatment of the fine grains in acid, pH was controlled to be above 3.

The coarse grain fraction was applied to a high-density liquid solution (sodium polytungstate) to separate minerals using the differences in mineral density. Due to the fact that all coarse grain fractions were rich of quartz, 2.70 and 2.62 g/cm^3 of the liquid density were applied in this step to obtain quartz fractions. Since the radiation of alpha particles irradiated to the mineral was only less than 25 μm and the correction of effects from the alpha radiation was complicated, coarse grain quartz samples were further etched by 38% HF for ca. 50 minutes (Aitken, 1985). Then 90-200 μm in diameter grains were attached to a 1-cm-diameter disc.

The fine grain fraction (silt size) was applied to Atterberg cylinders to extract grain sizes between 4 and 11 μm principled by Stoke's law to get a polymineral fine grain fraction for luminescence measurements. When sufficient sample material was available, the polymineral fraction was treated in H_2SiF_6 for the removal of feldspar grains and the enrichment of quartz to gain a quartz fine grain fraction. The fine grain fraction was attached to a 0.8-cm disc through the pipet technique.

1.3.3 *Luminescence measurement and statistical analysis*

The prepared discs were measured in a luminescence reader (Risø TL/OSL reader DA15). The reader is equipped with an EMI 9235Q UV sensitivity photomultiplier. An example of a quartz OSL decay curve read by the Risø reader from sample BT1555, which was taken from Songkhla in Study I, is presented in Figure 1.4.

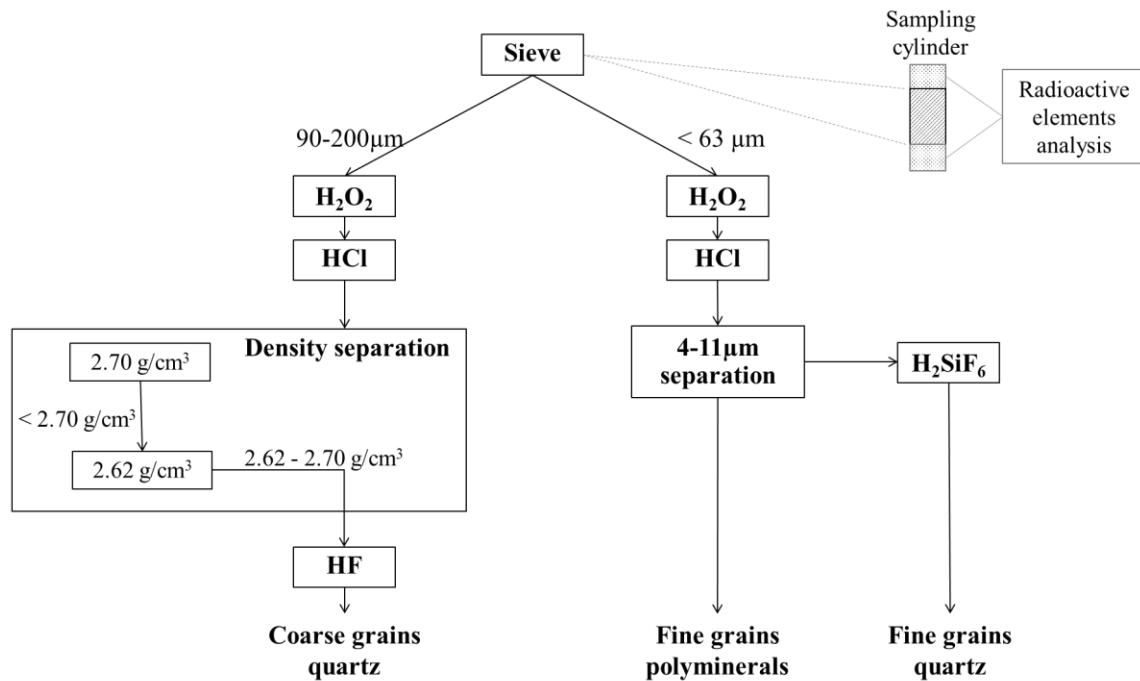


Figure 1.3 Steps of sample preparation of equivalent dose determination for both coarse and fine grains.

The SAR protocol was applied afterwards. The step measurement of the SAR protocol is presented in Table 1.1. The preheat plateau test and/or the dose recovery test were carried out for estimating the suitable temperature for preheating the sample in step 2 in Table 1.1 (Wintle and Murray, 2006). The heating in the Step 5 in Table 1.1 was applied by with a cut heat temperature to be the same as the preheat one. The SAR measurement was carried out for four cycles with various doses related to the estimated D_e and a repeat dose cycle and a zero dose cycle. The measuring cycles are presented in Figure 1.5. For quartz measurements, the purity of quartz was tested by infrared stimulation. When the infrared signal was almost similar to background, the measured aliquot was accepted.

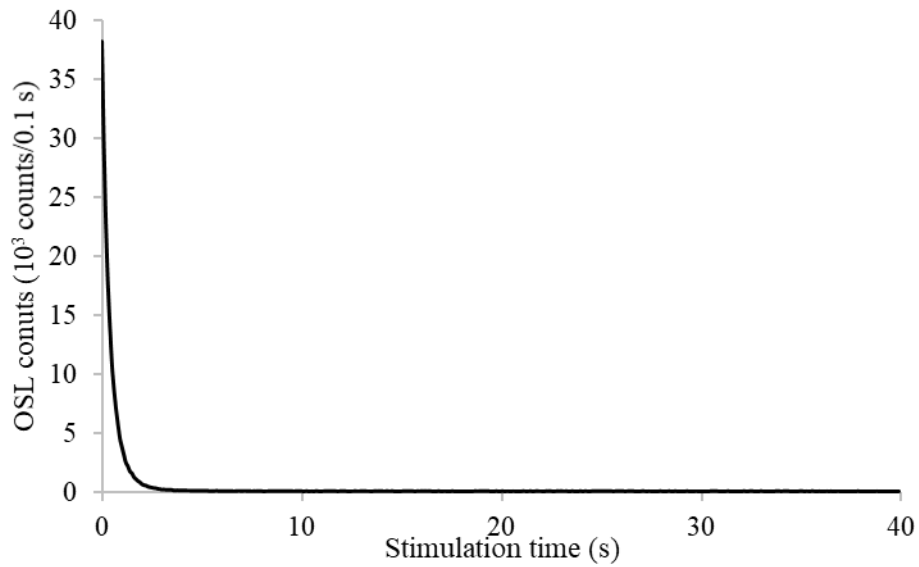


Figure 1.4 Example of natural OSL decay curve of BT1555.

Table 1.1 Measurement steps of the single aliquot regenerative dose (SAR) protocol
(Wintle and Murray, 2006)

Step	Treatment	Observed
1	Give dose*	-
2	Preheat	-
3	Stimulation	Lx
4	Given test dose	-
5	Heat	-
6	Stimulation	Tx
7	Return to 1	-

* During the first cycle of Step 1 the natural dose is measured.

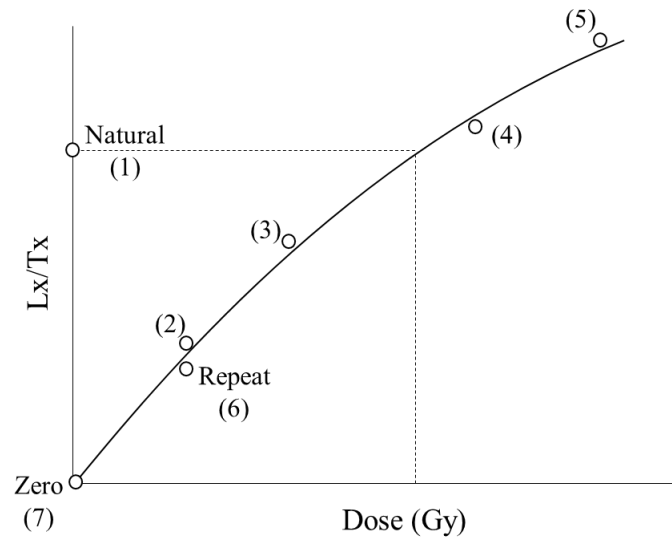


Figure 1.5 Measuring cycles of SAR protocol, which in brackets show ordering of measurements (dashed line shows an equivalent dose in Gy).

The quartz sample was stimulated by blue LED (470 nm, ca. 36 mW/cm²) for 40 s, while a polymineral sample was stimulated by infrared LED (870 nm, ca. 121 mW/cm²) for 100 s. The OSL signal was filtered by a UV filter (7.5 mm Hoya U340) for the quartz measurements, and blue-violet band interference filter (3 mm Chroma D410/30x) for polymineral measurements. All stimulation signals were emitted from LEDs in a continuous wave (CW) mode. Samples were then dosed by an in-built ⁹⁰Sr/⁹⁰Y β-source. The SAR was analysed by Analyst software (Duller, 2015). This considered signal and background signals of each study are presented in Table 1.2. In Study II, as all samples showed low D_e , the considered ranges were only at the beginning of the shine down curve. Growth curves were fitted by an exponential function,

$$y = a \left(1 - e^{-(x+c)/b} \right), \quad 1.1$$

where y represents a luminescence signal per test dose dose (Lx/Tx), x represents an applied dose. D_e distribution can be plotted in many types (Galbraith and Roberts, 2012), and some statistical information can be provided. Statistical methods were applied to improve the quality of the D_e via **R** (R Core team, 2018) with the luminescence package (Kreutzer et al., 2018). The central age model

(Galbraith et al., 1999), which has been integrated in the **R** luminescence package, was carried out to assume well bleached samples and fine grain samples. Overview's steps are presented in Figure 1.6.

Table 1.2 Integral and background subtraction ranges for Study I to III.

Study	Mineral	Signal integral range (s)	Background range (s)
I: Songkhla	Quartz	0-0.8	25-40
II: Trassenheide	Quartz	0-0.2	0.2-1.7
III: Ephesus	Quartz	0-0.8	25-40
	Polyminerals	0-2.0	90-100

For the IR measurement of polymineral dating, the fading phenomenon was observed. The correction of fading was measured based on Huntley and Lamothe (2001). Then, the fading rate was reported as g in % decade after the measurement. The faded ages were corrected following Huntley and Lamothe (2001) via the luminescence package (Kreutzer, 2018).

1.3.4 Dose rate and age calculation

The outer part of the cylinder sample, which was taken in the field (see 1.3.2), was further processed under normal light conditions. To determine the dose rate, the concentration of radioactive elements and the location of samples are required. Then two methods were carried out in the radioactivity analysis. The content of thorium and uranium were determined by a thick source alpha counting (TSAC), while the potassium content was analysed by inductively-coupled plasma- optical emission spectrometry (ICP-OES). For the TSAC technique, samples were prepared by crushing and the part with a grain size of less than 25 μm was attached above a ZnS (Ag) scintillator in a confined tray (Michael and Zacharias, 2000). After ca. 1-month storage, a prepared tray was measured in the alpha counter, which is located at the Chair of Geomorphology, University of Bayreuth. The ICP-OES was carried out by the BayCEER laboratory (University of Bayreuth).

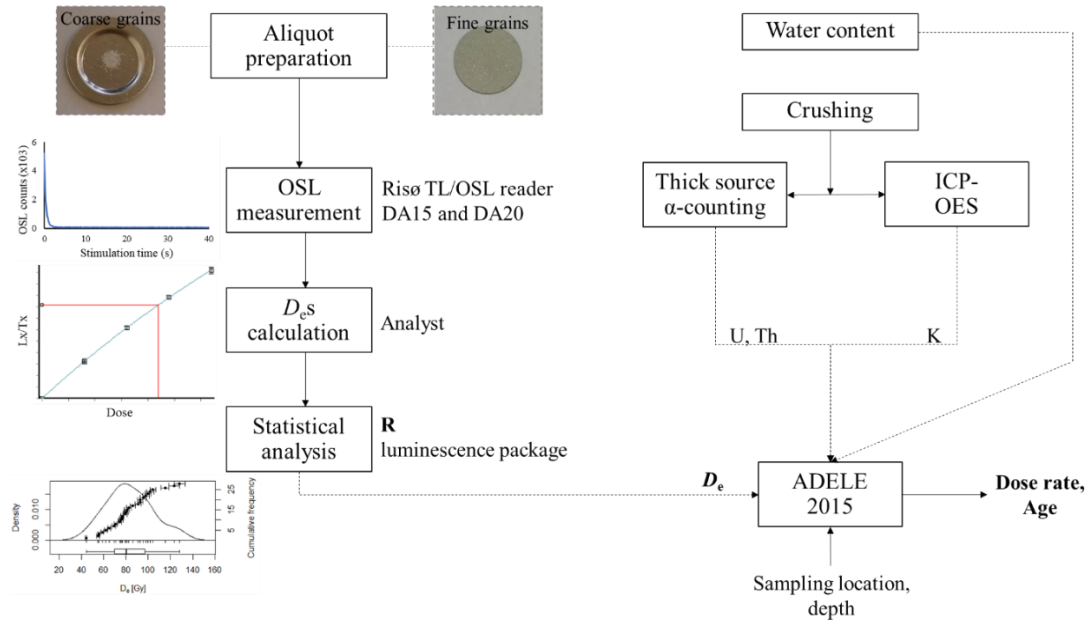


Figure 1.6 OSL measurements, data processing of equivalent dose, dose rate, and age calculation.

After that, results from radioactivity analysis were taken to determine the dose rate according to Aitken (1985) and Guerin et al. (2011). Moreover, the cosmic dose rate can be calculated using equations presented by Prescott and Hutton (1994). Age (t) was calculated by

$$t = \frac{D_e}{\dot{D}}, \quad (1.2)$$

where \dot{D} is the total dose rate (Gray per thousand years, Gy/ka) consisted of the cosmic dose rate and the external dose rate. The external dose rate consisted of the alpha, beta, and gamma dose rate which water contents correction was carried out following Aitken (1985) with the conversion factors by Guerin et al. (2011). In the calculation for coarse grain quartz, alpha dose rate was neglected as the zone of the mineral grains, which was affected by alpha particles, was removed by HF. For fine grain samples, the alpha dose rate was taken into account by using an alpha efficiency 0.035 ± 0.005 of quartz (Lai et al., 2008) and 0.08 ± 0.02 of polymineral (Zöller et al., 2013). Using these principles,

Kulig (2005) developed the software for calculating the dose rate and age called ADELE. The current version of ADELE, v2015, was also applied to this study; ADELE provides dose rate and age.

1.4 Study areas, results and discussions

Obtained D_e s were between 0.56-153 Gy. Growth curves of high D_e s showed stronger curvatures. However, no saturation was observed. All distribution plots are presented in Appendix 2. The distribution curves of the fine grain measurements were closer to the ideal Gaussian distribution than coarse grain measurement. This can be described by the number of grains in an aliquot which has a degree of a million for fine grain and hundreds for coarse grain (Heer et al. 2012). Moreover, most of the coarse grain measurements showed outliers. The outliers might occur from a few grains which were attached to a high radioactive mineral and received more ionizing radiation. It was significant that the average \dot{D} of the sand rich samples, 0.91 ± 0.30 Gy/ka (wave/wind transported), was lower than of the silty ones (harbour/lagoon/lake/delta sediments), 2.74 ± 0.80 Gy/ka. Lower \dot{D} of the sand rich samples lead to an extend of the OSL age ranges. However, higher \dot{D} can result in lower age errors. The D_e s and \dot{D} s resulted in OSL ages between 0.59-160 ka with less than 10% error. The introduction of each study area is briefly discussed with the OSL results here. In-depth details are presented in the following chapters.

1.4.1 Study I: Songkhla, Thailand

Songkhla is at the eastern coast of Southern Thailand (7.1 °N, 101.6 °E). Quaternary geomorphology of Songkhla's coastal areas was investigated by Chaimanee and Tiyaipirach (1983) and classified into three types of sedimentary units: beach ridges, old lagoon, and tidal flat (more details in Study I). In nearby areas, there were some investigations and summary on coastal evolution and Holocene sea level change by Horton et al. (2005). However, the Quaternary geological evolution of the Songkhla area has not yet been investigated due to the lack of chronological information, especially on the sandy rich sediments.

Sand size grains were observed in all sedimentary units. OSL dating (blue LED stimulation) to sediments consisting of sand was applied to this study. The OSL ages range from 160 to 4.5 ka. All samples had no significant incomplete bleaching. The oldest sample, from wave-transported sediment (ca. 3 m at location A in Figure 1.7), showed evidence of weathering (poor in potassium content), which resulted in an overestimated age. This was corrected by a time dependence dose rate model.

The corrected age was at 127 ka and agreed with the time of the last interglacial when the sea level was similar to the present. This sample proved the last interglacial sea level highstand and was evidence of the sea level of at least 5 m above present.

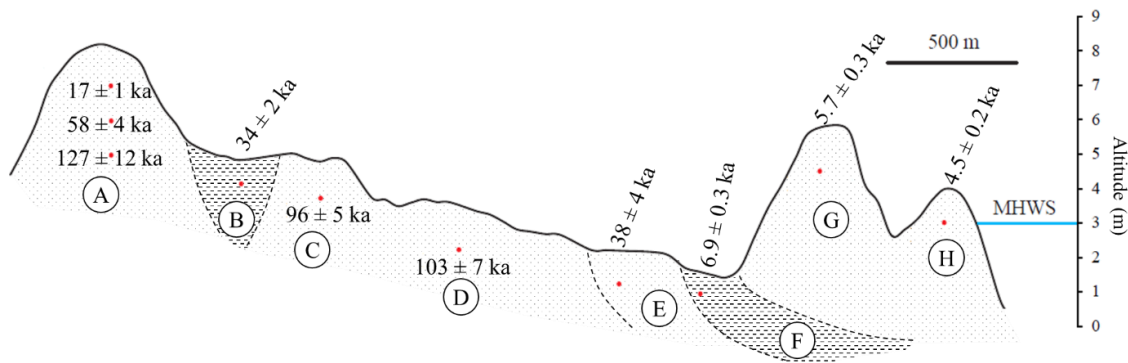


Figure 1.7 OSL dating results on the cross-section to the sea (right hand side). Unit B and F were sandy clay, while others were sandy rich.

During the global glacial period, the sea level regressed, and Songkhla was located hundreds of kilometres from the coastline (Kershaw et al., 2001). Songkhla's environment was dominated by wind depositing aeolian sand (reactivated from interglacial marine sand) based on evidenced by the top and middle part of location A, C, and D in Figure 1.7. Moreover, lacustrine and fluvial sediments, evidenced by area B and E in Figure 1.7, were found at ca. 38-34 ka which had a slightly humid climate (Dheeradilok and Kaewyana, 1986). The OSL age at location B and Pleistocene sea level curve lead to improve the regional geological map which suggested that it was an old lagoon. Holocene samples, with the ages of ca. 6.9-4.5 ka, were from the old lagoon and the sand dune ridge. The clay-silt rich sedimentary unit F in Figure 1.7 shows the possible old lagoon. Moreover, the higher altitude G and H sandy unit was deposited by wind. These findings can prove the hypothesis of a mid Holocene sea level highstand which was ca. 0.4 to 4.7 m above the present sea level. More details are explained in Chapter 2.

1.4.2 Study II: Trassenheide, Germany

Trassenheide is located on Usedom Island in the Baltic Sea of Germany. The classification of dunes in this area was based on degrees of soil podsolization (Keilhack, 1914) as a relative dating method

for three dune formations: Brown (the oldest), Yellow, and White (the youngest). In this study, OSL dating was employed to the parallel-to-coastline dunes in order to provide insights into the Holocene phases of dune formation, stability phases, and mobilization.

Blue OSL was applied to 90-200 μm sized quartz minerals. The overall distributions of D_e s showed complete beaching before burial. Coastal sand dunes here showed 0.67-1.05 Gy/ka dose rates and provided OSL age ranges of 0.59 to 2.46 ka. OSL results proved that coast-parallel dunes were mainly formed during the Roman Warm Period, RWP (ca. 2.5-1.6 ka). Then there was a hiatus of dune's development due to no sand supplying to the Trassenheide coast. Around ca. 0.59 ka in the Medieval Warm Period, OSL age results showed that strong winds brought new sand above the closest to shore dune which was formed in the RWP. This study further found that the Yellow Dune, classified in 1914, has already changed to yellowish brown colour. During 1914 to present, it might be that the podsolization changed the subsoil colour from yellow to yellowish brown (10YR 4/4). OSL ages might be a good indicator of dune generation compared to the degree of the soil podsolization which can change over time. More details are mentioned in Chapter 3.

1.4.3 Study III: Ephesus, Turkey

Ephesus is an ancient Roman harbour located in Turkey. It has been intensively studied since the 1990s. This study attempted to apply an OSL chronology from quartz and feldspar of polymineral fine grains and compared it to nearby core data from previous studies (Delile et al., 2015; Stock et al., 2016) and ^{14}C ages from bulk sediments.

Collected sediments were mainly fine grains (silt size) and originally from marine, delta, intensive used harbour, and lake sediments. Dose rates were 2.74 ± 0.80 Gy/ka in average. Samples 4 to 7 were successfully dated (1.06-3.13 ka). The unsuccessfully dated samples showed a problem of incomplete bleaching having younger numerical ages of quartz than feldspar in polyminerals. This problem was studied by Godfrey-Smith et al. (1988) stating that quartz was easier to bleach than feldspar in polyminerals. Moreover, ^{14}C ages of bulk sediments were all overestimated. The overestimation of ^{14}C might relate to the problem that sampled sediments derived from older ones. For these kinds of sediments only one dating method cannot be relied on. Successfully dated ages (see Figure 1.8) were applied to the Bayesian age-depth model as presented by Zeeden et al. (2018).

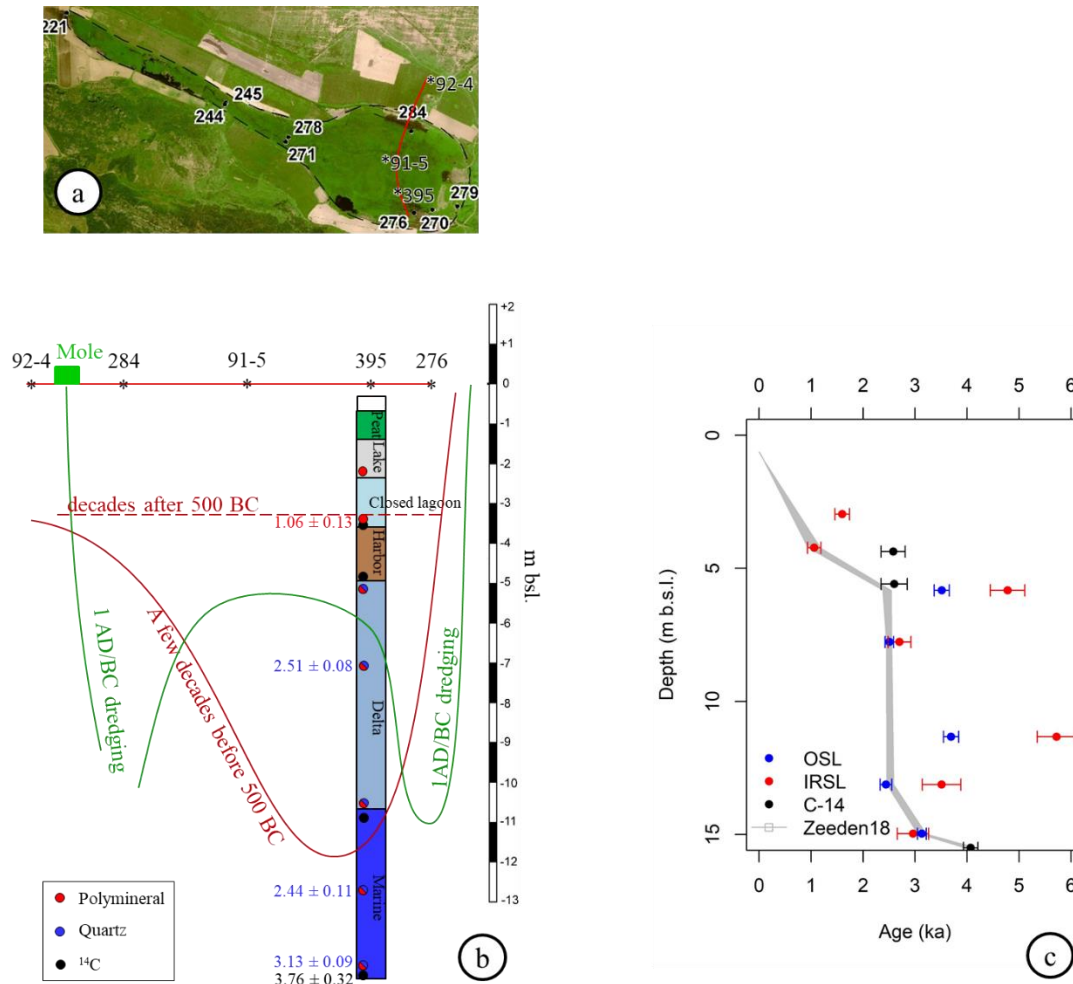


Figure 1.8 (a) Location of cores in previous and this studies (395), (b) deposition environments and successfully dated results of the core 395 combined with the possible bathymetry during 500 BC and 1 AD/BC, (c) Bayesian age-depth model (Zeeden et al., 2018) from the successfully dated samples

This study showed that before 500 BC this area was dominated by marine sediments. Until ca. 500 BC, the advance of the Küçük Menderes Delta implied a very high deposition rate (ca. 65 mm/year) covering the study area. Then Romans occupied this area and protected the harbour by moles (Stock et al., 2016) ca. 1 AD/BC. The possible bathymetry of the study area is presented in Figure 1.8a. Since the harbour was inactive, this area became a lake environment. More details are narrated in Chapter 4.

1.5 Conclusion

The SAR protocol of OSL dating is a useful tool to date various kinds of coastal sediments such as coastal dunes, marine sands, lagoon deposits, and harbour deposits. Wind and wave transported material showed complete bleaching, while delta and harbour sediments had a possibility of incomplete bleaching. There is a higher possibility of sand dunes and marine sands to date older depositions compared to lagoon and harbour sediments due to the dose rate. From these three studies two major problems were identified generating overestimated numerical ages, incomplete bleached sediments and weathering.

Incomplete bleaching was found in the harbour sediments possibly due to an effect on turbid water. The incomplete bleaching can be clearly observed when the age obtained from quartz is younger than the polymineral ages. For the harbour (and delta) environment, only one chronological method might not be enough. Weathering after deposition effected the concentration of radioactive elements and leaded to have a variable dose rate. This study succeeded in correcting the overestimated age due to weathering using the time dependence dose rate model.

With the combination and integration of other information, such as sea level, paleoclimate, and paleontology, dated OSL ages can well describe various paleo-coastal environments from the Late Pleistocene, both in geological and archaeological contexts. For sea level reconstruction, OSL is a useful tool to determine ages especially when less organic material is available.

1.6 References

- Aitken, M.J. (1985). Thermoluminescence dating. Academic Press, London.
- Bøtter-Jensen, L., McKeever, S.W.S., Wintle, A.G. (2003). Optically stimulated luminescence dosimetry. Elsevier, Amsterdam, London.
- Chaimanee, N., Tiyapirach, 1983. Quaternary Geology of Songkhla. Geology Division, Bangkok.
- Choi, K.H., Choi, J.-H., Kim, J.W. (2013). Reconstruction of Holocene coastal progradation on the east coast of Korea based on OSL dating and GPR surveys of beach-foredune ridges. *The Holocene* 24 (1), 24–34.

- Delile, H., Blichert-Toft, J., Goiran, J.-P., Stock, F., Arnaud-Godet, F., Bravard, J.-P., Brückner, H., Albarède, F. (2015). Demise of a harbor: A geochemical chronicle from Ephesus. *Journal of Archaeological Science* 53, 202–213.
- Dheeradilok, P., Kaewyana, W. (1986). On the Quaternary Deposits of Thailand. *Bulletin of the Geological Society of Malaysia* 19, 515–532.
- Duller, G.A.T. (2015). The Analyst software package for luminescence data: overview and recent improvements. *Ancient TL* 33(1), 35–42.
- Finkl, C.W. (2004). Coastal Classification: Systematic Approaches to Consider in the Development of a Comprehensive Scheme. *Journal of Coastal Research* 201, 166–213.
- Fuchs, M., Kreutzer, S., Fischer, M., Sauer, D., Sørensen, R. (2012). OSL and IRSL dating of raised beach sand deposits along the southeastern coast of Norway. *Quaternary Geochronology* 10, 195–200.
- Galbraith, R.F., Roberts, R.G. (2012). Statistical aspects of equivalent dose and error calculation and display in OSL dating: An overview and some recommendations. *Quaternary Geochronology* 11, 1–27.
- Galbraith, R.F., Roberts, R.G., Laslett, G.M., Yoshida, H., Olley, J.M. (1999). Optical dating of single and multiple grains of quartz from Jinmium rock shelter, Northern Australia: Part I, Experimental Design and Statistical Models. *Archaeometry* 41 (2), 339–364.
- Godfrey-Smith, D.I., Huntley, D.J., Chen, W.-H. (1988). Optical dating studies of quartz and feldspar sediment extracts. *Quaternary Science Reviews* 7 (3-4), 373–380.
- Guérin, G., Mercier, N., Adamiec, G. (2011). Dose-rate conversion factors: Update. *Ancient TL* 29, 5-8.
- Heer, A.J., Adamiec, G., Moska, P. (2012) How many grains are there on a single aliquot?. *Ancient TL* 30, 9-16.
- Horton, B.P., Gibbard, P.L., Milne, G.M., Morley, R.J., Purintavaragul, C., Stargardt, J.M. (2005). Holocene sea levels and palaeoenvironments, Malay-Thai Peninsula, southeast Asia. *The Holocene* 15 (8), 1199–1213.
- Keilhack, K. (1914). Erläuterungen zu Geologischen Karten von Preussen und benachbarten Bundesstaaten. Blatt Swinemünde, Berlin.

- Kershaw, P., Penny, D., van der Kaars, S., Anshari, G., Thamotherampillai, A. (2001). Vegetation and climate in lowland southeast Asia at the Last Glacial Maximum. In: Metcalfe, I., Smith, J.M.B., Morwood, M., Davidson, I. (Eds.) *Faunal and Floral Migrations and Evolution in SE Asia-Australasia*. A A Balkema, Netherlands, pp. 227–236.
- Kreutzer, S., Burrow, C., Dietze, M., Fuchs, M.C., Schmidt, C., Fischer, M., Friedrich, J., Mercier, N., Smedley, R.K., Christophe, C., Zink, A., Durcan, J., King, G.E., Philippe, A., Guerin, G., Fuchs, M. (2018). *Comprehensive Luminescence Dating Data Analysis*. R package version 0.8.2.
- Lai, Z.P., Zöllner, L., Fuchs, M., Brückner, H. (2008). Alpha efficiency determination for OSL of quartz extracted from Chinese loess. *Radiation Measurements* 43 (2-6), 767–770.
- Michael, C.T., Zacharias, N. (2000). A new technique for thick source alpha counting determination of U and Th. *Nuclear Instruments and Methods in Physics Research Section A: Accelerators, Spectrometers, Detectors and Associated Equipment* 439 (1), 167–177.
- Murray-Wallace, C.V., Woodroffe, C.D. (2014). *Quaternary sea-level changes. A global perspective*. Cambridge University Press, Cambridge, United Kingdom, New York.
- Prescott, J.R., Hutton, J.T. (1994). Cosmic ray contributions to dose rates for luminescence and ESR dating: Large depths and long-term time variations. *Radiation Measurements* 23 (2-3), 497–500.
- Preusser, F., Degering, D., Fuchs, M., Hilgers, A., Kadereit, A., Klasen, N., Krbetschek, M., Richter, D., Spencer, J.Q.G. (2008). *Luminescence dating: basics, methods and applications*. E&G – Quaternary Science Journal; Vol. 57 No 1-2; 95-149.
- R Core team (2018). *A language and environment for statistical computing*. R Foundation for Statistical Computing, Vienna, Austria.
- Reimann, T., Naumann, M., Tsukamoto, S., Frechen, M. (2011). Luminescence dating of coastal sediments from the Baltic Sea coastal barrier-spit Darss–Zingst, NE Germany. *Geomorphology* 122 (3-4), 264–273.
- Rohling, E.J., Grant, K., Hemleben, C., Siddall, M., Hoogakker, B.A.A., Bolshaw, M., Kucera, M. (2008). High rates of sea-level rise during the last interglacial period. *Nature Geoscience* 1 (1), 38–42.

- Stock, F., Knipping, M., Pint, A., Ladstätter, S., Delile, H., Heiss, A.G., Laermanns, H., Mitchell, P.D., Ployer, R., Steskal, M., Thanheiser, U., Urz, R., Wennrich, V., Brückner, H. (2016). Human impact on Holocene sediment dynamics in the Eastern Mediterranean - the example of the Roman harbour of Ephesus. *Earth Surface Processes and Landforms* 41 (7), 980–996.
- Williams, S.J. (2013). Sea-Level Rise Implications for Coastal Regions. *Journal of Coastal Research* 63, 184–196.
- Wintle, A.G. (1997). Luminescence dating: laboratory procedures and protocols. *Radiation Measurements* 27 (5-6), 769–817.
- Wintle, A.G., Murray, A.S. (2006). A review of quartz optically stimulated luminescence characteristics and their relevance in single-aliquot regeneration dating protocols. *Radiation Measurements* 41 (4), 369–391.
- Yukihara, E.G., McKeever, S.W.S. (2011). *Optically stimulated luminescence. Fundamentals and applications*. Wiley, Chichester West Sussex.
- Zeeden, C., Dietze, M., Kreuzer, S. (2018). Discriminating luminescence age uncertainty composition for a robust Bayesian modelling. *Quaternary Geochronology* 43, 30–39.
- Zöller, L., Richter, D., Masuth, S., Wunner, L., Fischer, M., Antl-Weiser, W. (2013). Luminescence chronology of the Grub-Kranawetberg site, Austria. *E&G – Quaternary Science Journal*; Vol. 62 No 2; 127–135; ISSN 0424-7116.

2 Study I

**Late Quaternary evolution of Songkhla coast, Southern Thailand,
revealed by OSL dating**

Prakrit Noppradit^{1, *}, Christoph Schmidt¹, Helmut Dürrast², Ludwig Zöller¹

¹ Chair of Geomorphology, University of Bayreuth, 95440 Bayreuth, Germany

² Department of Physics, Faculty of Science, Prince of Songkla University, Hatyai 90112,
Thailand

*corresponding author: prakrit.noppradit@uni-bayreuth.de

Submitted to

Chiang Mai Journal of Science

-Accepted-

Reprinted by permission from Chiang Mai Journal of Science's Editor



Chiang Mai J. Sci. 2019; 46(x) : 1-13
<http://it.science.cmu.ac.th/ejournal/>
 Contributed Paper

Late Quaternary Evolution of Songkhla Coast, Southern Thailand, Revealed by OSL Dating

Prakrit Noppradit* [a], Christoph Schmidt [a], Helmut Dürrast [b] and Ludwig Zöller [a]

[a] Chair of Geomorphology, University of Bayreuth, 95440 Bayreuth, Germany.

[b] Department of Physics, Faculty of Science, Prince of Songkla University, Hatyai 90112, Thailand.

*Author for correspondence; e-mail: prakrit.noppradit@uni-bayreuth.de

Received: 29 March 2018

Accepted: 1 August 2018

ABSTRACT

Coastal sediments in Songkhla Province (Southern Thailand) provide information on paleoenvironmental conditions; however, there is no geochronological data available for this area. This pilot study checks the suitability of optically-stimulated luminescence (OSL) dating to understand the geological evolution of the beach since the late Pleistocene. The single aliquot regenerative (SAR) dose technique of coarse grain quartz provided numerical ages from 160 ka to 4 ka. The oldest sample showed evidence of weathering, leading to an age overestimation due to leaching of radioelements. The overestimated age has been corrected based on a time dependent dose rate model. OSL ages provide a geochronological framework to interpret the geological and geomorphological evolution of the area since the last interglacial when the sea level was 5 m above present day sea level. Windblown sand overlying last interglacial deposits gave depositional ages of ca. 100, 58 and 17 ka. Moreover, during the period 34-38 ka ago, lacustrine and fluvial environments were prevalent, as deduced from sediment characteristics and sea level history. The OSL chronology established for windblown, lacustrine and fluvial deposits in Songkhla indicates the fluctuation of dry and humid climates during the last glacial period in Songkhla. Until the mid-Holocene, after the sea level had rapidly transgressed, a lagoon had been formed at around 1,100 m from the present coastline, supported by an OSL age of 6.8 ka. In the period 6.8-5.7 ka ago, the sea level reached its highstand and then regressed, resulting in two dunes deposited between 4 and 6 ka ago.

Keywords: OSL dating, late Quaternary, coastal evolution, Songkhla

1. INTRODUCTION

During the last interglacial in the global marine isotope stage MIS5e, 128-116 ka, the climate was similar to present conditions [1].

Due to this similarity, sea level changes during this period have been investigated by several studies (e.g. [2, 3]) in order understand and project future sea level dynamics [1]. For

example, around 130 ka and 120 ka ago, the sea level in Papua New Guinea, 6°S 147°E, was 5 m and 6.5 m above the present sea level, respectively [4, 5]. From then on, the climate became colder and drier and the sea level never reached the present day values until the mid-Holocene. During the last glacial

period in SE Asia the sea level was below the present state, up to -120 m at the late glacial maximum (LGM) [4, 5]. From then until the mid-Holocene the sea transgressed rapidly. The sea level history since the early Holocene has been summarized for various areas along the Malay Peninsula and central Thailand based on ^{14}C dating and paleontology [6, 7]. Moreover, local paleo-sea levels have been predicted by geophysical models, which were constructed from solid earth properties and global deglaciation history [6]. These models show that the sea level in Songkhla, Southern Thailand, was -22 m at 9.5 ka ago and rapidly increased until around 6 ka when the sea level was approximately +5 m. Since then the sea has regressed until present. This sea level trend is similar for the entire Gulf of Thailand; however, the difference is the degree of the sea level at the highstand [6].

Songkhla is located on the eastern coast of Southern Thailand (Malay Peninsula) facing the Gulf of Thailand (Figure 1a). The city is located on a small peninsula with an important fishing port and a deep sea port for cargo and petroleum exploration activities offshore. Songkhla is also a main hub for tourists from Malaysia, Singapore, and Indonesia. The climate in Songkhla is humid with two dominating monsoon seasons: May to October from southwest and October to January from northeast, with the latter one bringing the main rainfall. The average rainfall is 2,066 mm/year and the average temperature is 28 °C. Moreover, the tidal range of Songkhla is less than 1 m [8].

Quaternary geomorphology of Songkhla's coastal areas was investigated and classified into three types of sedimentary units: beach ridges, old lagoons, and tidal flats (Figure 1b). On the eastern coast of the small peninsula three areas dominated by

coastline-parallel relic (sandy) beaches can be found, which are demarcated by fine sediments of the old lagoon. In nearby areas there have been some investigations on coastal evolution and Holocene sea level change [6]. However, the Quaternary geological evolution of the Songkhla area has not yet been investigated due to the lack of chronological information, although sediments from nearby areas were dated using the ^{14}C method applied to organic rich parts. Nonetheless, ^{14}C dating has limitations, as it is only applicable for an age range less than ~50 ka [10] and as it requires organic material, which is not commonly found in sandy coastal sediments. Moreover, the current model of the local Holocene sea level for Songkhla [6] lacks evidence during the highstand.

Optically-stimulated luminescence (OSL) is a trapped charge dating method, which can be used to date various sediments [11] containing quartz and/or feldspar minerals. OSL dating is principally employed to measure the last time since minerals in sediments were exposed to sunlight (time of deposition). Its basic principle has been described in many studies [11-14, others]. OSL dating of quartz can provide age ranges from a few years to a few hundred ka depending on the detected luminescence signal and the environmental dose rate.

Due to the fact that the sedimentary units in Songkhla are quartz-rich [9], OSL dating has been applied to various coastal units in this study. The OSL ages provide a chronological framework for the coastal sediments in Songkhla from the late Pleistocene, which has led to a detailed understanding of the coastal evolution. Moreover, the geophysical models implying the sea level highstand in the last interglacial and the mid Holocene highstand can be confirmed by the results of this study

In addition, some sedimentary units with unclear formation could be classified as part of this investigation based on OSL ages and global sea level history.

2. GEOMORPHOLOGY OF SONGKHLA

Songkhla coast is a sandy coast extending NW-SE at the Gulf of Thailand and consists of a lagoonal system (Songkhla Lake) in the north. The sediments closest to the sea can be classified as sand beach composed mainly of medium to very coarse sand which was deposited by wind, wave action, and longshore current activities [9]. Moreover, at least two sandy paleo-ridges lie parallel to the coast. The inner ridges (westernmost) are located ca. 3 km from the coast line with a few hundred meters width and ca. 10 m height. These ridges show discontinuities due to the erosional processes. The middle ridge has a lower height comparing to others and is ca. 2.5-5 km wide [9].

The locations between sandy ridges consist of fine sediment plains above a sandy layer. The fine sediment plains are also made up of sand which was mixed to fine sediment due to wind action during the monsoonal season and were classified as old lagoons [9]. The outer plain (between recent and middle ridge) was formed because the offshore ridge protected it from wave action. The dominating lower energy of water resulted in the formation of a lagoon. All coastal sediments in this area were hypothesized to have been formed before the mid-Holocene [9].

Moreover, the western part of the study area consists of pre-Quaternary mountains and unconsolidated sediments. The unconsolidated sediments (colluvial,

terrace and alluvial) were deposited in this area by water flow from the pre-Quaternary mountains which ran parallel to the coast line.

3. METHODOLOGY

Geological maps and a 90 m resolution digital elevation model (DEM) were utilized to identify landforms within the study area. Samples for sedimentological characterization as well as OSL dating were collected along a single profile (Figure 1b, c), oriented perpendicular to the present coastline, and crossing the modern and ancient beaches and former lagoons (Figure 1b). For OSL dating, sediments were sampled with a PVC cylinder approximately 0.7 to 1.25 m below surface to avoid mixing of material due to soil development, except for the inner ridge (~3.5 km from coastline), where samples were collected at 1.2, 2.1, and 3.2 m depth (Figure 1c). Location and altitude of all samples were determined using Global Positioning System (GPS) and barometric altimetry. For the latter, a calibrated base station at Wat Ang Thong was used, 7°4'39.1022N 100°38'3.5722E, 10.7311 m orthometric altitude [15]. Note that in this study the orthometric height represents the present mean sea level (MSL). Details of the collected samples are shown in Table 1.

Sediment samples prepared for OSL dating require two portions of each sample: one for determining the equivalent dose (D_e), and the other for establishing the dose rate (\dot{D}) values in order to obtain an OSL age (t ; [12, 16]) according to the simplified equation:

$$t = \frac{D_e}{\dot{D}} \quad (1)$$

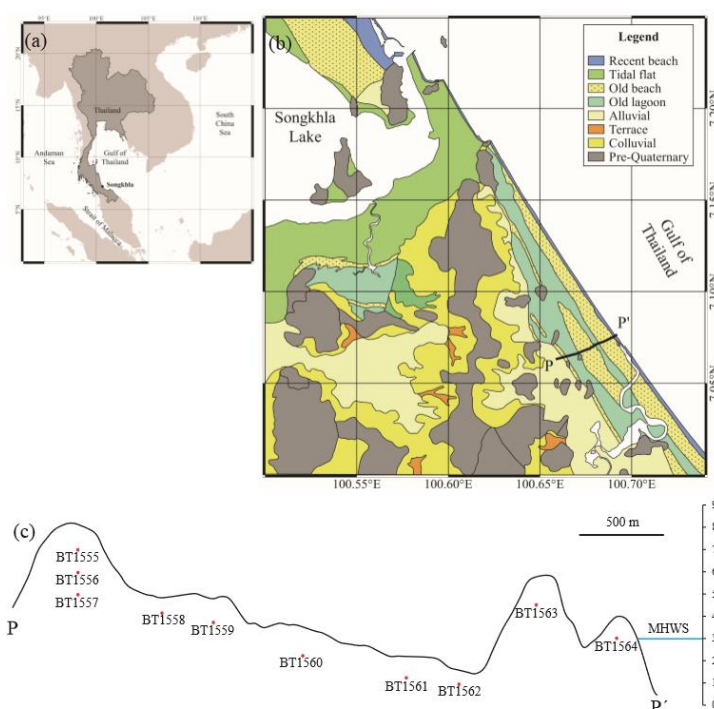


Figure 1. (a) Geographical location of Songkhla at the eastern coast of Southern Thailand, (b) Geomorphological map (redraw and modified from [11]), (c) Barometric altitude in m of the profile P-P' in (b) and sampling location; blue line indicates mean high water spring (MHWS), vertical scale shows orthometric height in meter.

Table 1. Detail of sample collection and OSL dating.

Sample ID	Latitude (°N)	Longitude (°E)	Surface altitude (m)	Depth (m)	Water content (%)	Th (ppm)	U (ppm)	K (%)*	D (Gy/ka)	n/N**	D _e (Gy)	Age (ka)
BT1555	7.0676	100.6602	8.2	1.10	0.4	5.32±0.61	1.32±0.19	0.023	0.866±0.076	25/25	14.85±0.83	17±1
BT1556	7.0676	100.6602	8.2	2.00	4.6	6.07±0.68	1.91±0.21	0.041	1.016±0.080	23/25	59.27±2.86	58±4
BT1557	7.0676	100.6602	8.2	3.20	5.2	1.64±0.22	0.68±0.07	0.007	0.392±0.039	24/25	62.58±2.59	***160±10
BT1558	7.0654	100.6670	4.9	0.75	26.2	19.11±1.71	5.79±0.51	0.136	2.344±0.146	28/34	80.55±3.78	34±2
BT1559	7.066	100.6700	4.9	1.12	24.3	13.98±0.93	2.04±0.28	0.376	1.593±0.089	15/25	152.61±6.41	96±5
BT1560	7.0669	100.6778	3.5	1.35	16.1	9.26±1.03	1.93±0.31	0.075	1.157±0.102	23/25	119.58±5.17	103±7
BT1561	7.0713	100.6794	2.1	1.10	13.5	0.76±0.18	0.89±0.10	0.082	0.457±0.039	25/25	17.33±1.52	38±4
BT1562	7.0723	100.6811	1.5	0.65	28.8	20.62±1.75	5.42±0.53	0.887	2.851±0.148	24/25	19.56±0.40	6.9±0.3
BT1563	7.0727	100.6851	5.9	1.30	4.2	10.30±0.90	2.51±0.27	0.121	1.532±0.103	25/25	14.85±0.83	5.7±0.3
BT1564	7.0753	100.6899	4.0	1.05	4.1	4.09±0.56	1.98±0.17	0.430	0.928±0.071	24/25	59.27±2.86	4.5±0.2

* Error of K content: 10%; ** Number of accepted aliquots *n* per measured aliquots *N*;

*** Age of Sample 1557 overestimated due to weathering, see text for further explanation.

The sample portion for determination was processed under red LED (640 ± 20 nm) conditions in the laboratory. Coarse grains ($90\text{-}200$ μm) were extracted by sieving; treatments with HCl (10%) and H_2O_2 (10%) removed carbonate and organic matter, respectively. Quartz was extracted by heavy liquid (sodium polytungstate solution) within a range of $2.62\text{-}2.70$ g/cm^3 . Then HF etching (48%) was applied for 45 min to remove the outer layer of the grains influenced by external α -radiation and to dissolve remaining feldspars. Finally, the quartz separates were rinsed in 10% HCl to destroy fluorides that could have precipitated during HF etching. The single aliquot regenerative dose technique, SAR [14], was applied to determine D_e values with a Risø DA15 TL/OSL reader, equipped with a $^{90}\text{Sr}/^{90}\text{Y}$ β -source delivering a dose rate of 0.12 ± 0.01 Gy/s to coarse grains. OSL signals were stimulated by blue LEDs emitting at 470 ± 5 nm for 40 s and detected with an EMI 9235QB15 photomultiplier tube through a 7.5 mm thick Hoya U340 glass filter. For determining the optimum preheat temperature of the SAR protocol, dose recovery tests were carried out while varying the preheat temperatures between 180 and 260 $^\circ\text{C}$ (in 20 $^\circ\text{C}$ increments) for samples BT1558 and BT1563 (Figure 2). Before administering a laboratory dose in the range of the expected burial dose, samples were bleached with an Osram Duluxstar lamp for 3 h to remove the natural signal. For each preheat temperature, three aliquots were measured. In addition, the D_e of natural aliquots was determined for different preheat temperatures (preheat plateau test; the range of tested preheat temperatures was the same as in the dose recovery experiment). The cutheat temperatures applied after irradiation with the test dose were set equal to the preheat

temperatures for all measurements. A preheat temperature of 240 $^\circ\text{C}$ showed least scatter between individual aliquots and measured D_e values were closest to the given dose compared to other preheat temperatures. For these reasons, 240 $^\circ\text{C}$ was applied for the preheating of all samples.

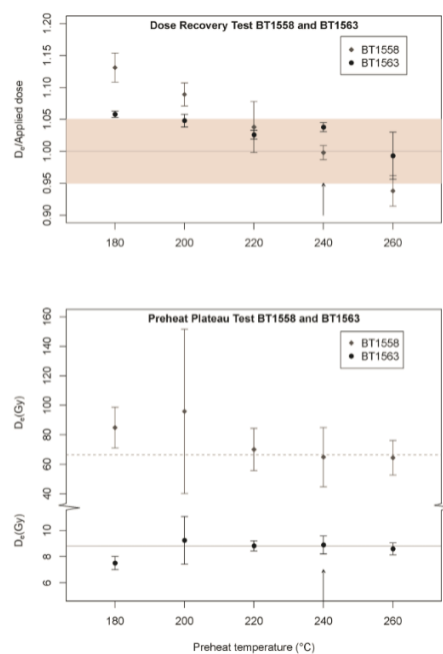


Figure 2. Dose recovery test for samples BT1558 and BT1563 for determining an appropriate temperature for preheating in the SAR protocol. Top: Equivalent dose (D_e) over applied dose versus preheat temperature. Band shows $\pm 5\%$ deviation from unity. Bottom: Equivalent dose (D_e) versus preheat temperature (preheat plateau test), the horizontal lines indicate the D_e plateau in the temperature range 220-260 $^\circ\text{C}$.

At least 25 aliquots per sample were measured for D_e determination. The obtained SAR data was processed via the software Analyst v.4.31.7 [17]. For constructing the dose response curve, the OSL signal was

integrated from 0 to 0.8 s, while a background averaged from the integral 25-40 s was subtracted. Data outside the range of the following quality criteria were rejected: a recycling ratio of 0.9-1.1, a test dose error <10%, and a recuperation ratio of <10% (relative to the natural signal). The central dose model (CDM) [18] was applied to the obtained D_e distribution using the **R** package ‘Luminescence’ (calc_CentralDose()) [18-20] and a σ_b value of 0.11 [21] because wave or wind transported sediments in coastal areas of lower latitudes are normally well bleached prior to deposition.

The dose rate (\dot{D}) was estimated from the concentrations of the radioactive elements (K, U, and Th) in the sediment. U and Th were determined by thick source α -counting, placing a <25 μm -crushed-bulk-sample above a ZnS (Ag) scintillator and using an α -counter [16]. The K content was determined by inductively coupled plasma-optical emission spectrometry (ICP-OES) of the bulk sample. Moreover, the cosmic dose rate (\dot{D}_c) was calculated from the geographical coordinates of the samples. Water contents were determined in the laboratory; their errors were assumed to be 5%. The D_e values resulting from the CDM, the K, U and Th concentrations as well as the geographical coordinates were fed in the ADELE [23] v2015 software for dose rate (beta, gamma, cosmic dose rate) and age calculation.

For sample BT1557, which was strongly weathered, the dose rate changed over time: $\dot{D}(t)$. In order to account for that, Equation (1) is transformed into Equation (2) to account for time-dependent dose rate variations. Under certain assumptions (see details in discussion part), Equation (3) and (4) were derived from Equation (2) and Figure 3, and Equation (5) is the error of t_0 resulting from Equation (4):

$$D_e = \int_0^{t_0} \dot{D}(t) dt = \int_0^{t_1} \dot{D}_0(t) dt + \int_{t_1}^{t_2} \dot{D}_1(t) dt + \dots + \int_{t_{n-1}}^{t_n} \dot{D}_{n-1}(t) dt + \int_{t_n}^{t_0} \dot{D}_n(t) dt \quad (2)$$

$$D_e = \dot{D}_1 t_1 + \frac{1}{2}(\dot{D}_0 + \dot{D}_1)(t_0 - t_1) \quad (3)$$

$$t_0 = \frac{2[D_e - \dot{D}_1 t_1 + \frac{1}{2}(\dot{D}_0 + \dot{D}_1)t_1]}{\dot{D}_0 + \dot{D}_1} \quad (4)$$

$$\delta t_0 = \sqrt{\left(\frac{\partial t_0}{\partial D_e}\right)^2 \delta D_e^2 + \left(\frac{\partial t_0}{\partial \dot{D}_1}\right)^2 \delta \dot{D}_1^2 + \left(\frac{\partial t_0}{\partial \dot{D}_0}\right)^2 \delta \dot{D}_0^2 + \left(\frac{\partial t_0}{\partial t_1}\right)^2 \delta t_1^2} \quad (5)$$

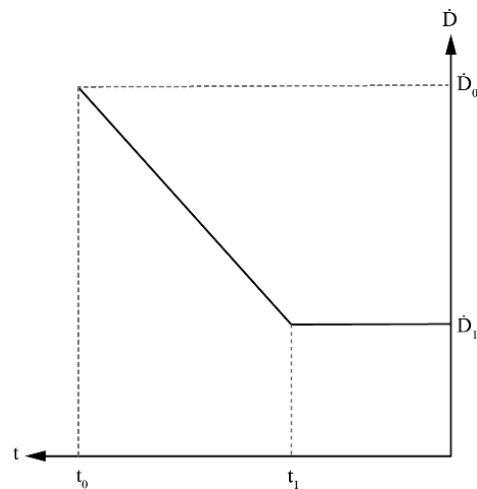


Figure 3. Time dependence dose rate model for estimating the age of the weathered sample, when the integral (area under the graph) of dose rate (\dot{D}) and time (t) is present day equivalent dose (D_e).

D_e is the measured equivalent dose; \dot{D}_1 is the present day dose rate; t_1 is the time when the dose rate became constant; \dot{D}_0 is the dose rate at the deposition time; t_0 is the deposition time. D_e and \dot{D}_1 are values which are obtained in ‘conventional’ age calculation. Note that the disequilibrium of U and Th series was not taken into account because this sample was below ground water only a short period after deposition (the last interglacial) and sediment above is unconfined. As α activity of U and Th and their daughters was measured by thick source

alpha counting a possible disequilibrium of U decay chains would be accounted for by the total count-rate. As the energies of α decays are not much different (with the exception of ^{214}Po which has an extremely short half-life) the calculation of the α dose-rate from the overall α count-rate is a good approach to the representative α dose-rate over the burial time even in case of disequilibrium.

4. RESULTS AND DISCUSSION

A topographic profile P-P' was constructed by using barometric altimetry (Figure 1c). Three possible dune ridges with surface altitudes of 8.2, 5.8, and 4.0 m above present sea level, respectively, were identified at approx. 3500, 650, and 200 m from the coastline. The lowest inland point (1.4 m) was 1100 m from the coastline, where the sediments had been classified as a former lagoon. The mean high water spring (MHWS) was measured at 3.0 m (orthometric height) from the beach cliff.

Representative examples of the form of the OSL dose response curve are depicted in Figure 4, with older samples (higher D_e) showing a stronger curvature (Figure 4 top), while younger samples (low D_e) have a weaker curvature (Figure 4 bottom). Between 60 and 100% (91% on average) of aliquots measured with the SAR protocol were accepted. This shows that the sediments in this area can be well dated by quartz SAR-OSL. The D_e values resulting from the CDM range between 4.2 and 153 Gy with 2-9% standard errors, while the effective dose rates vary from 0.392 to 2.851 Gy/ka with 5-10% standard errors. The dose rates of the sandy units (0.392-1.593 Gy/ka) are lower than of fine sediment units (2.344-2.851 Gy/ka). This typical observation can be explained by the fact that the smaller grain sizes consist of more clay minerals or mica tying or adsorbing more radionuclides than quartz grains. Calculated apparent

OSL ages cover a range of 4.5 to 160 ka with a relative error of 4 to 10%. All data are presented in Table 1. Note that the K concentrations are presented in % (%w/w). There were three samples giving Holocene ages and seven samples yielding Pleistocene ages. The obtained OSL ages help to classify geologic events since the onset of the Late Pleistocene.

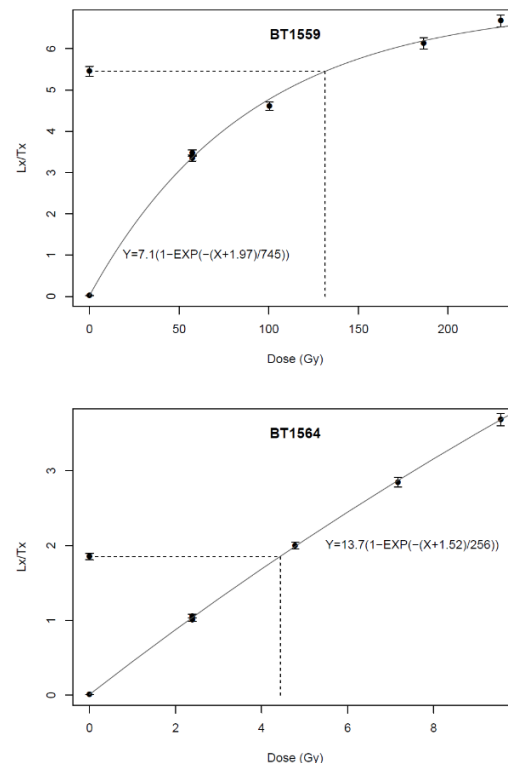


Figure 4. Examples of OSL growth curves of BT1559, which has the highest D_e (top), and of BT1564, which has the lowest D_e .

Overestimated OSL Age Due to Weathering and the Interglacial Highstand

Sample BT1557 (5 m above MSL, 3500 m from coastline) was the oldest sample, apparently some 160 ka old (older than the last interglacial). However, the very

low concentration of radioactive elements, especially K, with a concentration of 0.007% (other samples showed between 0.023-2.851% K), was an indication that the sample was altered by weathering processes. With regard to the dominant chemical weathering process of hydrolysis in the study area, K has a very high solubility, while U and, in particular, Th have low to almost none solubility [24]. The dissolved-weathering-products of K-bearing minerals can easily be translocated to adjacent porous sediments. Strong weathering processes in SE Asia during the last interglacial were confirmed by [25]. Due to its higher relief position, weathering products of sample BT1557 could easier be transported to lower areas. The loss of radioactive elements decreases over time and leads to an age overestimation if the present-day low dose rate is used for age calculation. BT1557 was collected beneath the pebble layer and marine shell fragments found at the same depth nearby. When the sampling site was a ridge, the only possibility is that the material of BT1557 was transported by very strong wave action. Thus, the time of global MIS5e (~125 ka) very likely represents the deposition time of BT1557.

This study attempted to correct the overestimated age of BT1557 by using the present day concentration of K in beach sediments of approximately 0.3% [26] with a 0.1% assumed error. Our correction method is based on the assumption that U and Th contents did not change substantially over the burial period since both radioelements are hardly soluble if sediments are well-drained. The change of \bar{D} over time is presented in Figure 3, where the assumption of t_1 was 34 ± 2 ka (BT1558), and for D_1 it was 0.66 ± 0.11 Gy/ka (based on present day potassium content, $\sim 0.3 \pm 0.1\%$, in beach sands [26], 40% water content, and present day uranium and thorium

contents). Moreover, a decrease of dose rate in a linear trend was assumed in a first approximation, accounting for a lack of more detailed information about the temporal evolution of the K leaching process. Finally, the calculation via Equations (4) and (5) resulted in a corrected age of 127 ± 12 ka. This age agrees with the geological conditions of the last interglacial when the sea transgressed above present day height. The correction of the weathering was applied only to BT1557, while other samples which formed after the last interglacial were not taken into account. However, to give a more accurate age, a precise translocation model of the weathering products would be required.

Late Pleistocene Events

Seven samples were dated in the late Pleistocene period. A ca. 3 m deep profile of the westernmost sand ridge was dated and the lowermost age corrected due to overestimation as explained in the previous section; the two samples above yielded ages of 58 ± 4 and 17 ± 1 ka. The inner fine sediment plain (BT1558) was dated to 34 ± 2 ka. OSL ages of the middle sandy unit (BT1559 and BT1560) are around 100 ka, while the east side of this ridge was dated to 38 ± 4 ka.

Marine shell fragments were found at few meters depth at the west side of the middle ridge (below BT1559). This site most likely formed during the same space of time within which BT1557 (westernmost ridge) was deposited during the last interglacial. To consider the altitude, the site of BT1557 was a beach berm, while the locations of BT1559 and BT1560 (middle sandy unit) were an offshore sand bar and the area beneath BT1558 was a trough between an offshore bar and a beach berm (Figure 5a). These evidences indicate that the sea level highstand during the last interglacial in

Songkhla was around 5 m above MSL. When the sea level fell after global MIS5e (interglacial), around 100 ka ago, this area was covered by aeolian sand suggested by the ages of samples BT1559 and BT1560 (Figure 5b).

According to the OSL ages and sea level history, there was no coastal event recorded during the time interval between 100 and 10 ka, i.e., during almost the entire last glacial when the sea level was less than -30 m (-120 m during the LGM) relative to MSL [4]. However, around 58 ka and 17 ka (Figure 5b, d), the dry climate [27] induced dune reactivation at the site of BT1557 (BT1556 and BT1555, respectively). Moreover, around 34-38 ka (Figure 5c), alluvial and lacustrine events occurred. Between interglacial berm and bar, fine sediments were observed indicating lake sediment depositions. Such fine sediments might be interglacial weathering products transported to low lying areas, indicated by a very high dose rate of BT1558. The 34 ka event is in agreement with related sediment classification by [9]: the area of BT1558, which was previously classified to be an old lagoon [9], has recently been reclassified as a paleolake. At the eastern side where an OSL age of 38 ka was obtained, the medium-coarse sand might indicate a fluvial environment eroding the interglacial marine sand bar. This may further point to higher precipitation [28] during this 34-38 ka interval (in global MIS3), which lacks further independent evidence for this area.

Holocene Events

Three samples were dated in the

Holocene (6.9 ka for the fine sediment unit, and 5.7 and 4.5 ka of recent beach ridge). The mid-Holocene, approx. 6.9 ka (Figure 5e), fine sediments were observed at the sampling site of BT1562 (1 km from present coastline), which was deposited in a low wave energy environment (lagoon). This could be explained by another near shore barrier during the transgression at that time. This sample can serve well as a sea level indicator. The barometric altitude showed 1.58 m and the sample depth was 0.65 m. This indicates that the sea level around 6.9 ka was ~0.9 m above MSL.

Between 6.9 and 5.7 ka, the sea level transgressed. The outer barrier was eroded and a new berm eastward of BT1562 formed. The high sediment budget induced dune formation [29] at BT1563 sample location at around 5.7 ka (Figure 5f). From observations of core H17 in [9], located near BT1564, it appears that the lagoon remains through the nearby BT1563 location at around -0.2 to 0.4 m above MSL. The sampling depth of BT1563 was at 1.2 m. There was no marine evidence observed between surface and 4.7 m above the sea level at this site. Thus, the sea level was between 4.7 and 0.4 m above MSL at 5.7 ka. In analogue, there was no observation of marine evidence between surface and 3 m from sea level at the location of BT1564. An OSL age of 4.5 ka can be interpreted that the sea level was 0.4 to 3 m above MSL at 4.5 ka. This showed an overall sea level regression and is in agreement with a study of [30] in Chumphon, approx. 500 km north of Songkhla also at the Gulf of Thailand side.

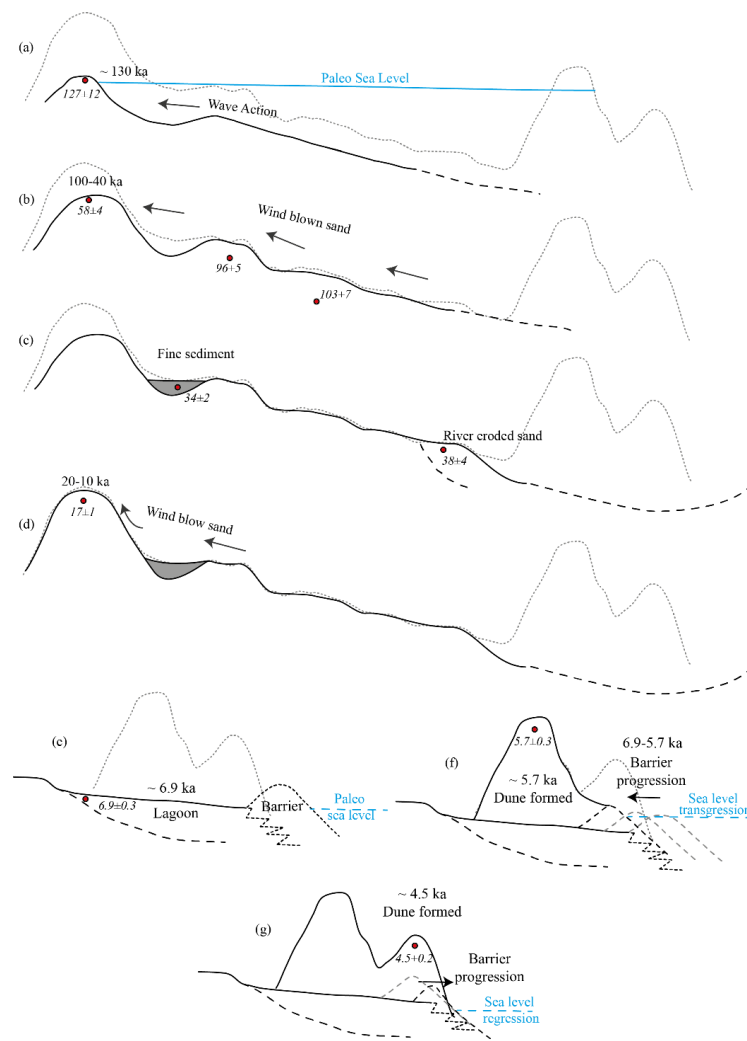


Figure 5. Late Quaternary coastal evolution along Profile P-P' in Songkhla (see Figure 1). OSL ages are given in italics. (a) Last interglacial sea level highstand when the sea level was +5 m from today, (b, c, d) after sea level regress since the interglacial, wind and water affected the development in the area, (e) before the Holocene sea level highstand, a lagoonal system occupied the area behind the barrier, (f) during the Holocene sea level highstand the barrier moved landward, inducing coastal sand dunes, (g) with sea level regression after the highstand, the barrier developed seaward and a dune ridge formed.

Moreover, there is a lagoon system observed in [9], but with no OSL ages available. However, from the sediment stratigraphy it can be assumed that this unit is between 4.5 and 5.6 ka old when the sea level was 2.6 m above the present level.

For this study, sea level indicators, here BT1563 and BT1564, show a range, which is too wide to construct an updated

sea level curve. However, sea level data of this study are in good agreement with a predicted sea level curve constructed by [6] (see Figure 6), especially confirming the sea level highstand at around 6 ka before present. In order to give more precise and accurate values on paleo-sea level altitudes, beach berms beneath the dunes need to be defined in future coring.

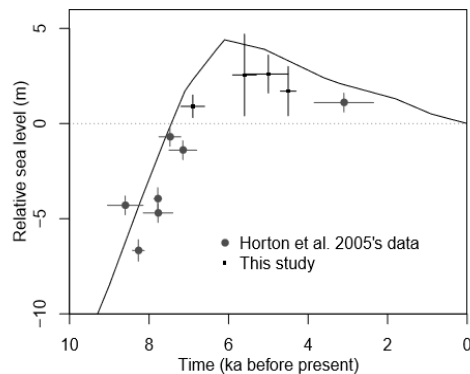


Figure 6. Relative sea level changes over time. Comparison of this study (black square) to local sea level curve of [7] (model in grey line, data in grey circles).

5. CONCLUSION

OSL dating of quartz using the SAR protocol provides a valuable chronological tool for obtaining further insights into the geological evolution and sea level history of the coastal area in Songkhla since the late Pleistocene. However, weathering process led to age overestimation for one sample which was deposited during the last interglacial period. A time dependent dose rate model was successful to correct the overestimated age.

Based on OSL ages, the geological evolutions of Songkhla's coast is now better understood. During the last interglacial (global MIS5e), the sea transgressed Songkhla ca. 3 km from the recent coast line. The very low K concentration in the last interglacial sample confirms the strong weathering process in that period. Humid and dry climates changed during the glacial period (100-17 ka) which was confirmed by aeolian (wind), lacustrine (lake), and fluvial sediments. The OSL age of the fine sedimentary units at the inner plain was helpful to reinterpret it to be lacustrine due to the sea level history. During the Holocene the lagoon and wave-dominated environments

were the prevalent features in this area. This confirms the geophysical model of sea level highstand during the mid-Holocene. However, the precision of paleo sea level altitude determination is still relatively low. To improve that, interdisciplinary studies (e.g. palaeontology, geophysics, and stratigraphy) in the greater study area, combined with further OSL dating would need to be completed.

ACKNOWLEDGEMENT

Authors would like to thank N. Chaimanee (Department of Mineral Resources, Thailand) for the supporting information, M. Fischer (University of Bayreuth) for assistance in the laboratory, and the Department of Groundwater Resource, Region 12 (Thailand) for sharing groundwater well data.

REFERENCES

- [1] Rohling E.J., Grant K., Hemleben Ch., Siddall M., Hoogakker B.A.A., Bolshaw M. and Kucera M., *Nat. Geosci.*, 2008; **1**: 38-42. DOI 10.1038/ngeo.2007.28.
- [2] Aharon P. and Chappell J., *Palaeogeogr. Palaeoc.*, 1986; **56**: 337-379. DOI 10.1016/0031-0182(86)90101-X.
- [3] Bloom A.L., Broecker W.S., Chappell J.M.A., Matthews R.K. and Mesolella K.J., *Quaternary Res.*, 1974; **4**: 185-205. DOI 10.1016/0033-5894(74)90007-6.
- [4] Kershaw A.P., Penny D., van der Kaars S., Anshari G. and Thamotherampili A., *Vegetation and Climate in Lowland Southeast Asia at the Last Glacial Maximum*; in Metcalfe I., Smith J.M.B., Morwood M. and Davidson I., eds., *Faunal and floral migrations and evolution in SE Asia-Australasia*, Balkema, Lisse, 2001: 227-236.

- [5] Voris H.K., *J. Biogeogr.*, 2000; **27**: 1153-1167. DOI 10.1046/j.1365-2699.2000.00489.x.
- [6] Horton B.P., Gibbard P.L., Mine G.M., Morley R.J., Purintavaragul C. and Stargardt J.M., *Holocene*, 2005; **15**: 1199-1213. DOI 10.1191/0959683605hl891rp.
- [7] Sinsakul S., *J. South. Asian Earth*, 1992; **7**: 23-37. DOI 10.1016/0743-9547(92)90012-Z.
- [8] Trisirisatayawong I., Naeije M., Simons W. and Fenoglio-Marc L., *Glob. Planet. Change*, 2011; **76**: 137-151. DOI 10.1016/j.gloplacha.2010.12.010.
- [9] Chaimanee N. and Tiya Pirach S., *Quaternary geology of Songkhla. Geological survey report No.008*, Geological Survey of Thailand, Bangkok, 1983.
- [10] Walker M., *Quaternary dating methods*, John Wiley & Sons, West Sussex, 2005.
- [11] Preusser F., Spencer J.Q.G., Degering D., Fuchs M., Hilgers A., Kadereit A., Klasen N., Krbetschek M. and Richter D., *E&G Quaternary Science Journal*, 2008; **57**: 95-149. DOI 10.3285/eg.57.1-2.5.
- [12] Aitken M.J., *An Introduction to Optical Dating. The Dating of Quaternary Sediments by the Use of Photon-Stimulated Luminescence*. Oxford University Press, Oxford, 1998.
- [13] Wintle A.G., *Radiat. Meas.*, 1997; **27**: 769-817. DOI 10.1016/S1350-4487(97)00220-5.
- [14] Wintle A.G. and Adamec G., *Radiat. Meas.*, 2017; **98**: 10-33. DOI 10.1016/j.radmeas.2017.02.003.
- [15] Kanplumit T., Sangkarat P., Koonpoon R. and Muenjorn S., *Local GPS Control Point Online Network at Changwat Songkhla*. Rajamangala University of Technology Srivijaya, Songkhla, 2015.
- [16] Aitken M.J., *Thermoluminescence Dating*. Academic Press, Orlando, Florida, 1985.
- [17] Duller G.A.T., *Ancient TL*, 2015; **33**: 35-42.
- [18] Galbraith R.F., Roberts R.G., Laslett G.M., Yoshida H. and Olley J.M., *Archaeometry*, 1999; **41**: 339-364. DOI 10.1111/j.1475-4754.1999.tb00987.x.
- [19] Kreuzer S., Schmidt C., Fuchs M.C., Dietze M., Fischer M. and Fuchs M., *Ancient TL*, 2012; **30**: 1-8.
- [20] Burow C., calc_CentralDose(): Apply the central age model (CAM) after Galbraith et al. (1999) to a given De distribution. Function version 1.3.2; in Kreuzer S., Dietze M., Burow C., Fuchs M.C., Schmidt C., Fischer M. and Friedrich J., *Luminescence: Comprehensive Luminescence Dating Data Analysis. R package version 0.7.5*. <https://CRAN.R-project.org/package=Luminescence>, 2017: 62-64.
- [21] R Development Core Team, R: *A Language and Environment for Statistical Computing*. R Foundation for Statistical Computing, Vienna, 2017.
- [22] Cunningham A.C. and Wallinga J., *Quat. Geochronol.*, 2012; **12**: 98-106. DOI 10.1016/j.quageo.2012.05.007.
- [23] Kulig G., *Erstellung einer Auswertesoftware zur Altersbestimmung mittels Lumineszenzverfahren unter spezieller Berücksichtigung des Einflusses radioaktiver Ungleichgewichte in der 238U-Zerfallsreihe*, B.Sc. Thesis, TU Bergakademie Freiberg, Germany, 2005.
- [24] Wilford J., *Geoderma*, 2012; **183-184**: 124-142. DOI 10.1016/j.geoderma.2010.12.022.
- [25] Verstappen H., *GeoJournal*, 1980; **4**: 45-54. DOI 10.1007/BF00586754.

- [26] Boonya M., *Analysis and interpretation of rock weathering index using airborne radiometric data in Songkha Province*, M.Sc. Thesis, Prince of Songkla University, Thailand, 2015.
- [27] Wurster C.M., Bird M.L., Bull I.D., Creed F., Bryant C., Dungait J.A.D. and Paz V., *PNAS*, 2010; **107**: 15508-15511. DOI 10.1073/pnas.1005507107.
- [28] Dheeradilok P. and Kaewyana W., *Geol. Soc. Malaysia Bulletin*, 1986; **19**: 515-532.
- [29] Hesp P., *Geomorphology*, 2002; **48**: 245-268. DOI 10.1016/S0169-555X(02)00184-8.
- [30] Nimnate P., Chutakositkanona V., Choowong M., Pailoplee S. and Phantuwongraja S., *ScienceAsia*, 2015; **41**: 55-63. DOI 10.2306/scienceasia1513-1874.2015.41.055.

3 Study II

**Geological evolution and optically stimulated luminescence (OSL) dating of the coastal dunes
at Trassenheide, Usedom Island, NE Germany**

Prakrit Noppradit^{1*}, Ludwig Zöller¹, Christoph Schmidt¹, Sebastian Lorenz², Henrik Rother³

¹ Lehrstuhl für Geomorphologie, Universität Bayreuth, Universitätsstr. 30, 95440 Bayreuth,
Germany

² LB Physische Geographie, Institut für Geographie und Geologie, F.-L.-Jahn-Str. 16, 17487
Greifswald, Germany

³ Landesamt für Geologie & Bergwesen Sachsen-Anhalt, Köthener Str. 38, 06118 Halle (Saale),
Germany

Corresponding author: prakrit.noppradit@uni-bayreuth.de

Submitted to

E&G Quaternary Science

-Under review-

3.1 Abstract

Late Quaternary sand dunes of Usedom Island in the southern Baltic Sea (NE Germany) were mainly studied on the south-eastern part at the Swina barrier. However, information of sand dune evolution in the north-western portion of Usedom is still scarce. This study tries to fill this gap by applying optically stimulated luminescence (OSL) dating on the so-called Yellow Dune generation, which was classified based on the colour of the subsoil, near Trassenheide (NE Usedom) using the single aliquot regeneration (SAR) technique of coarse-grain quartz. The resulting OSL ages between 0.6 and 2.5 ka allow constraining the evolution of the dune generation to the sea-level transgression during the Roman Warm Period. At this time, dunes progressed seaward. Furthermore, our new OSL data evidences (re)activation of the dune generation at the end of the Medieval Warm Period. The classification based on pedological processes of (former) Yellow Dunes in Trassenheide has been changed to be Brown Dunes, which is supported by the dark yellowish brown colour of the illuvial horizon. Finally, our results are compared to previous findings on the evolution of sand dunes on the Swina spit. Our OSL ages agree with those of the oldest generation of shoreline-parallel dunes (Brown Dune II) in Swina.

Keyword OSL dating, coastal evolution, coastal dune, Usedom

3.2 Introduction

Sand dunes are common geomorphological elements in coastal environments all over the world. Many previous studies have focused on explaining their evolution providing critical information that is necessary in the context of future coastal zone management (for example in urban planning, efficiency in using of resources), especially along the Baltic Sea coast which features people habitats, intense tourism and which hosts a diverse and fragile ecosystem. Reconstructing coastal evolution is typically based on geological evidence derived from field observations and sedimentary or paleontological laboratory analyses, but receives critical support from chronometric information obtained by numeric dating methods (e.g. Hoffmann et al., 2005, Bird, 2008, Reimann et al., 2010, 2011). In this respect, various dating techniques such as radiocarbon (C-14), lead-210, luminescence,

etc. can be applied, dependent on sediment composition and the required dating range (Magee et al., 2009).

Optically stimulated luminescence (OSL) dating is a technique that covers the entire age range from the Holocene to the Late Pleistocene (timescales of 10^2 – 10^5 years), and which is widely applied to ubiquitous natural minerals such as quartz and feldspar (e.g. Aitken, 1998, Schmidt and Zöller, 2016). An OSL age reflects the time that has elapsed since the dated sediment was last exposed to sunlight (usually during transport before burial). Thus, OSL represents the preferred dating technique when aiming to understand landscape dynamics through time, while it is particularly well suited for geochronological landform investigations on sandy coasts which are enriched in quartz due to the high mineral resistance to mechanical and chemical weathering.

Using a comparison of historical and recent maps and analyses of previous radiocarbon dates and historical data, Schumacher (2002) and Schwarzer et al. (2003) showed that the coastline of Usedom Island has changed rapidly over centennial and millennial timescales. The major body of literature on the late Quaternary evolution of Usedom Island focused on the eastern Usedom spit in Swina, central Usedom (Prusinkiewicz and Noryskiewicz, 1966, Osadczuk, 2002, Reimann et al., 2011) (cf. section study area). The classification of dunes in Usedom was based on the degree of podsolization (on illuviation, Keilhack, 1912, 1914) as a relative dating method for dune formation. Since soil formation is an ongoing process (considering the timeframe of this study), it cannot lead to discrete classes of dune generations. However, so far there is no chronostratigraphic information available for the coastal sand dunes in the northern part of Usedom. In this study, OSL dating was applied to the parallel dunes in Trassenheide, which were interpreted as Yellow Dunes, with the aim of providing insights into the Holocene periods of dune formation, stability phases and mobilization. Our results will be compared to the previous findings for other dunes in adjacent areas.

3.3 Study area

Trassenheide is located on the Baltic Sea side of the Peenemünde lowland in northeastern Usedom Island, Pomerania, Germany. On Usedom, the base of the Quaternary sediments at approximately - 75 m NN is formed by Cretaceous deposits, overlain by Pleistocene glaciofluvial and glaciolacustrine meltwater and till deposits (Persson, 1999, Hoffmann, 2002). The Pleistocene sequence is in turn partially overlain by Holocene sediments primarily including marine and aeolian sand and peat (Hoffmann, 2002, Hoffmann and Lampe, 2007).

Since the beginning of the Holocene, when the Baltic sea was not yet connected to the ocean, the sea level first rose until ~10.5 ka, followed by a period of stabilization between ~10.5–9.5 ka, before it continued to rise rapidly from around -25 m to the present-day level (Lampe, 2005, Uścińowicz, 2006). For the periods starting with the mid-Holocene Littorina transgression into the Baltic Sea Basin, Lampe (2005) presents detailed sea level reconstructions based on peat sequences with overlying marine sequences that developed along the German Baltic Sea coast in response to the Littorina transgression. During the post-Littorina time since approximately 4 ka, the sea level in the Baltic Sea developed slower and included at least three phases of regression at 2.8, 1.5, and in the Little Ice age at 0.5 ka cal BP approximately (Lampe, 2005).

Hoffmann et al. (2005) described the postglacial marine evolution of the Peenemünde lowlands, based on which early Holocene fluvial to lacustrine sands were deposited over glacial sediments. In the Atlantic period, marked by the onset of the Littorina transgression, the sea levels rose and marine sediments, derived from coastal erosion of Pleistocene sediments, were deposited. Following the formation of spit areas with surface above sea level, the development of sand dunes commenced along the Baltic sea coast which continues until the present time. There are three generations of sand dunes in the Peenemünde lowland. The Brown Dune generation formed partly perpendicular (NE-SW) to the coast, while the Yellow and White Dunes developed parallel (NW-SE) to the present coastline (Kliewe, 1960). The overall geological setting is presented in Figure 1. The ground penetrating radar (GPR) investigation by Hoffmann (2004; see Figure 3.1 for the location) showed that the contact between dunes and marine sands is approximately 2 m below present sea level. The only chronological information is a radiocarbon date of peat in the marine sequence yielding an uncalibrated age of $5,965 \pm 60$ years BP (Hoffmann, 2004).

Information on the postglacial sand dune evolution of Usedom island has mainly been derived from data obtained from the Swina barrier in the central part of Usedom at the Polish coast (~30 km SE of the study area). Three generations of transgressive dunes were differentiated based on the predominant sand colours resulting from varying degrees of podsolization (Keilhack, 1912, 1914). The formation of the first dune generation, the Brown Dunes (strong illuviation), commenced soon after the initial phase of the Littorina transgression was completed (Osadczuk, 2002). Radiocarbon dating from Prusinkiewicz and Noryskiewicz (1966) and OSL dating from Reimann et al. (2011) showed that the Brown Dunes evolved over the period from 6.6–2.5 and 1.7–1.3 ka. The first generation of Brown Dunes (Brown Dune I) is characterized by ridges perpendicular to the present coastline, whereas the second phase of Brown Dunes (Brown Dune II) development yielded dunes

that are oriented parallel to the present coastline. While these latter Brown Dunes (II) formed, the sea level continued to gradually rise, leading to continued coastal erosion and high sediment supply to the spit areas in the SE from longshore transport (Reimann et al., 2011). The second dune generation, locally referred to as Yellow Dunes (initial illuviation), formed ridges parallel to the Baltic Sea coast. Osadczuk (2002) suggested that the process started when the sea level had stabilized after the end of the initial transgression phase. Reimann et al. (2011) applied OSL dating to six samples of Yellow Dunes and constrained the period of formation to ~1.2–0.6 ka in the Swina barrier. The third generation of the dunes on Usedom, referred to as White Dunes (no illuviation) are also orientated parallel to the coast line. Osadczuk (2002), Reimann et al. (2011) and Hoffmann et al. (2002) suggested that it formed from ~0.49 ka until the present, based on OSL and ^{14}C ages.

3.4 Methodology

Prior to the field work, the coastal sand dunes of Usedom were studied using geological maps (Figure 1b), and a 30-m resolution digital elevation model (DEM, Figure 1c), which formed the basis for the selection of our sampling locations. The area of the Yellow Dunes was delineated based on mapping by Hoffmann and Lampe (2007). Then three drill-cores of 3 m length each (TRA I, II, III) were taken using a 20 kg motor-driven percussion coring system (model Atlas Copco Cobra TT), which provided 1-m long black plastic core tubes with a diameter of 6 cm from dunes near Trassenheide. The site selection covered the three classified dunes (after Keilhack 1914): The White Dune (TRA III), the Yellow Dune (TRA II and TRA III) and the Brown Dune near TRA I but not sampled for this study. All coring locations are shown in Figure 3.1 with coordinates given in Table 3.1. The cores were opened under dimmed red-light conditions at the University of Bayreuth in order to collect three to four OSL samples per core. The exact depths of sampling are provided in Table 3.1 and lithological descriptions of each core are given further below. Sediment colours were classified based on the Munsell soil colour chart.

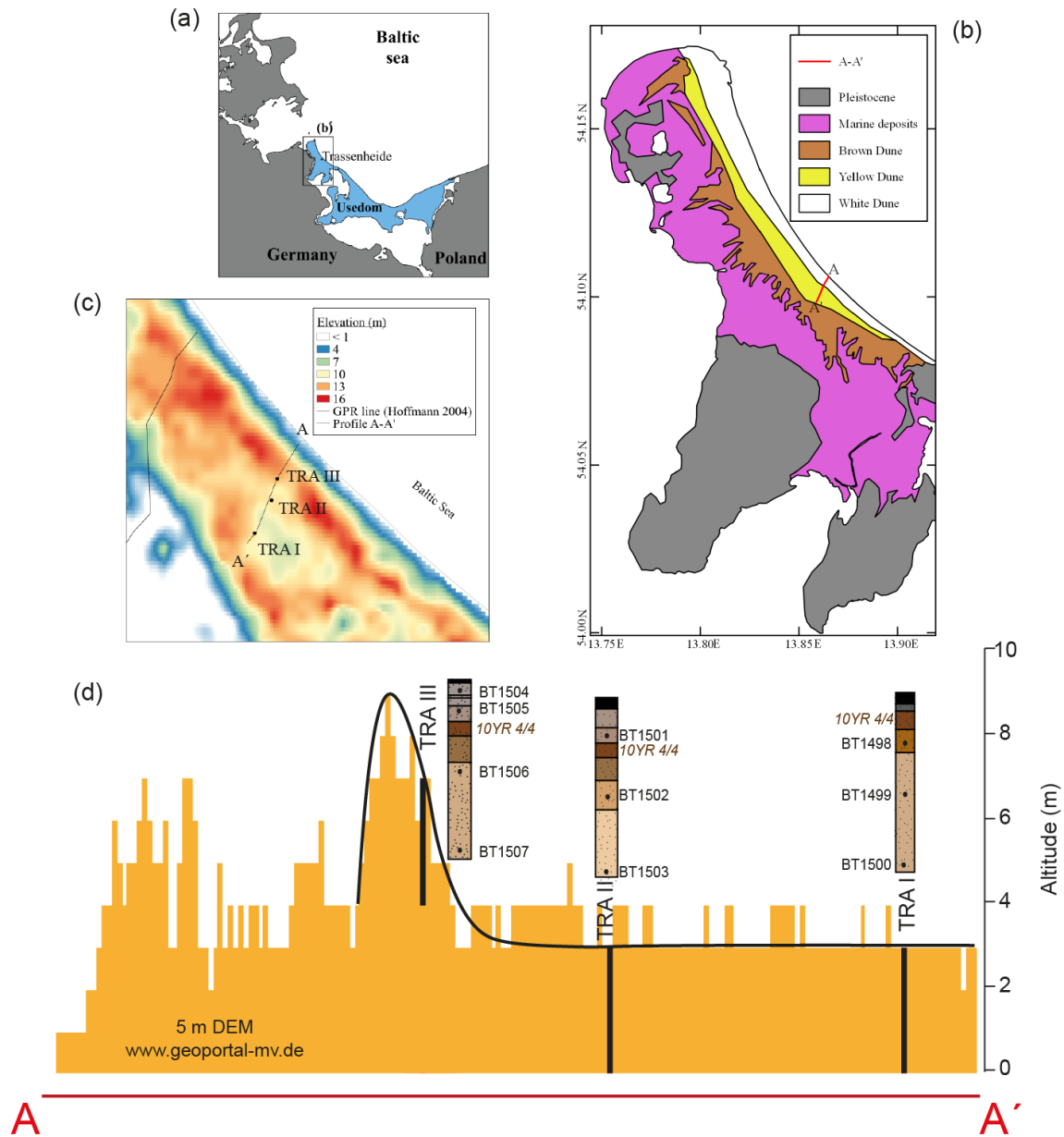


Figure 3.1 Study location: (a) overview map of the German-Polish coast in the southern Baltic Sea, where the blue colour shows the location of Usedom Island, (b) geomorphological map of northern Usedom (redrawn from Hoffmann and Lampe 2007), (c) 30 m digital elevation model (DEM) of Trassenheide and the nearby area, (d) topographic cross-section A-A' derived from the 5-m resolution DEM (www.geoportal-mv.de) as provided in the geomorphological map (b). Location of sediment coring sites (distance from coastline: 850 m for TRA I, 550 m for TRA II, and 350 m for TRA III). Moreover, the lithology of each core (brown italic text shows colours of illuvial horizon) and OSL laboratory numbers are presented.

The material obtained from the cores was separated into two parts, one (approximately 10 cm length from core) for equivalent dose (D_e) measurement, and the other (a few centimeters above and below the dose sample) for dose rate determination. For D_e measurement, samples were prepared by wet sieving (90–200 μm) and subsequent removal of carbonate (10% HCl) and organic matter (10% H_2O_2), and density separation (sodium polytungstate), as well as mineral surface etching (40% HF for 40 min), based on the standard laboratory protocol for the quartz inclusion technique as presented by Aitken (1985). OSL signals were measured using a Risø TL/OSL DA-15 reader with an in-built $^{90}\text{Sr}/^{90}\text{Y}$ β -source delivering $0.0336 \pm 0.0024 \text{ Gy s}^{-1}$ to quartz coarse grains on aluminum cups. The quartz samples were stimulated with blue LEDs ($470 \pm 5 \text{ nm}$; $\sim 36 \text{ mW cm}^{-2}$), and luminescence signals detected in the near UV range (Hoya U-340 glass filter, 7.5 mm) with an EMI 9235QB15 photomultiplier tube. The D_e of each sample was measured using the single-aliquot regenerative (SAR) dose protocol of coarse grain quartz (Murray and Wintle, 2000). Signals were integrated from 0–0.2 s (fast component dominated OSL), while background signals were averaged from the integral 0.2–1.7 s (slow and medium component dominated OSL) of the OSL decay curve based on the early background subtraction approach (Cunningham and Wallinga, 2010). Dose response curves were fitted using a single saturating exponential equation to calculate D_e values. Aliquots with a recycling ratio outside the range 0.9–1.1 and with test dose error exceeding 10% were rejected. In order to find appropriate preheating conditions for most accurate dose estimates, both preheat plateau (PHP) tests and dose recovery (DR) tests were carried out through varying the preheat temperatures in the range 200–280 $^{\circ}\text{C}$ (PHP test) and 180–260 $^{\circ}\text{C}$ (DR test). For the DR test, a recovery dose in the range of the expected D_e was used (2.01 Gy for BT 1499 and 1.34 Gy for BT1506).

Results from DR tests for samples BT1499 and BT1506 are presented in Figure 3.2. Recovery ratios ($D_e/\text{applied dose}$) for both samples were all between 0.95 and 1.05, indicating that a known β -dose can be accurately recovered within 5% with the chosen protocol and preheat temperatures. However, the dose recovery ratio of BT1499 did not fall in the range 0.9 – 1.1 (considering 1- σ uncertainty) for preheat temperatures of 180 $^{\circ}\text{C}$ and 240 $^{\circ}\text{C}$. Moreover, at BT1506 at 200 $^{\circ}\text{C}$ and 260 $^{\circ}\text{C}$, the errors of $D_e/\text{applied dose}$ were large. Based on these tests, a preheat temperature of 220 $^{\circ}\text{C}$ was henceforth adopted for the D_e measurements of all samples. The D_e values of individual aliquots were determined with the Analyst software (v.4.31.7; Duller, 2015). Since our samples derive from sand dunes, the OSL signals are assumed to have been completely bleached prior to burial. The final burial doses were then calculated using the arithmetic mean value along with the standard deviation (Guérin et al., 2017).

Table 3.1 Sampling locations and OSL dating results.

Sample ID	Core ID	Depth (m)	Altitude (m)	Latitude (°N)	Longitude (°E)	Water content (%)	Thorium (ppm)	Uranium (ppm)	Potassium* (%)	Dose rate (Gy/ka)	# of aliquots (<i>n/N</i>)**	D_e (Gy)	Age (ka)
BT1498	TRA I	0.8	10	54.0992	13.8595	1.9	1.10 ± 0.18	0.47 ± 0.05	0.546	0.896 ± 0.023	24/25	2.04 ± 0.27	2.28 ± 0.31
BT1499	TRA I	1.6	10	54.0992	13.8595	14.3	1.39 ± 0.20	0.52 ± 0.06	0.500	0.780 ± 0.030	26/27	1.93 ± 0.20	2.48 ± 0.27
BT1500	TRA I	2.8	10	54.0992	13.8595	16.4	1.00 ± 0.17	0.64 ± 0.05	0.871	1.048 ± 0.038	24/25	2.14 ± 0.27	2.04 ± 0.27
BT1501	TRA II	0.6	11	54.1015	13.8616	0.7	0.75 ± 0.01	0.40 ± 0.01	0.549	0.877 ± 0.021	24/25	1.68 ± 0.11	1.92 ± 0.13
BT1502	TRA II	1.55	11	54.1015	13.8616	2.3	0.77 ± 0.15	0.54 ± 0.05	0.460	0.790 ± 0.022	23/25	1.37 ± 0.13	1.73 ± 0.17
BT1503	TRA II	2.85	11	54.1015	13.8616	16.7	2.82 ± 0.29	0.58 ± 0.09	0.469	0.817 ± 0.030	25/25	1.33 ± 0.16	1.63 ± 0.21
BT1504	TRA III	0.25	12	54.1031	13.8623	3.7	1.49 ± 0.21	0.60 ± 0.06	0.540	0.965 ± 0.025	17/29	0.56 ± 0.04	0.58 ± 0.05
BT1505	TRA III	0.5	12	54.1031	13.8623	0.6	1.16 ± 0.18	0.41 ± 0.06	0.447	0.816 ± 0.025	25/25	1.41 ± 0.15	1.73 ± 0.24
BT1506	TRA III	1.5	12	54.1031	13.8623	2.0	1.26 ± 0.19	0.47 ± 0.06	0.411	0.764 ± 0.023	31/32	1.32 ± 0.19	1.73 ± 0.25
BT1507	TRA III	2.85	12	54.1031	13.8623	14.4	1.59 ± 0.01	0.48 ± 0.02	0.382	0.668 ± 0.023	26/27	1.27 ± 0.17	1.90 ± 0.26

* Overall uncertainty of K content is 10% according to the laboratory

** *n* = number of accepted aliquots, *N* = number of measured aliquots

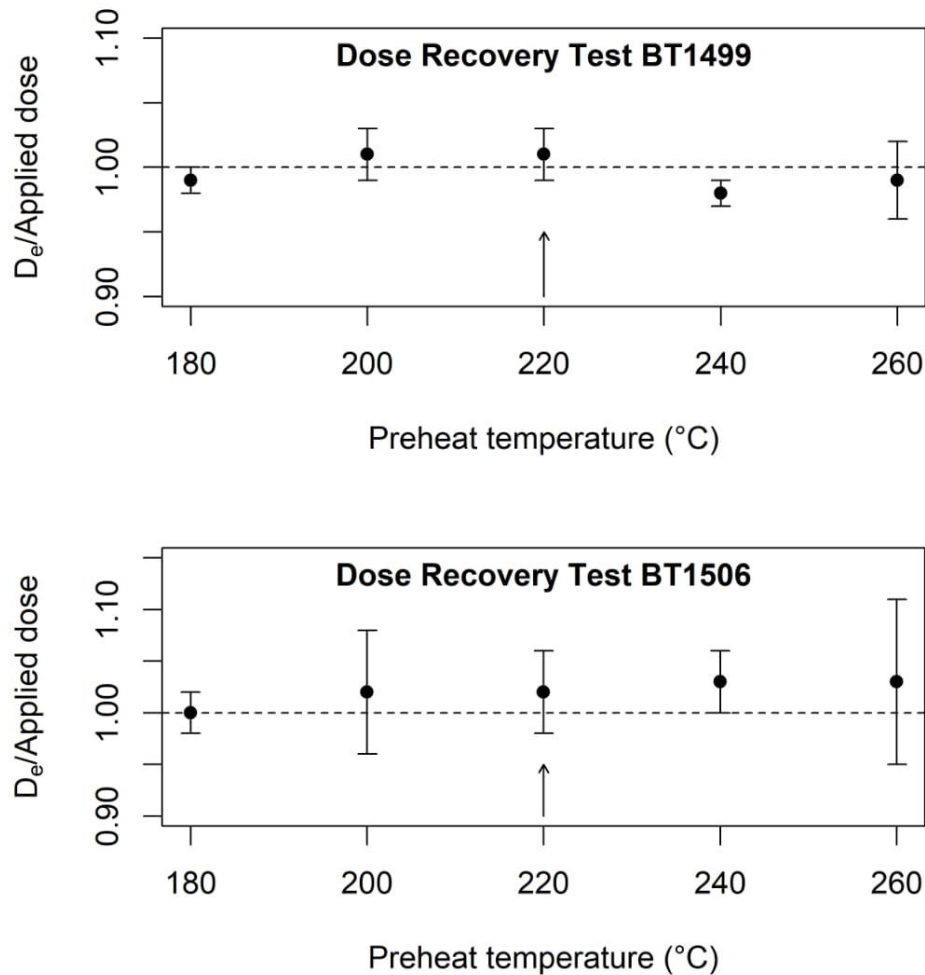


Figure 3.2 Results of dose recovery tests of samples BT1499 (top) and BT1506 (below). Three aliquots were measured at each preheat temperature setting, the results were then averaged. Error bars represent 1σ standard error.

For environmental dose rate determination, Thick-Source Alpha-Counting (TSAC) was carried out for measuring uranium and thorium contents (Aitken, 1985, Soumana, 1997), and Inductively-Coupled Plasma Optical Emission Spectrometry (ICP-OES) for measuring the potassium content. Total dose rates and ages were determined using the ADELE software (v2015 0.21a beta; Kulig, 2005) using information of geographical location, concentration of radioactive elements, present water content, and D_e .

3.5 Results

The colour of subsoil sediments, based on the Munsell soil colour chart, appeared dominantly brownish to pale brownish in colour in every core, with moderately well sorted to well sorted fine to medium sand except for the first 0.6 m of TRA III, which appeared greyish in colour. TRA III showed two organic rich units (soil layers) at the surface and at a depth of 33-46 cm, while the illuvial horizon was around 64-100 cm below surface. The illuvial horizon of all cores was dark yellowish brown (10YR 4/4). For TRA I and TRA II, the illuvial horizons were located at 30-65 cm and 75-78 cm from surface, respectively. Ten OSL samples were collected from these cores. Location and lithology are shown in Table 3.1 and Figure 3.1d).

At least 25 aliquots of each sample were measured to estimate the burial dose. An exemplary OSL decay curve of sample BT1501 is presented in Figure 3.3a indicating that the initial OSL signal is a fast component dominated OSL that falls to background level within a few seconds stimulation time (power density of $\sim 36 \text{ mW cm}^{-2}$). The average D_e values vary between 0.56 and 2.14 Gy. The range of dose rates between 0.668 and 1.048 Gy/ka is typical for coastal dunes. The calculated relative age errors are between 7 and 15%. An example of the D_e distribution of sample BT1501 is shown in Figure 3.3b. All relevant data for age calculation are compiled in Table 3.1.

Within 1σ uncertainty range, all ages of core TRA I (850 m from the present coast line) are statistically indistinguishable, giving an average OSL site age of $2.3 \pm 0.2 \text{ ka}$ (mean and standard deviation of samples BT1498–BT1500). The same applies to the samples from TRA II (BT1501–BT1503; 550 m from the present coastline) taken from depths $>0.5 \text{ m}$, resulting in an average OSL site age of $1.8 \pm 0.2 \text{ ka}$. For the third core TRA III (375 m from coastline), the topmost sample BT1504 (0.25 m) showed – in accordance with stratigraphy – the youngest age of $\sim 0.59 \pm 0.05 \text{ ka}$, while the remaining samples ($>0.5 \text{ m}$) from this core are again identical in age within uncertainties with an average of $1.8 \pm 0.1 \text{ ka}$.

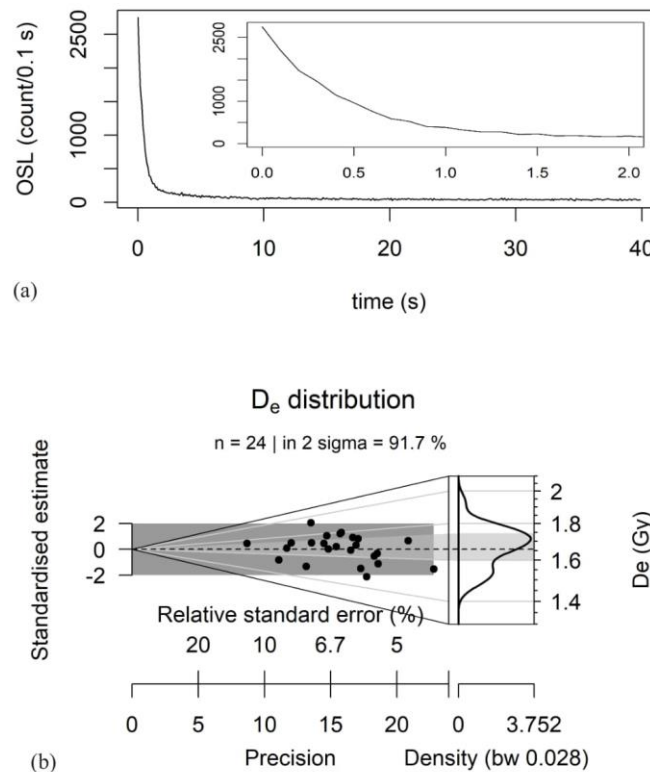


Figure 3.3 The OSL decay curve of sample BT1501 shows that the initial signal is dominated by the fast component (a), and D_e distribution of sample BT1501 presented in the form of an abancico plot (Dietze et al. 2016).

3.5 Discussion

The presented OSL age chronology ($n = 10$) from dune deposits on Usedom Island covers an age range from 2.5–0.6 ka (max. error envelope: 2.8–0.5 ka) consistent with dune deposition during the Subatlanticum stage of the late Holocene period. All ages from cores TRA I, II and III taken below 50 cm depth overlap within error, suggest a fast vertical development of the dunes. At around 2.3 ka ago the beach nearby TRA I was prograding northeastwards indicating positive coastal sediment budget. The first dune (at TRA I) began to develop at approximately 850 m from the present coast line. This dune was continuously progressing seaward until 1.8 ka. A further phase of dune formation started at around 1.8 ka as indicated by OSL ages below 0.5 m of 1.8 ± 0.2 ka (TRA II) and 1.8 ± 0.1 ka (TRA III). Interestingly, the TRA II and III sites yield identical ages within error bars although they appear to represent separate dune landforms located at a distance of 550 m (TRA II) and 350 m (TRA III) from the present coastline, respectively. This may suggest the dune evolution at TRA II and TRA III were formed in the same period. Figure 3.4 indicates the possible dune's surface during

1.9 and 1.7 ka. The wind blew sand via the ridge of the dune (at TRA III) and deposited it at the TRA III's lee and the flat area at TRA II. This information leads to a progression rate between 2.3 and 1.8 ka of at least 95 cm/year. However, there is another possibility that a contemporaneous formation of both dune systems took place, similar to the mechanism, which can be observed in parallel foredunes (Bird, 2008). In this scenario of the formation of swales separating parallel foredunes, the wind flows over a foredune, and splits into two branches, allowing deflating between dunes. One branch transports sand to the lee of the primary dune, while the other branch simultaneously delivers sand to accumulate at the stoss side of the next (secondary) foredune. Other models may be discussed here as well, which is, however, beyond the scope of this contribution.

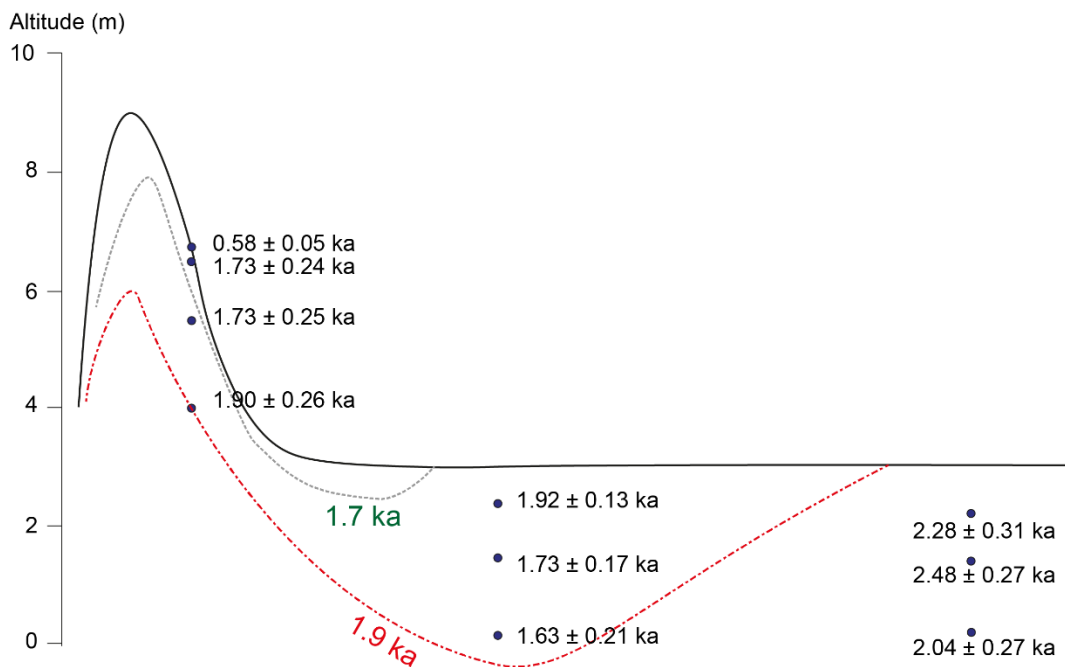


Figure 3.4 OSL ages and evolution model of the (classified) Yellow Dunes in Trassenheide (vertical axis = elevation in m above recent sea level, horizontal axis = distance in m from recent coastline, according to Figure 3.1). TRA I developed around 2.3 ka, then around 1.8 ka the dunes from which cores TRA II and TRA III were taken were generated contemporaneously. The red and grey dash indicates the possible dune surface at 1.9 and 1.7 ka, respectively. For lithological information please see Figure 3.1.

Such a model of concurrent sand accumulation at two adjacent dunes would explain the observed match of depositional ages of samples BT1501–1503 (TRA II) and BT1505–1507 (TRA III). During the period from 1.73 to 0.58 ka ago, the studied part of the dune system shows a break in sedimentation or an erosional hiatus, indicating a phase of coastal equilibrium or possibly limited coastal retreat with a balanced or slightly negative sediment budget (Hesp, 2002). When there was no sand input,

the organic layer was formed (ca. 33-46 cm in TRA III). At around 0.58 ka ago (sample BT1504, TRA III), it appears that there was a minor activation of the dune system. The present-day soil colour is grey-white. This activation is in agreement with and is related to the White Dune generation (Hoffmann, 2004, Reimann et al., 2011).

The presented OSL chronology suggests that the main phase of dune development at Trassenheide occurred between 2.5 and 1.6 ka during the Roman Warm Period (RWP), with a minor activation at around 0.58 ka at the end of the Medieval Warm Period (MWP) as defined by McDermott et al. (2001). The timing between 2.5 and 1.6 ka might support the hypothesis of the minor transgression phase (Figure 3.5) in the RWP along the Baltic Sea coast presented as “event TL3” in Lampe (2005) which is interpreted from the groundwater level. Under a transgressive coastal setting, waves and currents transported sand to the new coastline, promoting aeolian beach deflation. From a sediment dynamics perspective this leads to a very active coastal zone with little vegetation stabilizing the ground, allowing the wind to entrain and transport large amounts of sand further inland leading to the deposition of the dune belt.

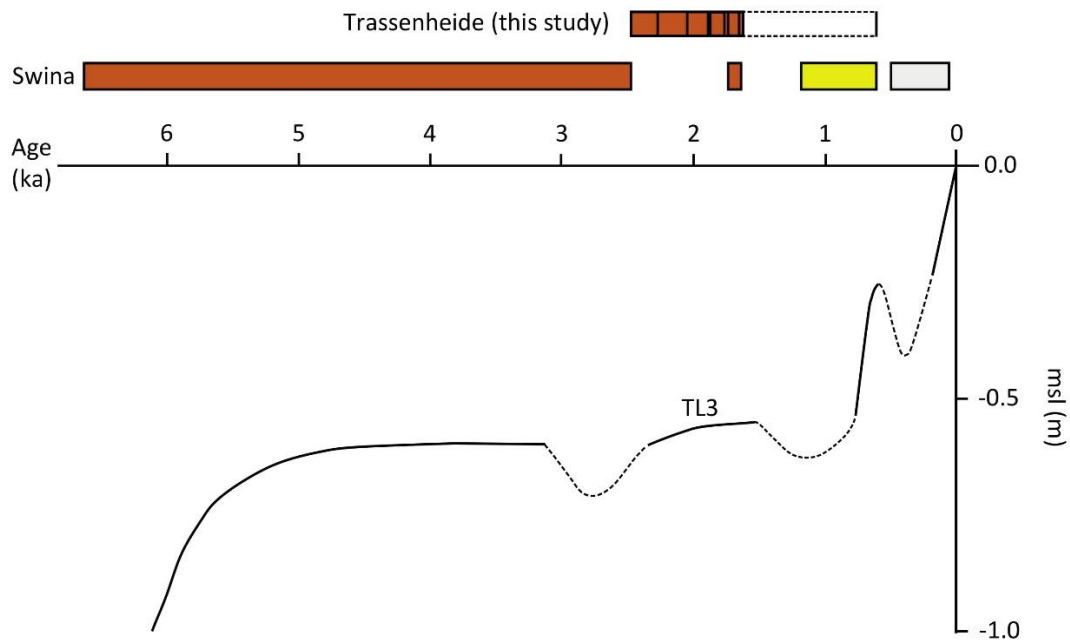


Figure 3.5 OSL dating results from this study (Trassenheide) and Swina with a relationship to Lampe (2005)'s hypothetical sea level curve (bar colour: brown = Brown Dune, yellow = Yellow Dune, white = White Dune; black line = OSL age).

A comparison of our data from Trassenheide with the OSL dune chronology from the Swina barrier (Reimann et al., 2011) indicates that the dunes at Trassenheide were deposited only after the

formation of Brown Dune I (meridional to coastline), coinciding with the timing of Brown Dune II formation (parallel to coastline) during the RWP. In contrast to the Swina barrier there appears to be no Yellow Dune accumulation in Trassenheide. This might be related to the very strong storm surge in the early 1300s (Jensen et al., 2008), which could have eroded some coastal dunes. Yet, we observe that the younger age of dune deposition at TRA III at around 0.58 ka, nominally coincides with the age of the Yellow Dune in Swina. However, this dune system at Trassenheide (previously classified as White Dune generation) lacks the characteristic degree of soil development (illuviation).

Using the Munsell colour chart, subsoil colours of the three cores were determined to range from yellowish brown to pale brown. This might indicate that the classification based on the pedological processes (as estimated by the colour of the subsoil) in 1912 cannot be used anymore for the Yellow Dune. On the TRA III dune, there are two separate organic-rich layers, where the lower organic-rich layer is interpreted as a fossil soil and therefore as an evidence for dune (re)activation. As the terms “Brown Dune” and “Yellow Dune” reflect the maturity of soils developed in these dunes, the observed diachrony between the Yellow Dunes from Swina and Trassenheide might as well be explained by timing of the classification (in 2011 and in 1912). The studied dunes which were classified as Yellow Dune in 1912 could have developed into Brown Dune since then.

3.6 Conclusion

Our study shows that late Holocene sand dunes near Trassenheide on the Island of Usedom are suitable for OSL dating of coarse grain quartz using the SAR protocol. A correlation could be established between the ages of dune formation, the climatic record and minor post-Littorina Baltic Sea level fluctuations. OSL thus proved to be a valuable tool in obtaining insights into the chronostratigraphy and depositional evolution of sand dunes along the Baltic Sea coast.

Based on the presented OSL chronology we find that the dunes in Trassenheide mainly formed during the period 2.5–1.6 ka. Thus, the formation of these dunes falls primarily into the Roman Warm Period, but we also document a (re)activation phase at ca. 0.6 ka in the Medieval Warm Period. Compared to the sand dune development on the nearby Swina peninsula (Reimann et al., 2011), the shore parallel dunes at Trassenheide were deposited at about the same time as the Brown Dunes II generation documented on the Swina barrier. Based on the soil colour results at Trassenheide, the Yellow Dune as classified by Keilhack (1912, 1914) can now be re-classified as Brown Dune.

3.7 Acknowledgement

The authors would like to thank PD Dr. Klaus-Martin Moldenhauer for help during fieldwork and Mr. Manfred Fischer for suggestions regarding the OSL measurements. Moreover, we thank Dr. Tony Reimann, an anonymous reviewer and the editor who provided very useful comments.

3.8 References

- Aitken, M. J.: Thermoluminescence dating, Academic Press, London, 1985.
- Aitken, M. J.: An introduction to optical dating, Oxford University Press, Oxford, 1998.
- Bailey, R. M., and Arnold, L. J.: Statistical modelling of single grain quartz D_e distributions and an assessment of procedures for estimating burial dose, *Quaternary Sci. Rev.*, 25, 2475–2502, doi:10.1016/j.quascirev.2005.09.012, 2006.
- Bird, E. C. F.: Coastal geomorphology: An introduction, John Wiley, Chichester, 2008.
- Cunningham, A. C. and Wallinga J.: Selection of integration time intervals for quartz OSL decay curves, *Quat. Geochronol.*, 5 (6), 657–666, doi:10.1016/j.quageo.2010.08.004, 2010.
- Dietze, M., Kreutzer, S., Burow, C., Fuchs, M., Fischer, M., and Schmidt, C.: The abanico plot: Visualising chronometric data with individual standard errors, *Quat. Geochronol.*, 31, 12–18, doi:10.1016/j.quageo.2015.09.003, 2016.
- Duller, G.: Single-grain optical dating of Quaternary sediments: Why aliquot size matters in luminescence dating, *Boreas*, 37, 589–612, doi:10.1111/j.1502-3885.2008.00051.x, 2008.
- Duller, G.: The Analyst software package for luminescence data: overview and recent improvements, *Ancient TL*, 33, 35–42, 2015.
- Galbraith, R., Roberts, R. G., Laslett, G., Yoshida, H., and Olley, J.: Optical dating of single and multiple grains of quartz from Jin-mium rock shelter, Northern Australia. Part I: Experimental Design and Statistical Models, *Archaeometry*, 41, 339–364, doi:10.1111/j.1475-4754.1999.tb00987.x, 1999.
- Guérin, G., Christophe, C., Philippe, A., Murray, A., Thomsen, K., Tribolo, C., Urbanova, P., Jain, M., Guibert, P., Mercier, N., Kreutzer, S., and Lahaye, C.: Absorbed dose, equivalent dose,

- measured dose rates, and implications for OSL age estimates: Introducing the Average Dose Model, *Quat. Geochronol.*, 41, 163-173, doi:10.1016/j.quageo.2017.04.002, 2017.
- Hesp, P.: Foredunes and blowouts: initiation, geomorphology and dynamics, *Geomorphology*, 48, 245-268, doi:10.1016/S0169-555X(02)00184-8, 2002.
- Hoffmann, G.: The geological evolution of Usedom Island, in: *Holocene Evolution of the South-Western Baltic Coast - Geological, Archaeological and Palaeo-environmental Aspects*, Lampe R. (ed.), Geographisches Institut der Ernst-Moritz-Arndt-Universität Greifswald, Greifswald, 89-94, 2002.
- Hoffmann, G.: *Rekonstruktion und Modellierung der Küstenevolution im Bereich der Pommerschen Bucht in Abhängigkeit von holozänen Meeresspiegelschwankungen*, Ph.D. thesis, Ernst-Moritz-Arndt-Universität Greifswald, Greifswald, 2004.
- Hoffmann, G. and Lampe, R.: Sediment budget calculation to estimate Holocene coastal changes on the southwest Baltic Sea (Germany), *Mar. Geol.*, 243, 143–156, doi:10.1016/j.margeo.2007.04.014, 2007.
- Hoffmann, G., Lampe, R., and Barnasch, J.: Postglacial evolution of coastal barriers along the West Pomeranian coast, NE Germany, *Quatern. Int.*, 133-134, 47–59, doi:10.1016/j.quaint.2004.10.014, 2005.
- Hoffmann, G., Lampe, R., Ziekur, R., and Schuricht, R.: The Peenemünde-Zinnowitz area – the Holocene evolution of a coastal lowland. in: *Holocene Evolution of the South-Western Baltic Coast - Geological, Archaeological and Palaeo-environmental Aspects*, Lampe R. (ed.), Geographisches Institut der Ernst-Moritz-Arndt-Universität Greifswald, Greifswald, 137-144, 2002.
- Jensen, J., and Müller-Navarra, S.H.: Storm Surges on the German Coast. *Die Küste*, 74 ICCE (2008), 92-124, 2008.
- Keilhack, K.: Die Verlandung der Swinepforte, in: *Jahrbuch der Königlich-Preussischen Geologischen Landesanstalt XXXII*, 209-244, 1912.
- Keilhack, K.: *Erläuterungen zu Geologischen Karten von Preussen und benachbarten Bundesstaaten*, Blatt Swinemünde, Berlin, 1914.

- Kliewe, H.: Die Insel Usedom in ihrer spät- und nacheiszeitlichen Formentwicklung, VEB Deutscher Verlag der Wissenschaften, Berlin, 1960.
- Kulig, G.: Erstellung einer Auswertesoftware zur Altersbestimmung mittels Lumineszenzverfahren unter spezieller Berücksichtigung des Einflusses radioaktiver Ungleichgewichte in der ^{238}U -Zerfallsreihe, B.Sc. thesis, Technische Universität Freiberg, Freiberg, 2005.
- Lampe, R.: Lateglacial and Holocene water-level variations along the NE German Baltic Sea coast: Review and new results, *Quatern. Int.*, 133-134, 121–136. doi:10.1016/j.quaint.2004.10.005, 2005.
- Magee, J. W., Miller, G. H., Spooner, N. A., Questiaux, D. G., McCulloch, M. T., and Clark P. A.: Evaluating quaternary dating methods: radiocarbon, U-series, luminescence, and amino acid racemization dates of a late Pleistocene emu egg, *Quat. Geochronol.*, 4, 84–92, doi:10.1016/j.quageo.2008.10.001, 2009.
- McDermott, F., Matthey, D. P., and Hawkesworth, C.: Centennial-scale Holocene climate variability revealed by a high-resolution speleothem delta ^{18}O record from SW Ireland. *Science*, 294, 1328–1331, doi:10.1126/science.1063678, 2001.
- Murray, A. S. and Wintle, A. G.: Luminescence dating of quartz using an improved single-aliquot regenerative-dose protocol, *Radiat. Meas.*, 32, 57–73, doi:10.1016/S1350-4487(99)00253-X, 2000.
- Osadczyk, K.: Evolution of the Świna barrier spit, in: *Holocene Evolution of the South-Western Baltic Coast - Geological, Archaeological and Palaeo-environmental Aspects*, Lampe R. (ed.), Geographisches Institut der Ernst-Moritz-Arndt-Universität Greifswald, Greifswald, 119-126, 2002.
- Persson, K. M.: Lithostratigraphy and paleoenvironmental development recorded in the coastal cliffs of SE Usedom, Germany, *E&G – Quaternary Science Journal*, 49, 71-83, doi:10.3285/eg.49.1.05, 1999.
- Prusinkiewicz, Z. and Noryskiewicz, B.: Zagadnienie wieku bielicy na wydmach brunatnych mierzei swiny w swieterze analisy palynologicznej i datowania radiowęglem ^{14}C , *Geografia*, 14, 75–88, 1966.

- Reimann, T., Naumann, M., Tsukamoto, S., and Frechen, M.: Luminescence dating of coastal sediments from the Baltic Sea coastal barrier-spit Darss–Zingst, NE Germany, *Geomorphology*, 122, 264–273, doi:10.1016/j.geomorph.2010.03.001, 2010.
- Reimann, T., Tsukamoto, S., Harff, J., Osadczuk, K., and Frechen, M.: Reconstruction of Holocene coastal foredune progradation using luminescence dating — An example from the Świna barrier (southern Baltic Sea, NW Poland), *Geomorphology*, 132, 1-16, doi:10.1016/j.geomorph.2011.04.017, 2011.
- Schumacher, W.: Coastal dynamics and coastal protection of the Isle of Usedom, in: *Holocene Evolution of the South-Western Baltic Coast - Geological, Archaeological and Palaeo-environmental Aspects*, Lampe R. (ed.), Geographisches Institut der Ernst-Moritz-Arndt-Universität Greifswald, Greifswald, 131-134, 2002.
- Schmidt, C., and Zöller, L.: Lumineszenzdatierung als Schlüssel zur Vergangenheit. *Chemie in unserer Zeit*, 50, 188-197, doi:10.1002/ciuz.201600703, 2016.
- Schwarzer, K., Diesing, M., Larson, M., Niedermeyer, R.-O., Schumacher, W., and Furmanczyk, K.: Coastline evolution at different time scales - Examples from the southern Baltic Sea (Pomeranian Bight), *Mar. Geol.*, 194, 79–101, 2003.
- Soumana, S., Fain, J., Miallier, D., Montret, M., Pilleyre, T. H., and Sanzelle, S.: Alpha counting using scintillation techniques: Observation on TSAC calibration and gas cell use, *Radiat. Meas.*, 27, 365–372, 1997.
- Strebler, D.: *Use of Minerals other than Quartz and Feldspars for Luminescence Dating*, M.St. thesis, University of Oxford, Oxford, 2013.
- Uścińowicz, S.: A relative sea-level curve for the Polish Southern Baltic Sea. *Quatern. Int.*, 145-146, 86–105. doi:10.1016/j.quaint.2005.07.007, 2006.

4 Study III

Methodological approach for dating harbor sediments by using luminescence dating – a case study in Ephesus, Western Turkey

Prakrit Noprakrit¹, Anika Symanczyk³, Ludwig Zöller¹, Helmut Brückner³, Friederike Stock^{2,3}

¹Institute of Geography, University Bayreuth, Universitätsstr. 30, 95440 Bayreuth, Germany

²Federal Institute of Hydrology, Am Mainzer Tor 1, 56068 Koblenz, Germany

³Institute of Geography, University of Cologne, Albertus-Magnus-Platz, 50923 Cologne, Germany

Published in

Archaeological and Anthropological Sciences

DOI: 10.1007/s12520-018-0739-y

Reprinted by permission from Springer Nature (License Number: 4470100258333)

4.1 Abstract

For this study, a 15-m sediment core from the Roman harbor of Ephesus has been dated with the luminescence technique. ^{14}C age estimates from the same and a neighboring core were used for comparing and validating the luminescence dating results via a single aliquot regenerative dose (SAR) protocol: infrared stimulation of polymineral and blue stimulation of quartz. The results reveal new insights into the deposition of the sediments of the Roman harbor from 2000 BC to AD 1500 approximately. Some samples showed incomplete bleaching. The difference between the polymineral and the quartz techniques described the bleaching condition before burial. When both approaches give consistent ages, complete bleaching can be assumed. Consistent ages were further applied to the Bayesian age-depth model and discussed within the archeological context. Based on the Bayesian age-depth model, a high sedimentation rate of ca. 65 mm/year was calculated for the period of ~ 700–400 BC suggesting a fast advance of the delta front. However, other age estimates suggest a fast advance for the period 200 BC to ca. AD 100. This is probably due to incomplete bleaching of the luminescence samples and the use of bulk samples for ^{14}C for this new study. Comparing the results with nearby cores suggests that dredging was conducted in the southern part of the Roman harbor at a depth of ca. 5 m b.s.l.

Keywords: Luminescence dating, radiocarbon, drill core, geoarchaeology, Western Anatolia, Ephesus

4.2 Introduction

Ancient harbors are often characterized by fine-grained sediments during the time of their intensive use. Marriner and Morhange (2006) denote the fining-upward sequence as the “Ancient Harbour Parasequence.” In the Mediterranean, several Roman-Byzantine harbors such as Alexandria (Bernasconi et al. 2006; Véron et al. 2006), Yenikapı (Algan et al. 2011), Naples (Delile et al. 2016), Marseille (Morhange et al. 2003), Miletus (Brückner et al. 2014), Portus (Mazzini et al. 2011; Salomon et al. 2012), and Troy (Kraft et al. 2003) have been intensively studied by geoarchaeologists in the last decades. The chronostratigraphy of these harbor sequences mostly relies on radiocarbon ages.

Another method for dating sediments is luminescence, a quaternary dating technique which is used for determining the last deposition, i.e., the last time a mineral was exposed to sunlight before being covered by sediments (Huntley et al. 1985). Various luminescence techniques have successfully been applied to date different kinds of sediments, depending on mineral types and sizes (Aitken 1985, 1998). Two major mineral types commonly used are quartz and feldspar. For Holocene samples, quartz is more suitable than feldspar (Preusser et al. 2008), since it is easier to bleach by sunlight (Godfrey-Smith et al. 1988) and no fading phenomena have been observed (Aitken 1985, 1998). However, in some sediments, quartz grains cannot be extracted; polymineral dating, including feldspar, is then carried out (Huntley et al. 1985).

The study area is the Roman harbor of the ancient city of Ephesus which is located at the southern flank of the Küçük Menderes graben at the west coast of Turkey. The city was one of the largest cities in the Eastern Roman Empire and the capital of the province Asia (Knibbe 1998). During the Roman and Byzantine periods, Ephesus had its most prosperous time, among others due to the importance of the harbor (Zabehlicky 1995). However, the delta advance of the Küçük Menderes river and its tributaries has silted up the formerly ca. 20-km-deep embayment during the last seven millennia, starting ca. 7000 years ago (Kraft et al. 2000; Brückner 2005; Stock et al. 2013, 2015; Brückner et al. 2017). The construction of a harbor mole in the second century BC (Strabo 14, 1, 24) and a protected harbor basin as well as a canal around the turn of the eras (Stock et al. 2016) could not stop this siltation (Zabehlicky 1995, 1999; Kraft et al. 2000, 2001; Steskal 2015). Along with the delta progradation, the harbors also had to be shifted following the retreating coastline during the Roman-Byzantine times (Kraft et al. 2000, 2007; Stock et al. 2014).

Ephesus has been the subject of geoarchaeological research since the beginning of the 1990s. Intensive research has been conducted in the environs of the city and the different harbors. Especially Kraft et al. (2000), Delile et al. (2015), Stock et al. (2016), and Schwarzbauer et al. (2018) focused on environmental changes and human impacts during the last three millennia by using the Roman harbor basin and the canal as geo-archives.

Delile et al. (2015) and Stock et al. (2016) published radiocarbon ages of core Eph 276 which show four similar age estimates in the lower 6 m. A deeper core of 15 m length (Eph 395) has been retrieved in the direct vicinity in order to establish a new chronostratigraphy for the harbor basin. For this study, luminescence dating of fine-grained minerals, both polymineral and quartz, was applied to this core. For better comparing and validating the luminescence ages, ^{14}C ages of the same core and of core Eph 276 were used. Then, the Bayesian age-depth model presented by Zeeden et al. (2018) was applied. The results should lead to a better understanding of the harbor evolution and the environmental setting.

4.3 Drill cores from the Roman harbor basin

The Roman harbor of Ephesus is nowadays located ca. 5 km to the east of the present coastline (Figure 4.1). Several drill cores have been retrieved from the harbor basin. Stock et al. (2016) published the sedimentology and geochemistry as well as the microfauna and palynology of core Eph 276 and several other cores in the Roman harbor and the harbor canal. These geobio-archives were also used for studies of major and trace elements as well as lead isotopes (Delile et al. 2015), organic compounds (Schwarzbauer et al. 2018), and intestinal parasites (Ledger et al. 2018).

The harbor sediments may be separated into different units reflecting the harbor use (Stock et al. 2016; Schwarzbauer et al. 2018). The lowermost part represents the pre-harbor use with laminations of grayish brown clayey silts, deposited earlier than 600 BC. On top, follow grayish silts of the open harbor unit. Intercalated layers of fine sand originate from the advancing Küçük Menderes delta. A sudden change occurs ca. 200 BC. Along with the construction of the protected harbor basin, grayish brown and pale yellow silts were deposited. A strong human impact can be detected in this layer. It is characterized by elevated lead and copper values, abundant pollen from fruit trees and eggs of intestinal parasites (Delile et al. 2015; Stock et al. 2016; Ledger et al. 2018). Moreover, organic compounds related to anthropogenic activities are present in this layer (Schwarzbauer et al. 2018). With the continuous advance of the delta, the post-harbor phase (from 1500 BC onwards) can be traced in the sediment by a decrease of the anthropogenic indicators and the change in microfossil assemblages. The harbor lost its connection to the sea, and a closed lagoon-like lake evolved, which later turned to freshwater. The uppermost part of all drill cores is dominated by peat which has been growing during the last ca. 800 years (Stock et al. 2016).

4.4 Methodology

With a vibracorer Cobra pro (Atlas Copco), the sediment core Eph 395 of 15 m length and of 6 cm diameter was retrieved from the southern part of the Roman harbor. Elevation above present mean sea level (m.s.l.) were leveled with a Topcon HiPer pro GPS (precision: 2 cm in all dimensions). In the laboratory, the cores were opened and 49 samples (every 20–30 cm) were taken for analyses of grain size and loss on ignition (LOI) (see Stock et al. 2016 for details).

For grain size analysis, the samples were dried and pestled and the organic content removed using hydrogen peroxide. Grain size <2 mm were measured with a laser diffraction particle sizer (Beckmann Coulter LS13320 Mikro). The parameters are based on Folk and Ward (1957); results were processed using the GRADISTAT software (Blott and Pye 2001). Loss on ignition (LOI) was measured in a muffle furnace (c. 5 g of sediment heated for 12 h at 105 °C, and 4 h at 550 °C),

For the chronostratigraphy, four bulk samples from Eph 395 were radiocarbon dated (see Table 4.1). Moreover, seven samples from the different phases of the harbor's life cycle (pre-, open, protected, and post-harbor phases) were dated with the luminescence technique. For equivalent dose (De)-determination, the samples were prepared in a dark laboratory with dimmed red light. Four- to eleven-micrometer grain size was prepared by using an Atterberg cylinder. The treatment with HCl and H₂O₂ was carried out to remove carbonates and organic materials. After these steps, polymineral fine grains were measured. If enough sample material remained after polymineral measurements, it was further prepared for the fine grain quartz technique via etching by H₂SiF₆ for 1 week to remove feldspar.

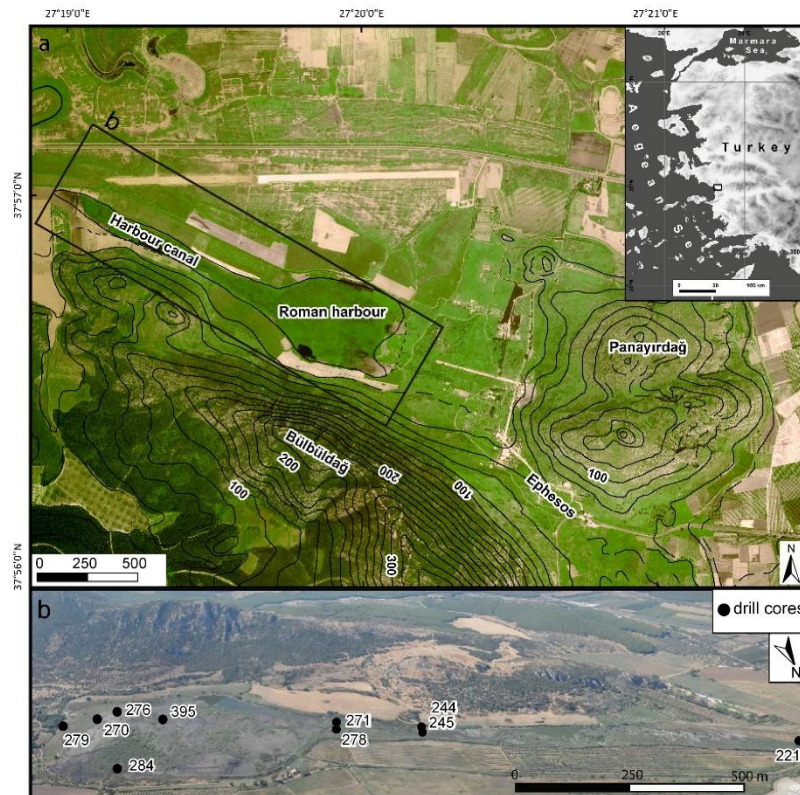


Figure 4.1 Location of the drill cores in the Roman harbor basin and the canal. Eph 395 is located in the southern part of the basin (Stock et al. 2016, modified)

Single aliquot regeneration protocol (SAR: Murray and Wintle 2000) was carried out through Risø TL/OSL reader DA15 with an in-built $^{90}\text{Sr}/^{90}\text{Y}$ β -source. Polymineral fine grain measurement was adapted from Banerjee et al. (2001) with $\sim 121 \text{ mW cm}^{-2}$ infrared (IR, 870 nm) LED and detection through interference filter (blue-violet band). The stimulation by IR directly had an effect on feldspar, but no one on quartz. For quartz fine grain, the method was adapted from Murray and Wintle (2000), stimulating with 470 nm blue LED ($\sim 36 \text{ mW cm}^{-2}$) and detection through U340 filter (ultraviolet band). The preheating temperature, required in SAR, was tested by the dose-recovery test (DRT). The DRT results of 240 °C for quartz and 220 °C for polymineral were adopted to the preheat step of SAR.

The measured luminescence signals were determined Des via Analyst 4.31.7 (Duller 2015) and fitted by an exponential function. The dose-response curve was constructed from the integrated luminescence signal from 0 to 0.8 s for quartz and 0–2 s for polymineral, while the 25–40 s of quartz

and 90–100 s feldspar were subtracted as a background. The obtained equivalent doses outside these ranges were rejected: 0.9–1.1 recycling ratio, < 10% test dose error, and < 10% recuperation ratio. The central age model (Galbraith et al. 1999) was applied to improve statistical values from accepted De. For the polymineral samples, the anomalous fading was tested through the method presented by Huntley and Lamothe (2001).

The environmental dose rate was determined from concentrations of radioactive elements. Uranium and thorium concentrations were measured via alpha counting, while potassium was measured by the inductively coupled plasma–optical emission spectroscopy (ICP-OES). Then the total dose rate and age were calculated by ADELE v.2015 software (Kulig 2005). The alpha efficiency values of polymineral and quartz were assumed to be 0.08 ± 0.02 (Zöller et al. 2013) and 0.035 ± 0.003 (Lai et al. 2008), respectively. For the polymineral samples, the effects from fading phenomena were corrected by a function “calc_FadingCorr” in R luminescence package (Kreutzer et al. 2017).

Table 4.1 ^{14}C dating results of sediment core Eph 395 from the Roman harbor basin. Dating was carried out at the Radiocarbon Dating Facility, Queens University Belfast, UK. The conventional ages were calibrated with Calib 7.1 (Reimer et al. 2009). They are presented with two sigma standard deviation (probability of 95.5%). b.s.l., below sea level; b.s., below surface.

Sample Code	Lab code	Material	Depth (m) b.s.	Depth (m) b.s.l.	^{14}C age (BP)	Age cal BC/ cal AD (2σ)
EPH395/374-375	UBA-34955	Sediment (bulk sample)	3.74	4.37	2405±29	730 – 400 BC
EPH395/496-497	UBA-34956	Sediment (bulk sample)	4.96	5.59	2452±35	760 – 410 BC
EPH395/1144-1145	UBA-34957	Sediment (bulk sample)	11.44	12.07	5491±42	4450 – 4250 BC
EPH395/1487-1488	UBA-34958	Sediment (bulk sample)	14.87	14.87	3675±32	2150 – 1950 BC

4.5 Results and interpretation

4.5.1 Sedimentology of Eph 395

Eph 395 from the southern part of the harbor basin with a total length of 15 m can be divided into six different units (Figs. 2 and 3), comparable to the neighboring core Eph 276 with a length of 12 m (for its detailed description of Eph 276 see Stock et al. 2016 and Schwarzbauer et al. 2018). The units of Eph 395 are as follows: unit 1, pre-harbor phase 15–10.90 m b.s.; unit 2, open harbor phase, 10.90–5.11 m b.s.; unit 3, protected harbor, 5.11–3.74 m b.s.; unit 4, closed lagoon, 3.74–2.66 m b.s.; unit 5, freshwater lake, 2.66–1.47 m; unit 6, peat layer, 1.47–0 m b.s., post-harbor units 5 and 6.

The grain size measurements reveal fine-grained sediments at the base of the core in the pre-harbor unit 1 with laminated clayey silts and a low mean of 8–15 μm . They were deposited in a protected marine embayment with freshwater input from the direct environs (cf. Stock et al. 2016). The organic content varies between 6 and 10%. The open harbor unit 2 is still dominated by silts (6–25 μm), but contains more fine sands (mean 35–57 μm). They originate from the advancing Küçük Menderes river and the increased erosion in the hinterland during the Roman period (cf. Stock et al. 2016). The organic content decreases to 3–9%. The higher LOI values of 13–16% towards the top of the unit can be explained by the transition to the protected harbor phase. After the construction of the harbor mole and the canal around the turn of the eras, the protected harbor unit is deposited (unit 3) with silts and a decreasing mean of (9–15 μm) as well as organic contents of 10–20%. In unit 4 (closed lagoon-like lake), follow silts with a higher content of clay and sand. Therefore, the sorting rises from 3–4 (below) to 5.6; moreover, lower organic contents (7–12%) are present. The post-harbor unit 5, the freshwater lake, is characterized by coarser sediments (mean up to 18–57 μm , very bad sorting of 8) and similar LOI values. The turning to freshwater can be seen in the microfossil assemblage (Stock et al. 2016); it indicates that the harbor was not connected to the sea anymore. The peat in the uppermost part has high organic contents of 28–56%. The small amount of clastic sediments is characterized by fine sand to coarse silt with a mean of 33–151 μm .

4.5.2 Chronology

Radiocarbon ages:

Four bulk sediment samples were radiocarbon-dated (Table 4.1). The results are between 4450 BC and 400 BC. An age inversion occurs in the lower part.

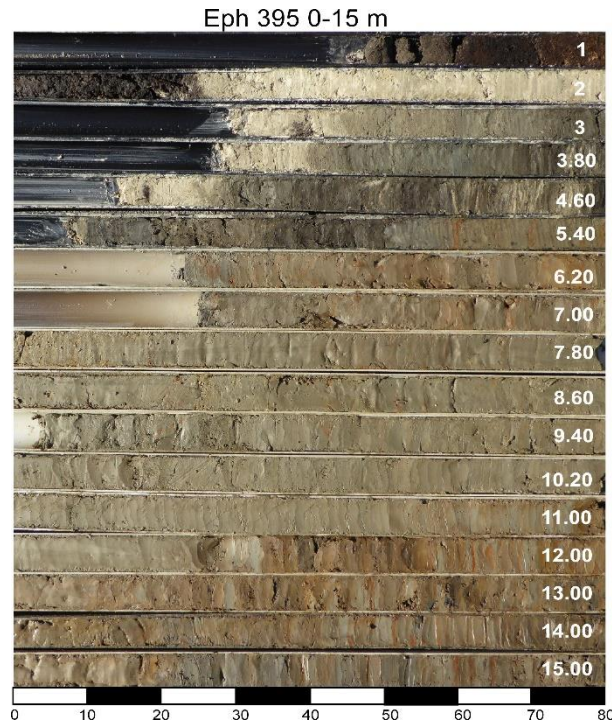


Figure 4.2 Photo of drill core Eph 395 from the Roman harbor basin. In order to minimize the problems with collapsed material and compaction, the section between 3 and 11 m were drilled with 80-cm segments only (Photo: F. Stock 2015)

Luminescence dating:

The dose rates of the samples were calculated between 1.0 and 3.5 Gy/ka; the ones for quartz were lower than the ones for feldspar due to the alpha efficiency. The major reason of the dose-rate variation is possibly linked to their provenance. The sediments of the shallow part were derived by runoff and karstic spring (Delile et al. 2015) which leads to lower radioelement concentration. The results of radioactive elements and dose rates are presented in Table 4.2.

Seven samples were dated by polymineral, while five of these were dated by quartz. Samples BT1408 and BT1509 from a depth of 2.34 and 3.60 m b.s., only reveal polymineral ages due to the limitation of the sample amount. The g values, indicating how strong the fading phenomenon of polymineral is, have decays between 0.89 and 2.81%, of which BT1408's g values were zero within their errors. Therefore, BT1408 was not applied to fading correction. For quartz dating, the remaining feldspar grains were tested by the measurement of IR signal stimulation. Since the signals were in the background level, they indicate that all feldspars were completely removed by H_2SiF_6 .

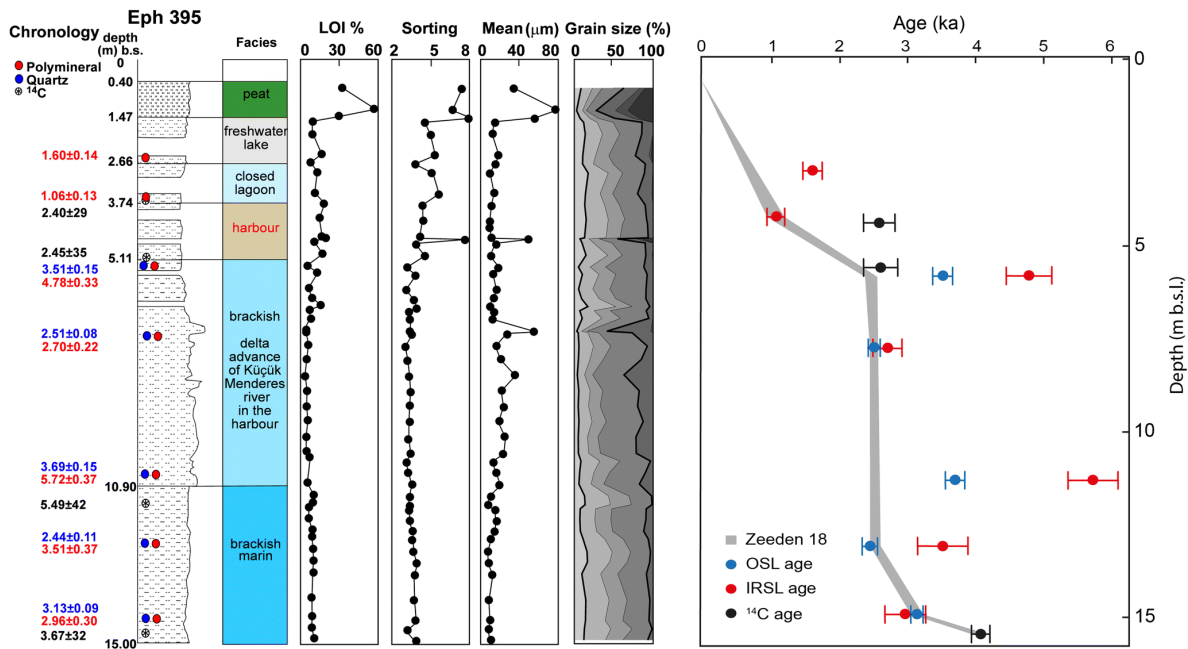


Figure 4.3 Left: stratigraphy and the results of grain size analyses, loss on ignition and the chronology (^{14}C and luminescence ages). Right: luminescence and ^{14}C ages (OSL: quartz age, IRSL: polymineral age) as well as age-depth model (gray band) following Zeeden et al. (2018)

All samples were well fitted with the exponential function in the dose-response curve with showing less than 5% relative standard errors D_e . An example of the dose-response and dose-distribution curves of polymineral (sample BT1409) is shown in Fig 4.4. The obtained ages of polymineral were dated between 1 and 5 ka with 2–12% of age errors, while ages obtained from quartz were dated between 2.5 and 3.7 ka with 3–5% of age errors. Luminescence dating results are presented in Table 4.2 and Figure 4.3.

Sedimentation rate:

For the luminescence ages, which are in agreement with the stratigraphy (see discussion), an age-depth model was calculated (Figure 4.3). The most probable ages were included in the model. A sedimentation rate of 0.6 mm/year was calculated for the period ca. 2000–1000 BC. It rises up to 3.0 mm/year until 500 BC. Then, 6–7 m of sediments are deposited in 200–300 years (sedimentation rate of 65 mm/year). From 500 BC to 1000 AD, only 1.1 mm/year were deposited in the harbor basin. From that time until today, the rate rises again to 3.4 mm/year.

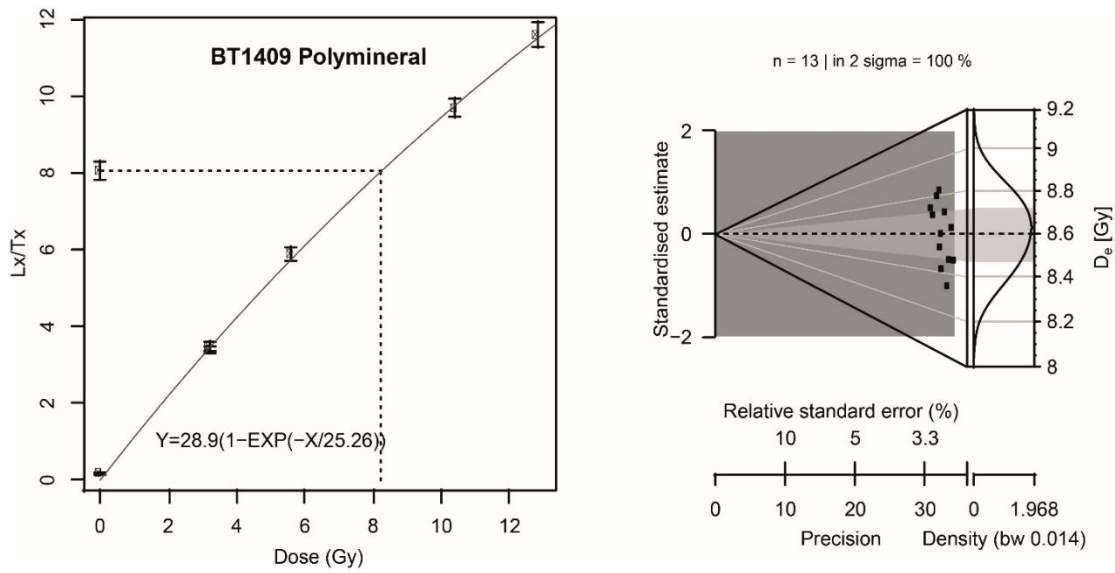


Figure 4.4 Dose response curve of BT1409 polymineral (right) and Abanico plot showing the D_e distribution of BT1409 polymineral.

4.6 Discussion

4.6.1 Validity of luminescence ages

The samples in this study were prepared for the fine-grain technique; thus, the distribution curve of D_e shows a Gaussian (normal) distribution (example in Figure 4.4). This can be described by the millions of mineral grains (Heer et al. 2012) on a disc which provide almost an average of luminescence signal (population of a sample). The observation of incomplete bleaching by the outliers of high D_e is not possible. However, incomplete bleaching can be observed comparing luminescence ages from quartz and polymineral fine grains.

Table 4.2 Luminescence dating results, both polymineral and quartz.

Lab ID	Depth (m b.s.)	Th (ppm)	U (ppm)	K (%)	\dot{D}_{PM} (Gy/ka)	\dot{D}_Q (Gy/ka)	D_{ePM} (Gy)	g value (% decade)	Polymineral age (ka)	^b Polymineral age (AD/BC)	D_{eQ} (Gy)	Quartz age (ka)	^b Quartz age (AD/BC)**
BT1408	2.34	3.75 ± 0.93	1.97 ± 0.27	0.87 ± 0.03	1.03 ± 0.11	-	1.65 ± 0.07	0.89 ± 3.67	1.60 ± 0.14	276-556 AD	-	-	-
BT1509	3.60	8.04 ± 0.93	1.92 ± 0.28	1.94 ± 0.06	2.19 ± 0.19	-	2.00 ± 0.01	1.92 ± 1.10	1.06 ± 0.13	^a 826-1086 AD	-	-	-
BT1510	5.20	16.12 ± 1.86	3.44 ± 0.56	2.71 ± 0.08	3.50 ± 0.35	3.09 ± 0.20	13.97 ± 0.07	2.08 ± 0.36	4.78 ± 0.33	3094-2434 BC	10.86 ± 0.22	3.51 ± 0.15	1644-1344 BC
BT1409	7.14	14.18 ± 1.86	4.28 ± 0.56	2.94 ± 0.09	3.63 ± 0.33	3.20 ± 0.19	8.60 ± 0.07	1.53 ± 0.32	2.70 ± 0.22	904-464 BC	8.03 ± 0.10	2.51 ± 0.08	^a 574-414 BC
BT1511	10.70	16.25 ± 1.86	3.02 ± 0.56	2.66 ± 0.08	3.34 ± 0.33	2.95 ± 0.20	16.27 ± 0.11	2.81 ± 0.29	5.72 ± 0.37	4074-3334 BC	10.88 ± 0.12	3.69 ± 0.15	1824-1524 BC
BT1512	12.50	11.01 ± 1.86	3.47 ± 0.56	1.83 ± 0.05	2.98 ± 0.33	2.59 ± 0.20	9.09 ± 0.01	1.58 ± 1.82	3.51 ± 0.37	1864-1124 BC	6.32 ± 0.13	2.44 ± 0.11	^a 534-314 BC
BT1410	14.34	10.26 ± 0.93	3.12 ± 0.29	2.71 ± 0.08	2.76 ± 0.21	2.46 ± 0.11	6.97 ± 0.05	1.88 ± 0.82	2.96 ± 0.30	1244-644 BC	7.72 ± 0.30	3.13 ± 0.09	^a 1204-1024 BC

^a Ages consistent with the stratigraphy and archaeological events

^b AD/BC converted from 2016 (the samples were measured during late 2015- early 2018).

The samples BT1409 and BT1410 (7.14 and 14.34 m b.s.) agree between quartz and polymineral ages at around 2.5 and 3.0 ka, respectively. This indicates a good bleaching before deposition (burial); it well represents the last time the sediments were exposed to light. Thus, quartz ages represent the burial age in this study due to the smaller age errors. Samples BT1510 to BT1512 show that polymineral ages are higher than the quartz ages. The differences can be explained by incomplete bleaching since quartz is more easily bleached than feldspar (Godfrey-Smith et al. 1988). However, the quartz age of sample BT1512 is closer to the age of sample BT1409. This suggests a complete bleaching of quartz and an incomplete bleaching of feldspar in the polymineral fraction.

The individual polymineral age of BT1408 at 2.34 m b.s. (1.60 ka) derives from freshwater sediments; the ^{14}C age of this unit in the neighboring core Eph 276 is around 0.5 ka, (see Figure 4.5 and Delile et al. 2015; Stock et al. 2016). The polymineral age of BT1408 is overestimated due to incomplete bleaching. The individual polymineral age of BT1509 at 3.60 m b.s. (1.06 ka), however, which was classified as a closed lagoon, is in agreement with the ^{14}C ages presented by Delile et al. (2015) and Stock et al. (2016).

Within 1σ luminescence age ranges, four of seven luminescence ages of the core Eph 395 were successfully dated and agreed with the archeological context: BT1410 (3.13 ± 0.09 ka; 1200–1030 BC), BT1512 (2.44 ± 0.11 ka; 533–313 BC), BT1409 (2.51 ± 0.08 ka; 571–407 BC), and BT1509 (1.06 ± 0.13 ka; 836–1086 AD). The ^{14}C age of UBA-34956 which was derived from the active harbor unit shows an overestimation compared to cores presented by Stock et al. (2016). This might be due to the reworking of organic material from the underlying sediment (related to BT1510). To construct the realistic age-depth model (see Figure 4.3), the ^{14}C age of Eph 395 (UBA-34956) was applied instead of the luminescence age of BT1510.

The BT1410 age of 1030–1200 BC, which was lithologically classified to be a brackish-marine deposit, has a good agreement with the results from Eph 278 in Stock et al. (2016). The luminescence age-depth model showed that a very high deposition rate occurred around 700–400 BC (2.7–2.4 ka) in the open harbor unit. The high deposition rate around 500 BC (cf. Brückner 2005) may indicate the fast delta advance of the Küçük Menderes and the change from a brackish-marine to a brackish environment. However, these results are 500 years older than the ones for Eph 276 and the other cores of the harbor and the canal (Figure 4.5). Thus, a dredging dump site at the southern part of the harbor basin may be a possible explanation (Stock et al. 2016).

The problem of incomplete bleaching was also described by Sanderson et al. (2003), Alappat et al. (2010), and Lauer et al. (2011). In this study, it can be explained by the fact that the delta advanced into the marine embayment with a higher sediment flux and suspension. The turbidity in the harbor and the difficult transmission of light through the sediment-loaded water column might be the major reason for incomplete bleaching. Moreover, light intensity is a factor of the bleaching process. If a fast deposition occurs during the night, triggered by intensive rainfall, there may not be enough light arriving at the mineral grains which results in incomplete bleaching. Subaqueous erosion of older sediments may cause incomplete bleaching as well.

4.6.2 Comparison with other results in the Roman harbor and canal

The results of this study can not only be integrated into the results of Eph 276 (discussed above), but also to the other ^{14}C age estimates from seeds, pollen, plant fragments, and wood, published by Stock et al. (2016). Moreover, new radiocarbon dates of Eph 278 (see Figure 4.5) can be compared with the results of this study. Eph 395 reaches 3 m deeper into the basin than all other drill cores (see Figure 4.5). Thus, the sediments give new insights into the development of the harbor basin. The lowermost ^{14}C age estimate dates the laminated clayey silts, i.e. the pre-harbor sediments, to 2100–1950 BC. At this time, the city of Ephesus was not yet located between Bülbüldağ and Panairdağ mountains (see Figure 4.1); Lysimachos refounded the city at this location around 300 BC (Kraft et al. 2000). Therefore, the hypothesis by Stock et al. (2016) can be confirmed that the laminated sediments were deposited in an open marine embayment. Moreover, the lowermost age of Eph 278 also reveals an age older than 1000 BC for the marine sediments. The relatively young ages of Eph 271 and 276 in 11–13 m b.s.l. (below sea level) may be caused by dredging activities (Stock et al. 2016). The ^{14}C age of Eph 395 dating to 4450–4250 BC at 12 m b.s.l. (Figure 4.5) is probably too old and should not be taken into account. Loughheed et al. (2017) dated bulk sediments of estuarine environments with the radiocarbon method; the results reveal that the bulk sediments are older than if other material was dated. An overestimation of the bulk sample is therefore well probable.

The open harbor (11–6 m b.s.; Figure 4.6) as well as the closed harbor units (6–4 m b.s., Figure 4.5) of Eph 395 were dated to ca. 700–400 BC by means of luminescence and ^{14}C . Delile et al. (2015) and Stock et al. (2016) dated the open harbor until the turn of the eras, and the protected harbor from that time until the sixth/seventh century AD (Eph 270, 276, 278). However, the ^{14}C result of this study (Eph 395) is based on the bulk sediment (760–400 BC) which is approximately 500–1000 years older

than the results of Eph 276. Again, the overestimation of bulk samples (see Lougheed et al. 2017) should be taken into account. In addition, the new results of Eph 278 for the intensive harbor use layer also clearly reveal a deposition of the protected harbor unit between the first century BC to the seventh century AD (Figure 4.5). The overestimation of bulk sediment dated with ^{14}C ages in a harbor environment might be explained by the fact that older organic material accumulated in the harbor.

Kraft et al. (2007) already published ^{14}C ages outside the harbor (Eph 92–4) to 633–410 BC (3–4 m b.s.l.). Eph 91–5 in the middle of the protected harbor reveals evidence of dredging around 5 m b.s.l. The high sedimentation rate calculated by Stock et al. (2016) for cores Eph 276 and 284 for the open harbor layer might be related to dredging. Figure 6 shows a scenario for the harbor floor a few decades before 500 BC (blue line) and very fast deposition due to the delta advance (second century BC to first century AD; Stock et al. 2016). At that time, the depth of the studied site was around 3 m b.s.l. (evidence from Eph 92–4). Around the turn of the eras, the harbor was protected by moles and was probably dredged (green line). Evidence from this study and from Kraft et al. (2007) showed that it was ca. 5 m deep. The difference between the age estimates from sites outside and inside the harbor is best explained by the fact that the protected harbor basin (construction of a harbor mole) was dredged. After that operation, younger material was deposited in the basin. Already, from the first century AD, it is reported that a proconsul under Emperor Nero's reign ordered the harbor basin to be cleaned and dredged—an action which was repeated five times between the first to the third centuries AD (Kraft et al. 2000, 2011). At the beginning of the second century AD, a high priest gave an immense donation to reconstruct and enlarge the harbor area (Zabehlicky 1995). It is also known that in the middle of the second century AD, a proconsul prohibited the disposal of waste, debris, and construction rubble into the basin and the canal (Kraft et al. 2000; Zabehlicky 1995).

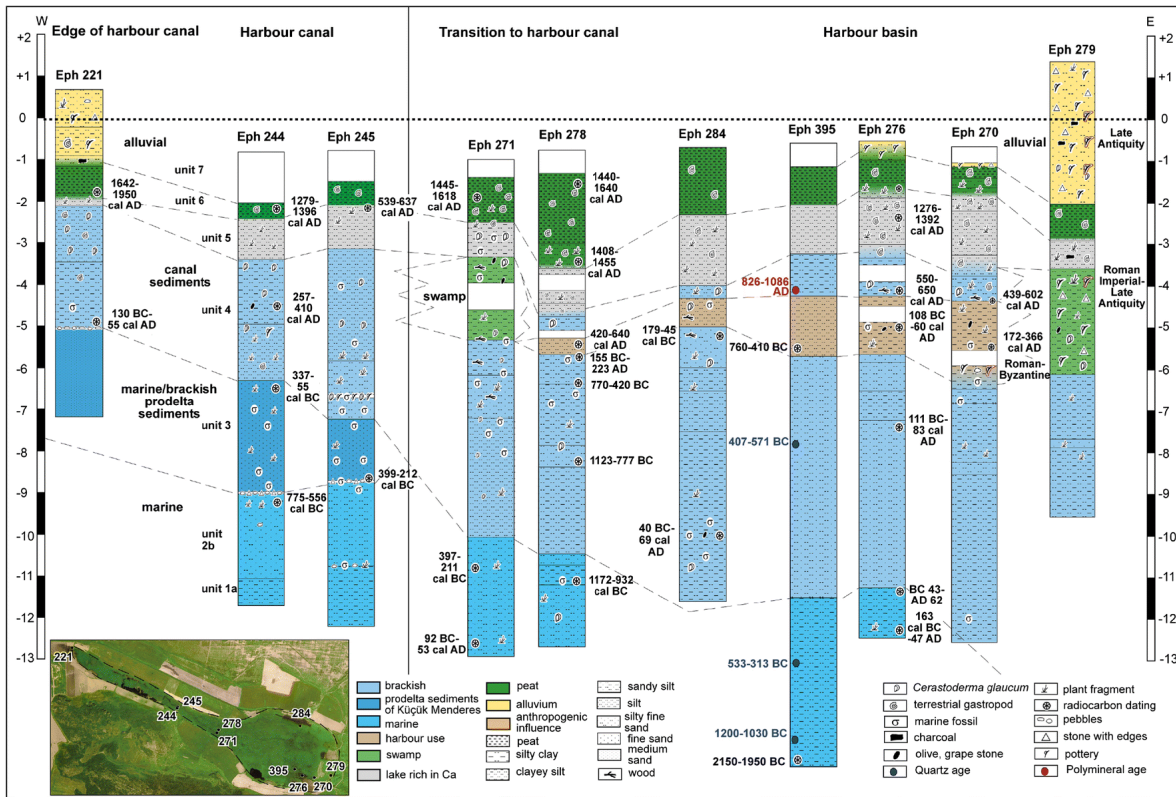


Figure 4.5 The results of the core Eph 395 from this study have been integrated into the harbor/canal sequence. Source: Stock et al. 2016, modified

4.7 Conclusion

For this study, sediments of the Roman harbor of Ephesus were dated with the luminescence and the radiocarbon methods. The results are complementary to already published results in the last years. They reveal that bulk samples of ^{14}C are probably too old and that luminescence ages in harbor sediments tend to overestimation due to incomplete bleaching. However, the interpretation of luminescence ages along with a comparison of quartz and polymineral grains are helpful to consider the bleaching condition. Ages in good agreement indicate the good bleaching of mineral grains before burial.

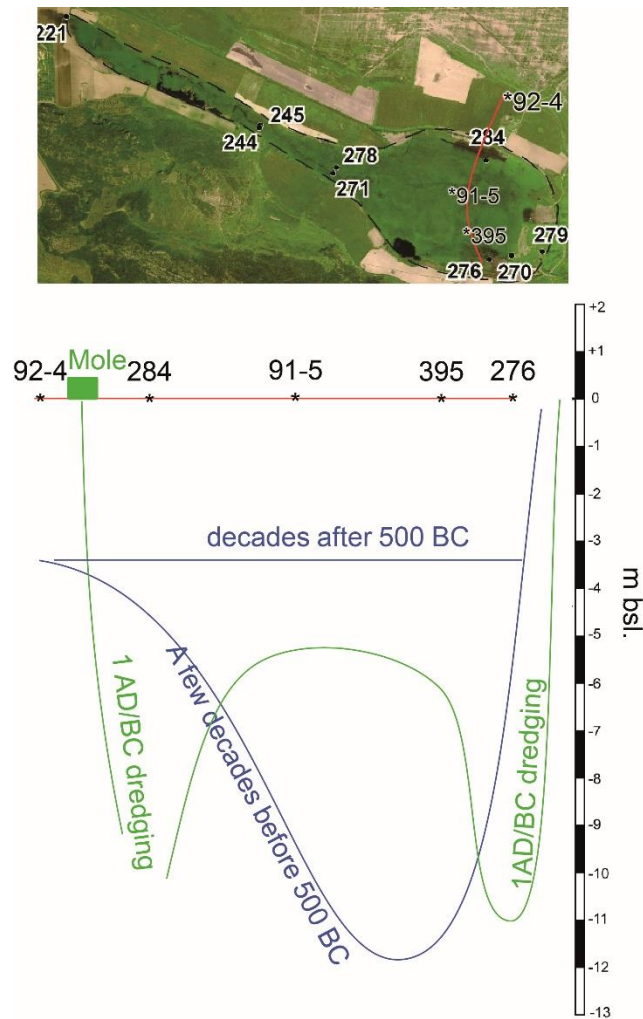


Figure 4.6 Possible harbor depth around decades before 500 BC (blue line), decades after 500 BC (blue dashed line) showing the very fast advance of the delta and around 1 AD/BC (green line) when the harbor was dredged

The ^{14}C and luminescence dating results provide ages between 2000 BC and 1500 AD in marine, brackish, lagoonal, and freshwater environments. The very fast advance of the Küçük Menderes delta around 2500 years ago (ca. 700–400 BC) is confirmed in this study. However, the ages seem to be overestimated. When the Romans used this harbor as main port, the harbor was protected by the mole. At a depth of ca. 5 m b.s.l., dredging activities probably took place.

4.8 Acknowledgements

The authors thank the Austrian Archeological Institute, especially the excavation director Sabine Ladstätter, for the continued financial and logistic support of our studies. The Turkish government authorities kindly granted the research permits. The new ^{14}C datings of Eph 395 and 278 were supported by the Austrian National Bank (grant number 17134).

4.9 References

- Aitken MJ (1985) Thermoluminescence dating. Academic Press, London.
- Aitken MJ (1998) An introduction to optical dating. Oxford University Press, Oxford.
- Alappat L, Tsukamoto S, Singh P, Srikanth D, Ramesh R, Frechen M (2010) Chronology of Cauvery Delta Sediments from Shallow Subsurface Cores Using Elevated-Temperature Post-IR IRSL Dating of Feldspar. *Geochronometria* 37:37-47. <https://doi.org/10.2478/v10003-010-0025-1>
- Algan O, Yalcin MN, Özdoğan M, Yılmaz Y, Sarı E, Kırıcı-Elmas E, Yılmaz İ, Bulkan Ö, Ongan D, Gazioğlu C, Nazik A, Ali Polat M, Meriç E. (2011) Holocene coastal change in the ancient harbor of Yenikape-Istanbul and its impact on cultural history. *Quaternary Res* 76:30–45. <https://doi.org/10.1016/j.yqres.2011.04.002>
- Banerjee D, Murray AS, Bøtter-Jensen L, Lang A (2001) Equivalent dose estimation using a single aliquot of polymineral fine grains. *Radiat Meas* 33:73-94. [https://doi.org/10.1016/S1350-4487\(00\)00101-3](https://doi.org/10.1016/S1350-4487(00)00101-3)
- Bernasconi MP, Melis R, Stanley JD (2006) Benthic biofacies to interpret Holocene paleoenvironmental changes and human impact in Alexandria's Eastern Harbor, Egypt. *The Holocene* 16(8):1163–1176. <https://doi.org/10.1177/0959683606069423>
- Brückner H. 2005. Holocene shoreline displacements and their consequences for human societies: the example of Ephesus in western Turkey. *Z Geomorphol Supp* 137: 11–22.
- Brückner H, Herda A, Müllenhoff M, Rabbel W, Stümpel H. (2014) On the Lion Harbour and other harbours in Miletos: recent historical, archaeological, sedimentological, and geophysical research. *Proceedings of the Danish Institute at Athens (PDIA)*, vol. VII: 49–103. Aarhus.

- Delile H, Blichert-Toft J, Goiran, J-P, Stock F, Arnaud-Godet F, Bravard J-P, Brückner H, Albarède F, (2015) Demise of a harbor: A geochemical chronicle from Ephesus. *J Archaeol Sci* 53:202-213. <https://doi.org/10.1016/j.jas.2014.10.002>
- Delile H, Goiran J-P, Blichert-Toft J, Arnaud-Godet F, Romano P, Bravard J-P (2016) A geochemical and sedimentological perspective of the life cycle of Neapolis harbor (Naples, southern Italy). *Quaternary Sci Rev* 150:84–97. <https://doi.org/10.1016/j.quascirev.2016.08.026>
- Duller G A T (2015) The Analyst software package for luminescence data: overview and recent improvements. *Ancient TL* 33(1): 35-42.
- Galbraith RF, Roberts RG, Laslett GM, Yoshida H, Olley JM (1999) Optical dating of single and multiple grains of quartz from Jinmium rock shelter, northern Australia: Part I, experimental design and statistical models. *Archaeometry* 41(2):339-364. <https://doi.org/10.1111/j.1475-4754.1999.tb00987.x>
- Godfrey-Smith DI, Huntley DJ, Chen WH (1988) Optical dating studies of quartz and feldspar sediment extracts. *Quaternary Sci Rev* 7(3-4):373-380. [https://doi.org/10.1016/0277-3791\(88\)90032-7](https://doi.org/10.1016/0277-3791(88)90032-7)
- Heer AJ, Adamiec G, Moska P (2012) How many grains are there on a single aliquot?. *Ancient TL* 30:9-16.
- Huntley DJ, Godfrey-Smith DI, Thewalt MLW (1985) Optical dating of sediments. *Nature* 313:105-107. <https://doi.org/10.1038/313105a0>
- Huntley DJ, Lamott M. (2001) Ubiquity of anomalous fading in K-feldspars and the measurement and correction for it in optical dating. *Can J Earth Sci* 38(7):1093-1106. <https://doi.org/10.1139/cjes-38-7-1093>
- Knibbe D (1998). *Ephesus – Geschichte einer bedeutenden antiken Stadt und Portrait einer modernen Großgrabung im 102. Jahr der Wiederkehr des Beginnes österreichischer Forschungen (1895-1997)*. –Peter Lang, Frankfurt a. Main.
- Kraft JC, Kayan I, Brückner H, Rapp G (2000) A geological analysis of ancient landscapes and the harbors of Ephesus and the Artemision in Anatolia. *Jahreshefte Des Österreichischen Archäologischen Institutes in Wien* 69:175-233.

- Kraft JC, Kayan İ, Brückner H (2001) The geological and paleogeographical environs of the Artemision. In: Muss U (ed), *Der Kosmos der Artemis von Ephesos*. Sonderschriften 37. Österreichisches Archäologisches Institut, Wien, pp 123–133
- Kraft JC, Rapp G, Kayan İ, Luce JV (2003) Harbor areas at ancient Troy: Sedimentology and geomorphology complement Homer's Iliad. *Geology* 31(2), 163–166.
[https://doi.org/10.1130/0091-7613\(2003\)031<0163:HAAATS>2.0.CO;2](https://doi.org/10.1130/0091-7613(2003)031<0163:HAAATS>2.0.CO;2)
- Kraft JC, Brückner H, Kayan İ (2005) The sea under the city of ancient Ephesus. In: Krinzing F, Brandt B, Gassner V, Ladstätter S (eds), *Synergia*. Festschrift vol. 1. Phoibos, Wien, pp 147–156
- Kraft JC, Brückner H, Kayan İ, Engelmann H (2007) The geographies of ancient Ephesus and the Artemision in Anatolia. *Geoarchaeology* 22(1), 121–149.
- Kraft JC, Rapp G, Brückner H et al. (2011) Results of the struggle at ancient Ephesus: natural processes 1, human intervention 0. *Geological Society London Special Publications* 35, 27–36.
- Kreutzer S, Burrow C, Dietze M, Fuch MC, Fischer M, Schmidt C (2017) Software in the context of luminescence dating: status, concepts and suggestions exemplified by the R package 'Luminescence'. *Ancient TL* 35(2): 1-11.
- Kulig G (2005) Erstellung einer Auswertesoftware zur Altersbestimmung mittels Lumineszenzverfahren unter spezieller Berücksichtigung des Einflusses radioaktiver Ungleichgewichte in der ^{238}U -Zerfallsreihe, B.Sc. Thesis, TU Bergakademie Freiberg.
- Lai ZP, Zöllner L, Fuchs M, Brückner H (2008) Alpha efficiency determination for OSL of quartz extracted from Chinese loess. *Radiat Meas* 43(2-6):767-770.
<https://doi.org/10.1016/j.radmeas.2008.01.022>
- Lauer T, Bonn R, Frechen M, Fuchs MC, Trier M, Tsukamoto S (2011) Geoarchaeological studies on Roman time harbour sediments in Cologne — comparison of different OSL dating techniques. *Geochronometria* 38(4):341-349. <https://doi.org/10.2478/s13386-011-0020-y>
- Lougheed BC, Obrochta SP, Lenz C, Mellström A, Metcalfe B, Muscheler R, Reinholdsson M, Snowball I, Zillén L (2017) Bulk sediment ^{14}C dating in an estuarine environment: How

- accurate can it be?. *Paleoceanography and Paleoclimatology* 32(2):123-131.
<https://doi.org/10.1002/2016PA002960>
- Marriner N, Morhange C (2006) The ‘Ancient Harbour Parasequence’: Anthropogenic forcing of the stratigraphic highstand record. *Sediment Geol* 186(1-2):13–17.
<https://doi.org/10.1016/j.sedgeo.2005.12.001>
- Mazzini I, Faranda C, Giardini M, Giraudi C, Sadori L (2011) Late Holocene palaeoenvironmental evolution of the ancient harbour of Portus (Latium, Central Italy). *J Palaeolimnol* 46(2), 243–256. <https://doi.org/10.1007/s10933-011-9536-7>
- Morhange C, Blanc F, Schmitt-Mercury S, Bourcier M, Carbonel P, Oberlin C, Prone A, Vivent D, Hesnard A (2003) Stratigraphy of late-Holocene deposits of the ancient harbour of Marseilles, southern France. *The Holocene* 13(4), 593–604.
<https://doi.org/10.1191/0959683603hl619rr>
- Murray AS, Wintle AG (2000) Dating quartz using an improved single-aliquot regenerative-dose (SAR) protocol. *Radiat Meas* 32(1):57-73. [https://doi.org/10.1016/S1350-4487\(99\)00253-X](https://doi.org/10.1016/S1350-4487(99)00253-X)
- Preusser F, Degering D, Fuchs M, Hilgers A, Kadereit A, Klasen N, Krbetschek M, Richter D, Spencer JQG (2008) Luminescence dating: basics, methods and applications. *E&G Quaternary Sci J* 57:95-149. <https://doi.org/10.3285/eg.57.1-2.5>
- Reimer PJ, Baillie MGL, Bard E, Bayliss A, Beck JW, Blackwell PG, Bronk Ramsey C, Buck CE, Burr GS, Edwards RL, Friedrich M, Grootes PM, Guilderson TP, Hajdas I, Heaton TJ, Hogg AG, Hughen KA, Kaiser KF, Kromer B, McCormac FG, Manning SW, Reimer RW, Richards DA, Southon JR, Talamo S, Turney CSM, van der Plicht J, Weyhenmeyer CE (2009) IntCal09 and Marine09 radiocarbon age calibration curves, 0-50,000 years cal BP. *Radiocarbon* 51(4):1111-1150.
- Salomon P, Delile H, Goiran JP, Bravard JP, Keay S (2012) The Canale di Comunicazione Traverso in Portus: the Roman sea harbour under river influence (Tiber delta, Italy). *Géomorphologie: relief, processus, environnement* 1:75–90.
<https://doi.org/10.4000/geomorphologie.9754>

- Sanderson DCW, Bishop P, Stark MT, Spencer JQ (2003) Luminescence dating of anthropogenically reset canal sediments from Angkor Borei, Mekong Delta, Cambodia. *Quaternary Sci Rev* 22:1111-1121. [https://doi.org/10.1016/S0277-3791\(03\)00055-6](https://doi.org/10.1016/S0277-3791(03)00055-6)
- Schwarzbaauer J, Stock F, Brückner H, Dsikowitzky L, Krichel M. (2018) Molecular organic indicators for human activities in the Roman harbor of Ephesus, Turkey. *Geoarchaeology*:1–12. <https://doi.org/10.1002/gea.21669>
- Steskal M (2015) Ephesus and its harbors: A city in search of its place. In Ladstätter S, Pirson F, Schmidts T (Eds), *Harbors and harbor cities in the Eastern Mediterranean (BYZAS 19)*. Ege Yayinlari, Istanbul, pp 325–338
- Stock F, Pint A, Horejs B, Ladstätter S, Brückner H (2013) In search of the harbours: New evidence of Late Roman and Byzantine harbours of Ephesus. *Quatern Int* 312:57–69. <https://doi.org/10.1016/j.quaint.2013.03.002>
- Stock F, Kerschner M, Kraft JC, Pint A, Frenzel P, Brückner H (2014) The palaeo-geographies of Ephesus (Turkey), its harbours and the Artemision – a geoarchaeological reconstruction for the timespan 1500–300 BC. *Z Geomorphol Supp* 58(2): 33–66. <https://doi.org/10.1127/0372-8854/2014/S-00166>
- Stock F, Ehlers L, Horejs B, Knipping M, Ladstätter S, Seren S, Brückner H (2015) Neolithic settlement sites in Western Turkey — palaeogeographic studies at Çukuriçi Höyük and Arvalya Höyük. *J Archaeol Sci: Reports* 4:565–577. <https://doi.org/10.1016/j.jasrep.2015.10.009>
- Stock F, Knipping M, Pint A, Ladstätter S, Delile H, Heiss AG, Laermanns H, Mitchell P, Ployer R, Steskal M, Thanheiser U, Urz R, Wennrich V, Brückner H (2016) Human impact on Holocene sediment dynamics in the Eastern Mediterranean – the example of the Roman harbour of Ephesus. *Earth Surf Proc Land* 41: 980–996. <https://doi.org/10.1002/esp.3914>
- Véron A, Goiran JP, Morhange C, Marriner N, Empeur JY (2006) Pollutant lead reveals the pre-Hellenistic occupation and ancient growth of Alexandria, Egypt. *Geophys Res Lett* 33:1–4. <https://doi.org/10.1029/2006GL025824>

- Zabehlicky H (1995) Preliminary views of the Ephesian Harbor. In: Köster H (ed), *Ephesus – Metropolis of Asia. An Interdisciplinary Approach to its Archaeology, Religion, and Culture*. Harvard Theological Studies 41, pp 201–216
- Zabehlicky H (1999) Die Grabungen im Hafen von Ephesus 1987–1989. In: Friesinger H, Krinzinger F (eds.), *100 Jahre österreichische Forschungen in Ephesus. Akten des Symposions Wien 1995*. Archäologische Forschungen 1, Denkschriften Wien 260, pp 479–484
- Zeeden C, Dietze M, Kreutzer S (2018) Discriminating luminescence age uncertainty composition for a robust Bayesian modelling. *Quat Geochronol* 43:30-39.
<https://doi.org/10.1016/j.quageo.2017.10.001>
- Zöller L, Richter D, Masuth S., Wunner L, Fischer M, Antl-Weiser W (2013) Luminescence chronology of the Grub-Kranawetberg site, Austria. *E&G Quaternary Sci J* 62:127-135.
<https://doi.org/10.3285/eg.62.2.04>

Appendix

A1 Own and authors contribution statements

Study I

Authors: Prakrit Noppradit, Christoph Schmidt, Helmut Dürrast, Ludwig Zöller

Title: Late Quaternary evolution of Songkhla coast, Southern Thailand, revealed by OSL dating

Status: Accepted by Chiang Mai Journal of Science

Own contributions: Study design 95%, Fieldwork 95%, Laboratory and data analysis 100%, Interpretation 80%, Manuscript preparation 100%.

Study was designed by PN and LZ, Fieldwork was carried out by PN and HD. Results were interpreted by PN, CS, HD, and LZ. Manuscript was improved by CS, HD, and LZ.

PN is the corresponding author.

Study II

Authors: Prakrit Noppradit, Ludwig Zöller, Christoph Schmidt, Sebastian Lorenz, Henrik Rother

Title: Geological evolution and optically stimulated luminescence (OSL) dating of the coastal dunes at Trassenheide, Usedom Island, NE Germany

Status: Under review by E&G Quaternary Science

Own contributions: Study design 25%, Fieldwork 25%, Laboratory and data analysis 100%, Interpretation 60%, Manuscript preparation 100%.

Study was designed by PN, LZ and HR, Fieldwork was carried out by PN, LZ, SL, and HR. Results were interpreted by PN, LZ, CS, and HR. Manuscript was improved by LZ, CS, SL, and HR.

PN is the corresponding author.

Study III

Authors: Prakrit Nopradit, Anika Symanczyk, Ludwig Zöller, Helmut Brückner, Friederike Stock

Title: Methodological approach for dating harbor sediments by using luminescence dating – a case study in Ephesus, Western Turkey

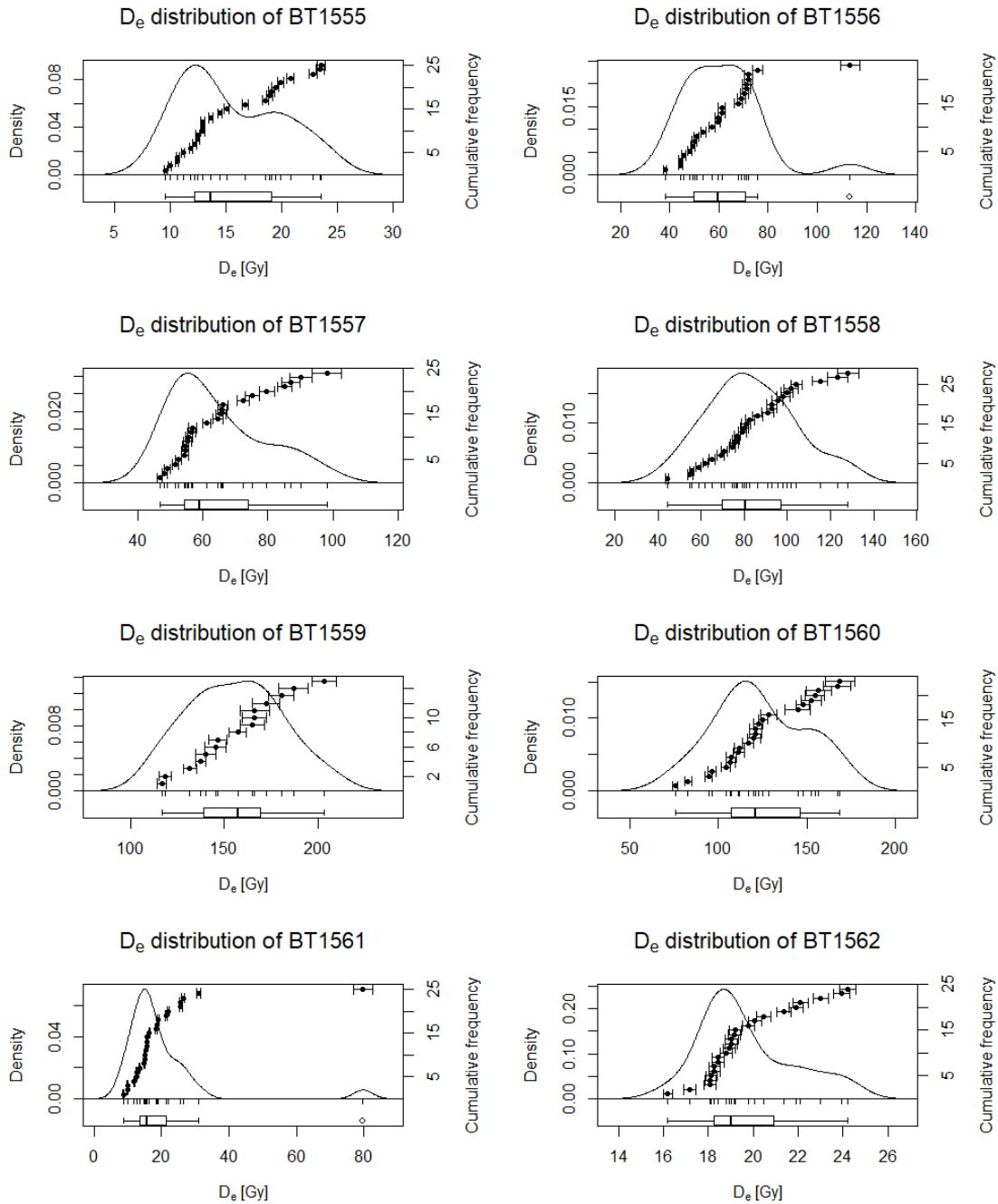
Status: Published in Archaeological and Anthropological Sciences

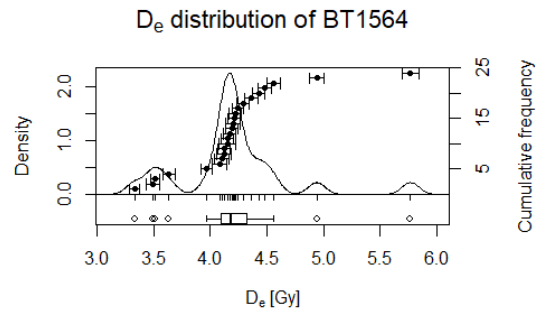
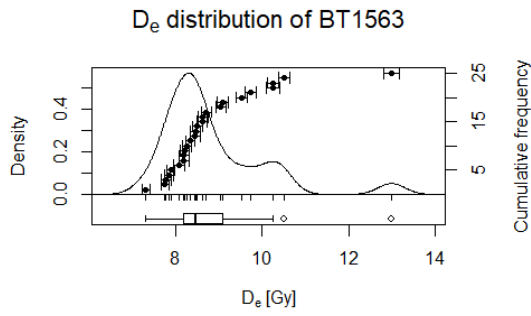
<https://doi.org/10.1007/s12520-018-0739-y>

Own contributions: Study design 50%, Laboratory and data analysis 60%, Interpretation and discussion 50%, Manuscript preparation 50%.

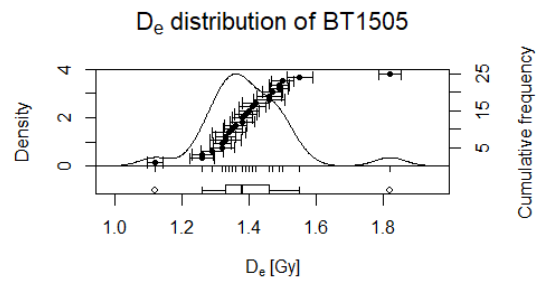
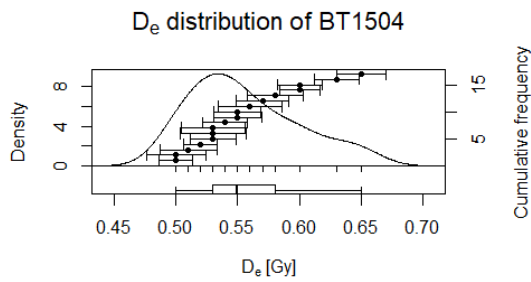
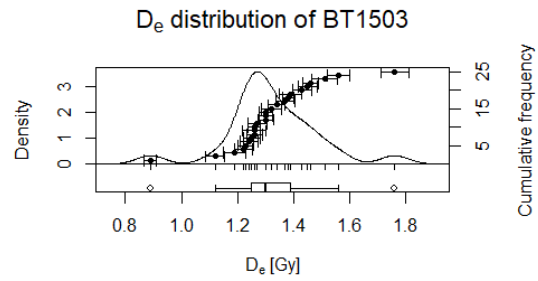
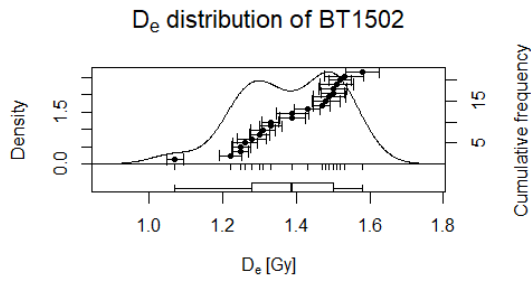
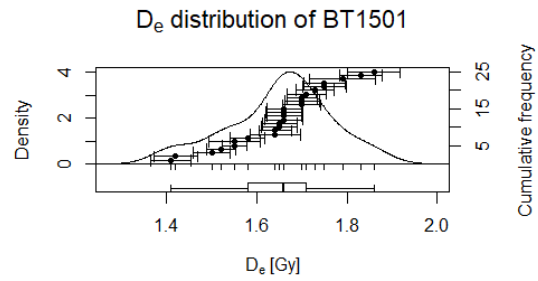
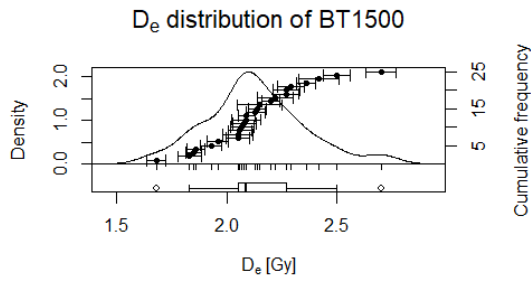
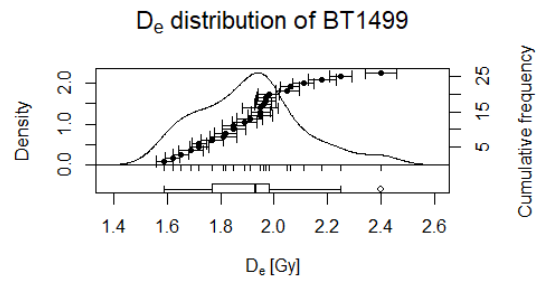
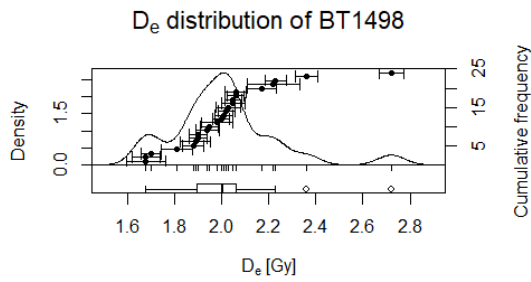
Study was designed by PN, FS, HB, and FS. Fieldwork was carried out by FS and HB. Laboratory and data analysis were carried out by PN, AS, and FS. Results were interpreted and discussed by PN, LZ, HB, and FS. Manuscript was prepared by PN and FS and was improved by LZ and HB.

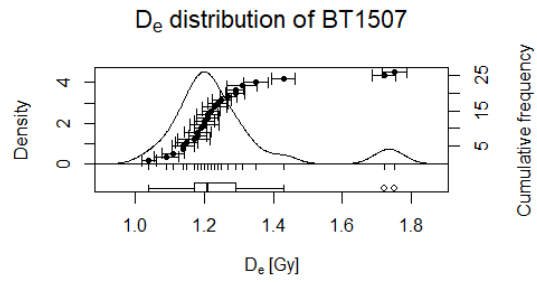
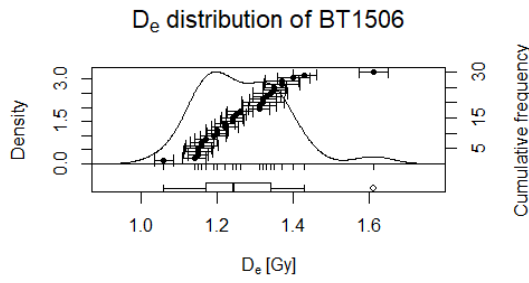
PN is the corresponding author.

A2 D_e distribution in Study I, II, and III*Study I: Quartz*

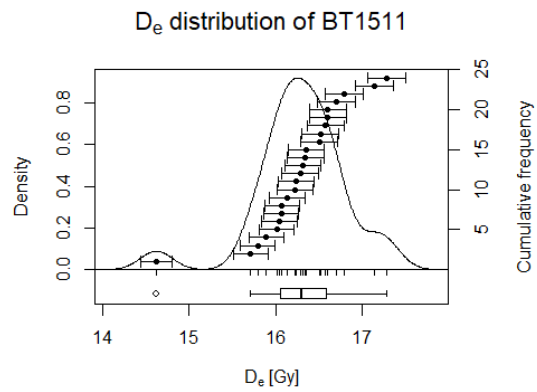
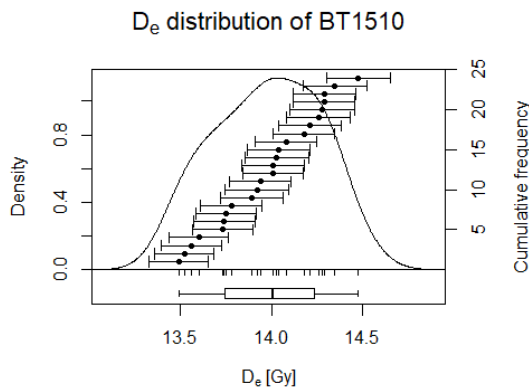
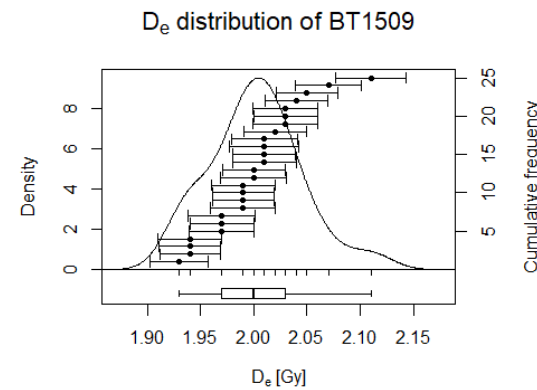
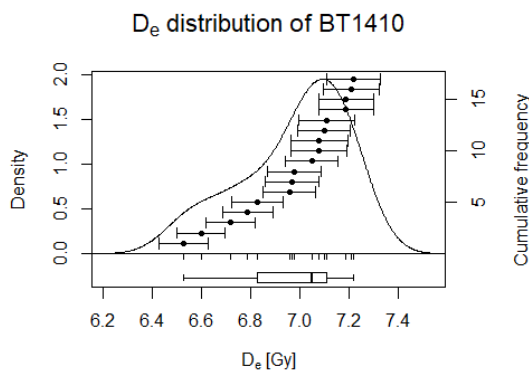
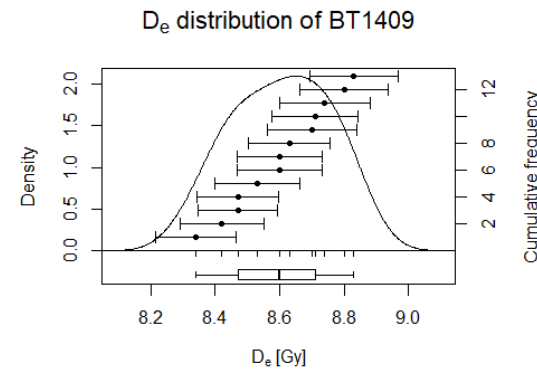
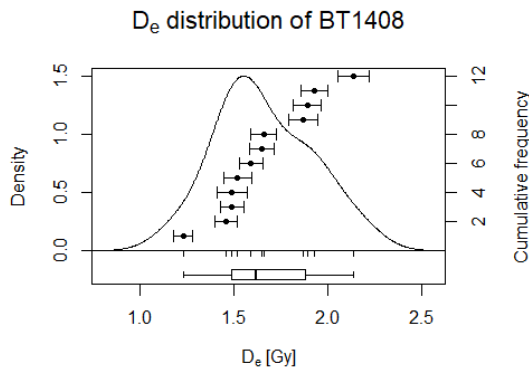


Study II: Quartz

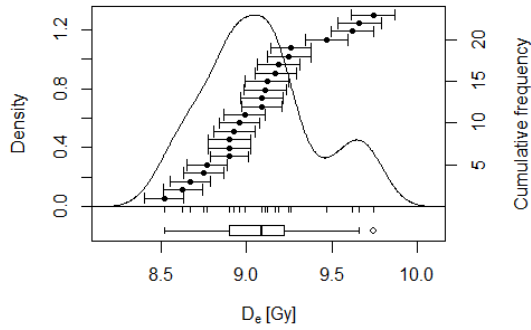




Study III: polyminerals

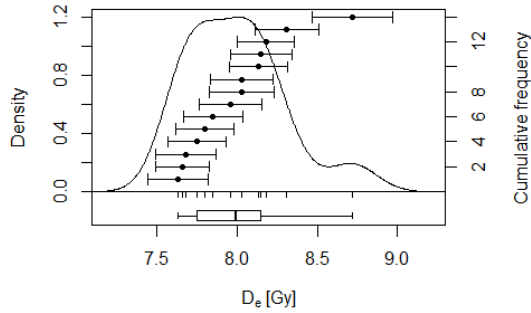


D_e distribution of BT1512

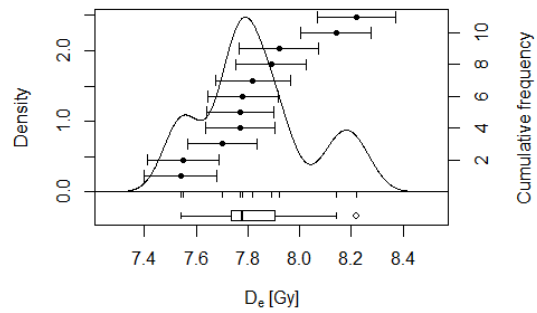


Study III: Quartz

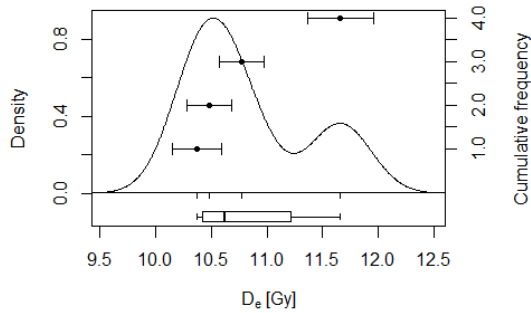
D_e distribution of BT1409



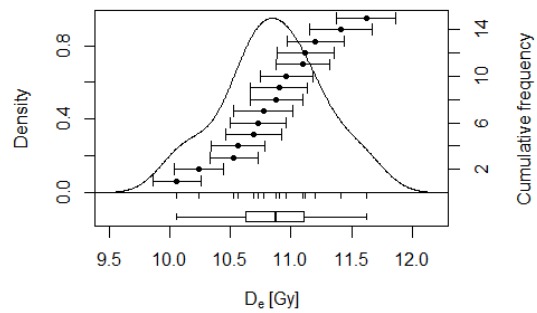
D_e distribution of BT1410



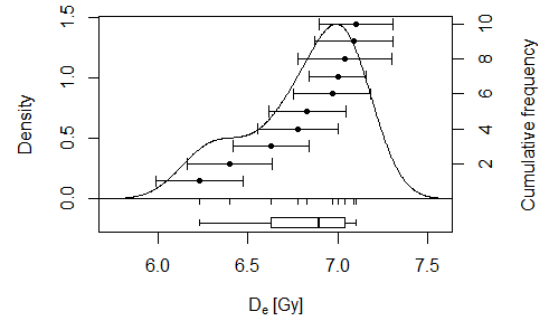
D_e distribution of BT1510



D_e distribution of BT1511



D_e distribution of BT1512

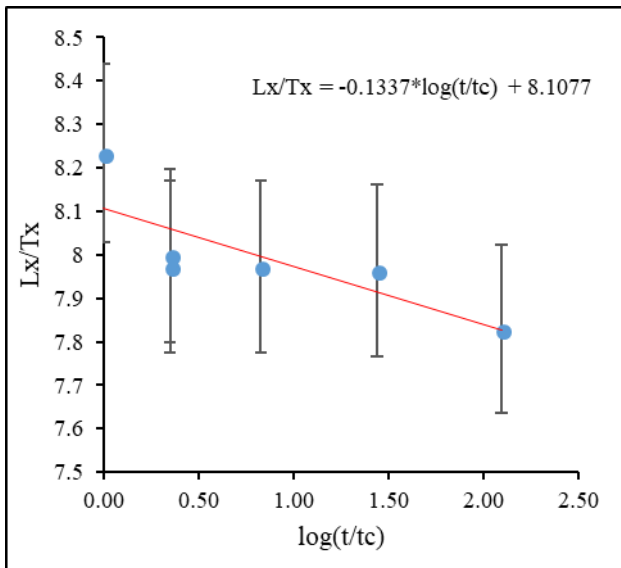


A3 Example of fading rate determination of polymineral fine grain

Measurement was following [a]. The equation was expressed by

$$I = I_c \left[1 - \frac{g}{100} \log_{10} \left(\frac{t}{tc} \right) \right].$$

an example of the fading measurement of BT1409 is presented in the figure below.



From the fitted equation (in Figure), I is Lx/Tx. After reformulated the equation above, g value was 1.65 % decade. At least 3 discs was measured per sample. The average value was applied to **R** luminescence package to correct the age due to fading phenomena [b].

[a] Huntley, D.J., Lamothe, M., 2001. Ubiquity of anomalous fading in K-feldspars and the measurement and correction for it in optical dating. *Canadian Journal of Earth Sciences*, 38, 1093-1106.

[b] Kreutzer, S. (2017). `calc_FadingCorr()`: Apply a fading correction according to Huntley & Lamothe (2001) for a given g-value and a given tc. Function version 0.4.2. In: Kreutzer, S., Dietze, M., Burow, C., Fuchs, M.C., Schmidt, C., Fischer, M., Friedrich, J. (2017). *Luminescence: Comprehensive Luminescence Dating Data Analysis*. R package version 0.7.5. <https://CRAN.R-project.org/package=Luminescence>

A4 Acknowledgement

This thesis could be finished smoothly only because a lot of people gave me their supervision, support, and advice. First, I would sincerely like to acknowledge Prof. Dr. Ludwig Zöller and Dr. Christoph Schmidt for supervising this thesis. They provided good supervision in terms of both academics and daily life during my stay in Germany. Moreover, I would like to thank Mr. Manfred Fischer for providing the good experience in luminescence dating laboratory. Then I would like to acknowledge all members of Chair of Geomorphology, University of Bayreuth that always gave me various guidance. All co-authors who appeared in cumulative works (cf. Chapter 2-4) and in poster presentations are all acknowledged for giving me good experiences.

I would like to specially thank Asist. Prof. Dr. Helmut Dürrast, geophysics lecturer at Prince of Songkla University, who motivated me to start Ph.D. and provided a great deal of assistance since I applied for the scholarship. I would also acknowledge my parents, my brother, and my friends (Chaloemlap Thammarat, Panet Sangkapan, and Mahan Sukawanno) who helped me a lot during my fieldwork in Thailand. Moreover, I am appreciated that Thai students in Bayreuth gave a good friendship since we met. Finally, I would like to thank my family who gave me the encouragement and motivation to finish my study successfully.

Living expenses during my Ph.D. have been provided by the Development and Promotion of Science and Technology (DPST) talent project (The Royal Thai Government). My stay in Germany is facilitated by the Office of Educational Affairs Berlin (OEA), the Royal Thai Embassy in Berlin. Both DPST and OEA also give useful consultants.

A5 Curriculum Vitae

Name Prakrit Noppradit

Date of birth 23rd February 1989

Place of birth Songkhla, Thailand

Post address

Thailand: 76 Moo 10 Thungwang, Muang district, Songkhla, 90000

Germany: Emil-Warburg-Weg 24, 95447 Bayreuth

Email address prakrit.noppradit@uni-bayreuth.de, prakrit.nop@gmail.com

Telephone No. +49 921 55 2054 (office), +49 1525 715 5010 (mobile), +66 83 534 2532
(Thailand)

Education

March 2011 B.Sc. (Physics) Prince of Songkla University, Thailand

September 2013 M.Sc. (Geophysics) Prince of Songkla University, Thailand

Scholarship

Development and Promotion of Science and Technology talent project (DPST), Thai's government

List of Publication (under revision process)

Noppradit, P., Schmidt, C., Dürrast H., Zöller L. (2019) Late Quaternary evolution of Songkhla coast, Southern Thailand, revealed by OSL dating. *Chiang Mai Journal of Science*, 46(x): 1-13.

Noppradit P., Symanczyk A., Zöller L., Brückner H., Stock F. (2018) Methodological approach for dating harbor sediments by using luminescence dating – a case study in Ephesus, Western Turkey, *Archaeological and Anthropological Sciences*, 38. DOI: 10.1007/s12520-018-0739-y

Noppradit P., Zöller L., Schmidt C., Lorenz S., Rother H., Geological evolution and optically stimulated luminescence (OSL) dating of the coastal dunes at Trassenheide, Usedom Island, NE Germany, *E&G Quaternary Science*.

List of Poster presentation and Proceeding (2014-2017)

- Noppradit P., Schmidt C., Dürrast H., Zöller L. (2017) OSL dating of weathered sand in Songkhla Province, Thailand. *German Luminescence and ESR Meeting 27th-29th October 2017*, Schney, Germany.
- Noppradit P., Schmidt C., Dürrast H., Zöller L. (2017) Coastal development in Songkhla Province, Thailand. *4th Central European Geomorphology Conference 9th-13th October 2017*, Bayreuth, Germany
- Noppradit P., Kreutzer S., Mercier N., Schmidt C., Zöller L. (2015) OSL Dating Study from the Dune du Pilat in France. *German Luminescence and ESR Meeting 6th-8th November 2015*, Berlin, Germany.
- Noppradit P. (2015) Paleoearthquakes of the Khlong Marui Fault Zone, Southern Thailand. *Proceedings of Thai Student Interdisciplinary Symposium 20th-22nd March 2015*, Heidelberg Germany.

A6 (Eidesstattliche) Versicherungen und Erklärungen

(§ 9 Satz 2 Nr. 3 PromO BayNAT)

Hiermit versichere ich eidesstattlich, dass ich die Arbeit selbstständig verfasst und keine anderen als die von mir angegebenen Quellen und Hilfsmittel benutzt habe (vgl. Art. 64 Abs. 1 Satz 6 BayHSchG).

(§ 9 Satz 2 Nr. 3 PromO BayNAT)

Hiermit erkläre ich, dass ich die Dissertation nicht bereits zur Erlangung eines akademischen Grades eingereicht habe und dass ich nicht bereits diese oder eine gleichartige Doktorprüfung endgültig nicht bestanden habe.

(§ 9 Satz 2 Nr. 4 PromO BayNAT)

Hiermit erkläre ich, dass ich Hilfe von gewerblichen Promotionsberatern bzw. -vermittlern oder ähnlichen Dienstleistern weder bisher in Anspruch genommen habe noch künftig in Anspruch nehmen werde.

(§ 9 Satz 2 Nr. 7 PromO BayNAT)

Hiermit erkläre ich mein Einverständnis, dass die elektronische Fassung meiner Dissertation unter Wahrung meiner Urheberrechte und des Datenschutzes einer gesonderten Überprüfung unterzogen werden kann.

(§ 9 Satz 2 Nr. 8 PromO BayNAT)

Hiermit erkläre ich mein Einverständnis, dass bei Verdacht wissenschaftlichen Fehlverhaltens Ermittlungen durch universitätsinterne Organe der wissenschaftlichen Selbstkontrolle stattfinden können.

Bayreuth, 21.11.2018
Ort, Datum, Unterschrift